ASSESSING THE IMPACT OF THE NOCTURNAL TRANSITION ON THE LIFETIME AND EVOLUTION OF SUPERCELL THUNDERSTORMS IN THE GREAT PLAINS

by

Matthew Edmund Gropp

A thesis submitted to the faculty of
The University of North Carolina at Charlotte
in partial fulfillment of the requirements
for the degree of Master of Science in
Earth Science

Charlotte

2017

Approved by:

_____
Dr. Casey Davenport

_____
Dr. Matthew Eastin

_____
Mr. Terry Shirley

ABSTRACT

MATTHEW EDMUND GROPP. Assessing the impact of the nocturnal transition on the lifetime and evolution of supercell thunderstorms in the Great Plains. (Under the direction of DR. CASEY DAVENPORT)

Predicting the evolution of supercell thunderstorms during and after the evening transition is a known challenge due to an incomplete understanding of how they evolve in response to associated environmental changes. As the low-level environment cools and stabilizes, supercells can dissipate, merge with other convection, grow upscale, or be sustained as either a surface-based or elevated supercell. The goal of this study is therefore to better predict how supercells will evolve during the evening transition by focusing on trends in environmental parameters that will lead to increased skill in forecasting. To quantify the connection between storm evolution and environmental changes during the nocturnal transition, a large number of initially isolated Great Plains supercell thunderstorms occurring between 2005 and 2016 are examined. Each supercell is categorized as either maintained, dissipating, growing upscale, or merging. Changes in the inflow environment are quantified using hourly RUC and RAP proximity soundings between one hour prior to local sunset time and five hours post sunset. Using these soundings, numerous thermodynamic and kinematic parameters are derived, including surface-based and most unstable CAPE and CIN, and low-level and deep-layer shear and storm-relative helicity. In general, the differences were large between evolution categories, but varied depending on the comparison; each classification existed in a unique set of kinematic and thermodynamic parameters. Statistical tests comparing trends and distributions of these parameters were most notable for maintained versus dissipated

cases; storm-relative helicity was identified as a key parameter in distinguishing these case types, with maintained supercells containing significantly higher storm-relative helicity values during the nocturnal transition. The benefit of stronger, sustained storm-relative helicity values is inferred to help maintain a robust rotating updraft despite increasing stability, while a decrease (as seen in other supercell evolution categories) would lead to a loss of supercellular characteristics.

ACKNOWLEDGEMENTS

Thank you to my adviser, Dr Casey Davenport, for taking me on as master's student. I am grateful for your guidance and scientific expertise shared with me over the last two years. Many thanks to my committee members, Terry Shirley and Dr Matthew Eastin, who provided numerous suggestions and ideas to help this work come to fruition. Words cannot express my gratitude to my fiancée, Christy Reuille, who was a constant source of support and motivation. To my parents, Julie and Rick Gropp, thank you for have being a steadfast source of inspiration and strength. Thank you to my family, Bill, Meag, and Jeff Gropp, for their scientific and personal input over the years. Finally, thank you to the Reuille Family for their tremendous support during my time at UNC Charlotte.

Table of Contents

LIST OF TABLES

LIST OF FIGURES

CHAPTER 1. INTRODUCTION

The stabilizing and cooling of the atmospheric boundary layer during the nocturnal transition leads to a series of thermodynamic and kinematic changes in the atmosphere, creating a challenging environment for forecasting the evolution of supercell thunderstorms. The primary environmental change that occurs during the nocturnal transition is cooling in approximately the lowest 1 kilometer; this begins shortly after sunset and continues until sunrise (Stull 1988). Since supercells tend to be long-lived, initiating in the afternoon and persisting for several hours, many supercells will exist during the nocturnal transition. Limited forecasting-based research exists regarding precisely how supercells evolve during the nocturnal transition; there are numerous temporal and spatial changes that occur in the supercell's local environment, and complex interactions exist between the storm and these variations. A lack of understanding regarding such interactions makes the accurate prediction of the lifetime a supercell challenging, which therefore makes quality forecasting of supercell track and strength difficult.

The governing dynamics of supercell thunderstorms have been well covered through various research studies (e.g., Lemon and Doswell 1979; Davies-Jones 1984; Rotunno and Klemp 1985; Klemp 1987). The numerous environmental factors that impact the strength, development, and severe weather production of supercells are also well-known, including favorable vertical wind, moisture, and temperature profiles

(Thompson et al. 2003); the nocturnal transition acts to modify these thermodynamic and kinematic aspects of the environment. As the environment evolves after sunset, there are four possible evolutions for an originally isolated supercell: 1) dissipation, 2) merge with other supercells, MCS or other convective cells, 3) grow upscale to a larger form of convection, or 4) maintenance either through becoming elevated or remaining surface-based (Colman 1990; Billings and Parker 2003; Nowotarski et al. 2011; Davenport and Parker 2015a; Davenport and Parker 2015b). The focus of this research will be to determine how the environment evolves differently to produce each of these evolution classifications, with an overall goal of promoting enhanced short-term forecasts. To achieve this goal, the nocturnal transition's environmental changes will be quantified through observational data; these changes will then be correlated with how a supercell is modified due to these changes.

CHAPTER 2. BACKGROUND

2.1 Environmental Changes during the Nocturnal Transition

The nocturnal transition is a period of both thermodynamic and dynamic modifications in the atmosphere, most strongly observed in the boundary layer. The boundary layer is defined as the portion of the atmosphere most affected by fluxes of energy, moisture and heat from the Earth's surface and observes a strong diurnal temperature dependence (Fig. 1; Stull 1988; Markowski and Richardson 2010; Cohen et al. 2015). Motion and processes in the boundary layer are also influenced by friction from the surface and turbulent processes (Stensrud 2007). During the nocturnal transition, the temperature decreases in the boundary layer at a rate dependent on numerous environmental conditions, including cloud cover, relative humidity, and precipitation (Markowski and Richardson 2010). The change in moisture and temperature fluxes are dependent on local conditions, such as valleys and tree coverage, therefore making it difficult to universally quantify the impact of the nocturnal transition (Acevedo and Fitzjarrald 2001).

The surface cooling quickly leads to stabilization of the potential temperature profile in the lowest levels of the boundary layer, which by extension directly impacts thermodynamic quantities including surface-based CAPE (SB CAPE) and surface-based CIN (SB CIN); specifically, SB CAPE decreases while SB CIN increases. The rate at which SB CIN increases with time during the transition is a function of how fast the

surface cools and the rate of moisture advection, if any. SB CAPE changes will inherently decrease as SB CIN increases, thus making the surface a more inhospitable environment for convection. Mixed-layer (ML) and most unstable (MU) parcels may respond differently to the surface cooling, since these parcels are not entirely dependent on the surface parcel. The ML and MU parcels may or may not be impacted by the surface cooling; a temperature profile with steep lapse rates in the mid- and upper-levels will be more likely to have MU parcels that are unaffected by surface tendencies, since the most unstable parcel generally develops near the interface with the nocturnal inversion.

In addition to thermodynamic changes, the nocturnal transition is also associated with changes to the wind profile, most notably a decrease in the surface wind speed and a formation of a low-level jet (LLJ; Stensrud 2007). The LLJ is defined as an area of high relative southerly wind speed, 12 m/s or greater, that forms on the top of the nocturnal boundary layer, at or below 1 km above ground level (AGL). This is primarily caused by a decrease in turbulent friction that occurs once the boundary layer begins to stabilize, and the differential cooling that can result along sloping surface; both of these effects need to be present in order to achieve observed LLJ magnitudes (Blackadar and Buajitti 1957; Stull 1988; Stensrud 2007; Cohen et al. 2015; Shapiro et al. 2016). The LLJ most frequently occurs in the central Great Plains primarily due to the gently sloping terrain, allowing for a horizontal temperature gradient to develop with differential cooling, as well as the region promoting strong radiative heating, leading to strongly turbulent boundary layer flow. The wind profile of the LLJ is unique as the maximum velocity will occur between 500 m and 1 km AGL, followed by relative minimum at or below 3 km

AGL (Fig. 2; Bonner 1968). This relative minimum distinguishes LLJ profiles from environments with winds greater 12 m/s throughout their depth. The LLJ plays an important role in providing the necessary ingredients for severe weather, primarily through transporting additional low-level moisture throughout the night, increasing low-level vertical wind shear, and also promoting upward motion through enhanced convergence along boundaries (Markowski and Richardson 2010; Coffer and Parker 2015). Given the importance of the LLJ in providing conditions conducive to storm development and maintenance, this aspect will be explored further to determine its influence on supercell evolution during the nocturnal transition.

Due to the LLJ and a decrease in surface wind speed, the nocturnal transition normally produces an increase in low level shear, primarily in the 0-1 km layer. Conversely, deep layer shear is a function of the larger synoptic environment, thus generally less impacted relative to low level. The LLJ's enhancement of low-level shear evolution during the transition not only influences speed shear, but directional shear as well. The changes in directional shear will lengthen the hodograph and potentially increase the amount of streamwise vorticity available for a supercell to ingest. Storm relative helicity (SRH; Kerr and Darkow 1996) in the 0-1 and 0-3 km layers are a measure of streamwise vorticity and is often used as a proxy for the strength of updraft rotation in a supercell. Average 0-1 km SRH values vary from around 100 m^2s^{-2} in weaker supercells to 300 m^2s^{-2} in stronger supercells (Thompson et al. 2007, hereafter TME07). Since SRH is a function of shear, it will vary with the phenomena like the LLJ and the nocturnal boundary layer where SRH values have been documented to increase

by up to 400 m^2s^{-2} during the early evening transition (Mead and Thompson 2011; Coffer and Parker 2015).

As a result of the low-level shear and SRH increases from the LLJ, the nocturnal transition presents a heightened risk for tornado related fatalities, despite increasing low level stability associated with boundary layer cooling; tornado occurrences after sunset make up 25% of total cases but cause 40% of total tornado fatalities (Ashley et al. 2008). Kis and Straka (2010) showed that nocturnal tornadoes tend to occur with shallow near-surface stable layers but strong LLJs, yielding extremely high low-level shear and SRH. Mean SB CIN for nocturnal tornado environments was greater than -100 J/kg; 0-1 km SRH values were greater than 300 m^2s^2. The distributions of SB CIN and SRH, however, indicate that tornadoes occurred in environments with -200 J/kg or more CIN, and with relatively small SRH magnitudes. This raises the question of what balance between rotation potential (as measured by SRH) and stability is necessary to produce tornadoes after sunset. Finding the preferential balance between low level CAPE, SRH, and SB CIN changes leading to tornado development would increase forecasting skill during the nocturnal transition, and also inform the potential of supercell maintenance during the transition.

In addition to shear and SRH changes, the LLJ modifies the thermodynamic environment via significant advection of moisture into the Great Plains; this increase in moisture then enhances elevated instability. This increase in elevated instability points to the importance of focusing on instability parameters that are not surface-based, as they may not be representative of the actual instability available to the supercell; high dew points just above the surface would cause a vertical gradient in CAPE and CIN. Clearly,

the presence of the LLJ during the nocturnal transition highlights the coupled nature of the thermodynamic and kinematic changes during the nocturnal transition, as surface cooling will lead to a LLJ, which increases moisture advection, which then in turn increase ML or MU CAPE.

2.2 Supercell Characteristics

The dynamics of isolated supercells has been a well-studied area of research over the last 40 years (e.g., Lemon and Doswell 1979; Davies-Jones 1984; Rotunno and Klemp 1985; Klemp 1987). Thermodynamically, supercells need a buoyancy force in order to develop, initiate, and sustain an updraft. Generally, CAPE values greater than 2000 J/kg is considered sufficient for supercell development and maintenance (Thompson et al. 2003). This threshold value assumes that the level of free convection (LFC) is reasonably close to the surface, so that the CAPE is not extremely elevated and easy to attain (i.e., minimal lifting needed). The amount of CIN present is also a factor in supercell development as well as maintenance in order to support minimal lifting of parcels. Increases in SB CIN (such as during the nocturnal transition) can cause weakening of a developed supercell, but in the presence of elevated instability, increasing SB CIN can also result in a supercell becoming elevated, primarily ingesting elevated parcels as opposed to near-surface parcels.

A supercell generally lifts a range of low-level parcels into its updraft (e.g., TME07; Nowotarski et al. 2011; Davenport and Parker 2015b). One method of assessing where a supercell may ingest parcels is the effective inflow layer. TME07 found that creating a unique layer for each individual storm (known as the effective layer) allowed

for a more physically representative layer of inflow parcels, in contrast to the relatively arbitrary 0-1 km or 0-3 km layers. The effective inflow layer is defined by the layer where parcels have more than 100 J/kg of CAPE and less than 250 J/kg of CIN; it is assumed that these parcels are buoyant enough to be ingested into the updraft (TME07). Using this layer, unique kinematic parameters such as effective shear and effective SRH value can be produced for every supercell, providing a more representative sense of the environment the supercell is utilizing for its maintenance. Changes in the depth and levels of the inflow layer, as well as modifications to effective parameters during the nocturnal transition will be used to yield information about storms evolve as surface parcels lose their buoyancy potential.

The amount of vertical wind shear is strongly correlated with supercell development, intensity, and maintenance (e.g., Lemon and Doswell 1979; Rotunno and Klemp 1985; Weisman and Rotunno 2000; Bunkers et al. 2006a; Coffer and Parker 2015). The average magnitude of the vertical shear in environments measured from the surface to 8 km varies from 20 m/s to 40 m/s, with the more intense and long-lived storms existing in the higher shear environments (e.g., Bunkers et al. 2006b). The vorticity vector resulting from this vertical wind shear is purely horizontal. The updraft of a supercell reorients the vorticity vector resulting from horizontal shear to the vertical by tilting, which can then be enhanced through stretching, via buoyant accelerations (Fig 3; Bluestein 1999). If the supercell's motion and the horizontal vorticity vector are in the same direction, streamwise vorticity is present. With tilting of the vertical shear and environmental streamwise vorticity, the cyclonic vertical vorticity is positioned in line with the updraft, creating the mesocyclone.

The development of the rotating updraft induces a negative pressure perturbation associated with the spin term in the pressure perturbation equation, and leads to enhanced vertical accelerations. Along with creation of the rotation in the updraft, vertical shear will also induce positive pressure perturbations upshear of the updraft and negative perturbations downshear of the updraft. With veering winds, the upshear high at the surface and the downshear low aloft will cause increased vertical acceleration (Fig 4; Davies-Jones 1984). The vertical pressure perturbation gradient force (VPPGF) plays a crucial role in storm supercell structure, maintenance, and lifetime (Markowski and Richardson 2010; Nowotarski et al. 2011).

Indeed, the connection between vertical wind shear and supercell thunderstorms bears out in forecasting-based research. For example, Bunkers et al. (2006b) found a strong correlation between vertical wind shear and the occurrence of long lived supercells while Thompson et al. (2003) found statistically significant differences in 0-1 km and 0-6 km shear between tornadic supercells, non-tornadic supercells, and ordinary thunderstorms. Since long-lived supercells on average will exist through the nocturnal transition, the amount of shear will likely play an important part in this current research (Bunkers et al. 2006b). However, since the wind profile will change during the nocturnal transition, shear will be time dependent due to the low level wind modification from decreasing turbulent drag and nocturnal cooling; how the updraft evolves in response to such changes in shear is not fully understood.

2.3 Interactions of Supercells with Temporally and Spatially Evolving Environments

The aforementioned changes that occur during the nocturnal transition present a complex and evolving forecasting environment. How a mature supercell responds to surface cooling or the development of a LLJ is an issue that previous research has only recently begun to explore.

When supercells are introduced to a stable surface layer, one possibility is that the supercell could become elevated (Colman 1990; Davenport and Parker 2015a). Convection that is not distinctly drawing air from the surface boundary layer is referred to as elevated convection (Colman 1990; Horgan et al. 2007). From a forecasting perspective, elevated supercells provide several challenges. Horgan et al. (2007) found that hail production is not mutually exclusive with elevated storms, like tornado or wind damage, as the formation of hail is not explicitly surface based. When determining whether or not a supercell has become elevated, a starting point is a discontinuation of wind and tornado reports, with continuing production of hail, as elevated storms tend to not produce tornadoes or severe wind damage. The difficulty with this method is that during and after the nocturnal transition, observing wind and tornado damage becomes much less likely due to lack of light.

Schultz and Corfidi (2008) attests that elevated convection cannot be thought of as a distinct type of convection, as its definition is fairly vague. This idea was also affirmed in several studies, where parcel trajectories computed in numerical modeling simulations demonstrated that supercells were ingesting parcels from a variety of surface and elevated layers (Parker 2008; Nowotarski et al. 2011; Billings and Parker 2012; Davenport and Parker 2015b; Coffer and Parker 2015). Based on this more recent

research, elevated convection should be thought of as “mostly elevated,” since even supercells that exhibit pure elevated characteristics are still ingesting in near-surface air. Idealized model simulations from Nowotarski et al. (2011) demonstrate that surface parcels are still able to be lifted and ingested into the updraft despite strong surface layer inhibition sustained throughout the simulation (Fig. 5). A strong vertical pressure perturbation gradient force in the updraft of a supercell was hypothesized to lift these stable near-surface parcels and is why the ‘mostly elevated’ definition was adopted (Nowotarski et al. 2011; Coffer and Parker 2015). Davenport and Parker (2015b; DP15b) also show that a supercell is able to lift parcels from the surface layer despite enhanced CIN, at least for a short time (Fig. 6); eventually, the CIN can be too great for the VPPGF to overcome and lift surface parcels into the updraft, akin to the more extreme stability cases seen in Nowotarski et al. (2011). Once a supercell completely stops ingesting surface parcels, a supercell will either dissipate or continue to persist, depending on the favorability of the elevated environment. ‘Mostly’ elevated supercells will be more likely to persist, relative to supercells that rely entirely on elevated inflow, since a ‘mostly’ elevated supercell would more easily retain its VPPGF due to easier lifting of moist low level parcels to their LFCs, further increasing the strength of the VPPGF and supercell maintenance.

Billings and Parker (2012) conducted a series of simulations based on a Bow Echo and MCV Experiment (BAMEX; Davis et al. 2004) case study from 22-23 June 2003 involving cold boundaries and elevated supercells. There were multiple types of convective systems and evolutions that occurred during this event, including discrete maintained supercells, merging supercells and the development of a squall line. The

simulations were run multiple times and each time another phenomenon (cell merging, preexisting cold pool, boundary layer cooling) was introduced. Billings and Parker (2012) came to the same conclusion as Nowotarski et al. (2011): the supercells were able to stay somewhat surface-based despite the presence of low level cooling (akin to the nocturnal transition), likely due to strong VPPGF that continued lifting air parcels despite the high CIN. Since the VPPGF has a non-linear response to changes in velocity and vorticity, small increases in the pressure perturbation or vertical accelerations could yield major impacts and accelerate buoyantly stable parcels into the updraft (Markowski and Richardson 2010).

In addition to studying the effects of a stable boundary layer, several studies introduced how temporal variations in environmental parameters can impact convection, such as low level cooling or increasing shear, mimicking the nocturnal transition. Parker (2008) showed how squall lines respond to low level cooling over time and found that squall lines were able to continue lifting surface air despite large CIN. The squall line in Parker (2008) showed the same ability to overcome surface stability as seen in Nowotarski et al. (2011), Billings and Parker (2012), and DP15b, indicating that the internal dynamics of organized convection can be remarkably resilient to changes in the local environment.

Coffer and Parker (2015) studied the effects of increasing low-level shear on two supercells from the Second Verification of the Origins of Rotation in Tornadoes Experiment (VORTEX2; Wurman et al. 2012) during the early evening transition. Using base-state substitution (Letkewicz et al. 2013), the kinematic environment around the mature supercell was modified over time to account for the development of the LLJ

associated with the nocturnal transition. As a result, surface storm relative helicity values increased significantly. This increase in shear and SRH during the nocturnal transition was found to enhance the VPPGF, thus preserving strong vertical accelerations and promoting convective maintenance.

Davenport and Parker (2015a) studied a dissipating supercell from VORTEX2 that also occurred during the early evening transition. In addition to nocturnal cooling, the storm in this study traveled into increasingly stable air through its lifetime by moving deeper into the cold side of a boundary, thus increasing near-surface convective inhibition. In contrast to Coffer and Parker (2015), however, the environment in this case exhibited decreases in 0-6 km shear, 0-1 km SRH, and 0-3 km SRH, which was hypothesized to weaken vertical acceleration of parcels due to less streamwise vorticity being ingested, thus weakening the mesocyclone. Interestingly, MUCAPE sufficient to sustain convection was present, yet the storm still dissipated. A follow-up idealized modeling study using base-state substitution found that it was the combination of weaker shear and SRH, as well as low-level stabilization that lead to the storm's demise (DP15b). This links well with Billings and Parker (2012), Coffer and Parker (2015), and Nowotarski et al (2011), since they also found that not just a single environmental change leads to a supercell dissipating. This highlights the difficulty in knowing when a supercell will become elevated and what set of environmental conditions lead to elevation versus dissipation. Since supercell maintenance is a function of multiple parameters providing different forcing, a balance between parameters could be necessary for maintenance; increasing shear could balance with increasing stability. These idealized simulation studies imply that there may be a combination of different parameters that will yield a

dissipating storm versus other types of outcomes. This is caused by the interplay between shear and SRH increases and SBCIN increases, which yields enhanced strength of the VPPGF but more stable parcels. Therefore, the amount of surface stabilization and the evolution of the wind profile are necessary factors in assessing supercell evolution during the nocturnal transition; this research aims to identify which environments tend to produce sustained (as a supercell or otherwise) versus dissipated convection.

Along with dissipated and maintained convection, upscale growth is another distinct possibility during the nocturnal transition. Supercells growing upscale into a convective line was explored more in depth in Billings and Parker (2012) via the development of gravity waves in the nocturnal or any stable boundary layer. These waves are theorized to lead to more linear convective development once the boundary layer cools by enhancing convergence and vertical motion. Linear convection can initiate along the crest of the wave, assuming the vertical motion is sufficient for the parcel to reach its LFC. Billings and Parker (2012) showed that a surface cold pool forced squall line that developed from upscaled supercells was able to remain surface based despite high CIN. This upscaled system also existed simultaneously with isolated supercells that remained partially surface-based as well. The LLJ jet will play a role in upscaling supercells, as it acts a source of convergence and vertical motion along the boundary of stable cold pools (Kumjian et al. 2006). Since the wind profile for linear systems is more unidirectional, the change in effective bulk wind shear during the nocturnal transition could yield information about the tendency of upscaled supercells.

The merger of a supercell with another convective feature is last type of evolution considered in this research. A supercell merging with a mature squall line is a common

occurrence and has been the focus of several recent studies. French and Parker (2012), using Rapid Update Cycle (RUC) analysis data, categorized 21 merger cases as either weakly or strongly synoptically forced based on the amplitude of the associated 500 mb trough. The strongly forced mergers existed in the warm sector of mid-latitude low pressure systems with much higher kinematic parameters (0-1 km SRH, 0-3 SRH, and 0-6 km shear) when compared to the weakly forced cases. In contrast, weakly forced cases tended to occur slightly ahead of the warm front away from the low pressure center. French and Parker (2012) implies that when in the warm sector and close to center of the low, mergers are more likely when 0-6 km shear and SRH are high.

Nowotarski et al. (2011), Billings and Parker (2012), and Parker and Coffer (2015) studied the impact of stable boundary layers on supercell maintenance, finding that supercells are notably resilient in response to increased CIN. This was attributed to a strong VPPGF in the updraft, allowing for continued lifting of parcels despite high CIN. Yet, with a weakening VPPGF, dissipation is also a possibility (DP15b). The results of these studies begs the question that this current research intends to answer; what set environmental parameters will significantly increase or decrease the strength of VPPGF? How large of increase in VPPGF is needed to compensate for a certain rate of stabilization? Within this, the environment needed for a supercell to become elevated is an area of limited research. For forecasting purposes, the parameters analyzed to assess the VPPGF strength and stabilization need to be those readily available to forecasters, including 0-6 km shear, effective SRH, SFC CIN, MU CIN, and MU CAPE; these parameters, among others, will be assessed in this study.

2.4 Spatial Heterogeneity

The nocturnal transition, owing to its multiple effects on temperature, wind, and moisture, will influence the spatial distribution of environmental parameters; indeed, the spatial distribution of thermodynamic and kinematic parameters in the inflow of supercells has been shown to be highly heterogeneous, partially driven by storm-induced perturbations, and can at times be quite large (e.g., Markowski and Richardson 2007; Parker 2014). Parker (2014), using VORTEX2 sounding and mesonet networks, illustrated that this variability tends to manifest as more favorable conditions closer to the supercell updraft. This study also showed that non-tornadic supercells tended to have strongly horizontally-heterogeneous wind profiles in the inflow region, with crosswise vorticity increasing towards the updraft. The results of these studies highlight that soundings from nearby NWS offices are likely not sampling the same environment that the supercell is occurring within as spatial variations can be large. For example, the nocturnal cooling may be more prevalent in the "far" regions from the supercells, while cooling will be less pronounced near the supercell thus creating a local temperature gradient. This gradient would modify CAPE, CIN and kinematic properties within the inflow, playing a role in the supercell's evolution and lifetime.

CHAPTER 3: DATA AND METHODOLOGY

3.1 Sample Supercell Collection

This research aims to create a climatology of supercell environments and the related modification of the environment due to the nocturnal transition in order to identify distinguishing characteristics between dissipating, merging, upscaled and maintained supercells. Ultimately, this research hopes to enhance our understanding of how supercells become elevated and develop a climatology that will be useful in forecasting supercell evolution.

Supercell cases utilized for this research were first identified using the Storm Prediction Center's Severe Thunderstorm Event Archive from 2005 to 2016, focusing on storms that occurred in the Great Plains of the United States. This region was chosen both for its propensity for supercells and its relatively flat, homogenous landscape, limiting the influences of terrain on storm evolution. All cases occurred during the months of March – June, as this is the time period of highest supercell frequency in the Great Plains. Cases were initially identified using national composite radar reflectivity to focus on isolated convection (e.g., cells of average supercell size and distinguishable from all other convection) that were present at 0000 UTC and had associated hail, wind, and/or tornado reports; these were flagged as possible supercells. 0000 UTC was used as proxy for the start of nocturnal transition only for the initial data gathering. A potential bias in this initial storm collection is that storm reports are only issued when a trained storm spotter

submits a report. Therefore, reports are far more likely in areas with larger populations. Synoptically, these isolated supercells were required to be in the warm sector of a low pressure system and/or displaced from frontal boundaries to avoid possible frontal interactions that could lead to enhancements not related to the nocturnal transition; quantifying the distance to the closest boundary will be discussed later in this section. This preliminary examination resulted in a total of 368 possible supercell cases collected.

In order to assess the impact of the nocturnal transition and account for the seasonal change in the onset of diurnal cooling, the sunset time was calculated for each supercell based on the date of the event and its latitude and longitude at 0000 UTC. This method allowed for a date and location-relative start time of the nocturnal transition. For example, for a supercell occurring on June 10, 2016 at 34.0° N and -100° W, sunset occurs at 0150 UTC so this sunset time would be rounded to 0200 UTC.

Each of the 368 potential cases initially identified were then examined in more detail to determine whether a supercell was indeed present after the start of the nocturnal transition. Supercells were identified by the presence of a Mesocyclone Detection Algorithm (MDA) flag at the calculated sunset time (SS); a combination of a characteristic hook echo in the reflectivity data and a distinct velocity couplet present in either the 0.5° or 1.5° elevation angles also sufficed in the absence of an MDA flag. The MDA performs two and three-dimensional analysis of azimuthal velocity shear at multiple elevation angles to flag a mesocyclone (Stumpf et al. 1998; Jones et al. 2004). The threshold shear values needed for a flag are dependent on range from the radar and common mesocyclone characteristics, such as width of maximum shear area in question. WSR-88D level 3 and level 2 data were used for all reflectivity, velocity and MDA data.

These methods all have shortcomings when the supercell is located too far from the radar in use. In these cases, the radar beam would simply hit too high in the supercell to detect any rotation and the weak echo region is also likely to not be present. In these questionable cases, a combination of the storm damage type (tornado, large hail), storm motion and the limited radar data was used. Figure 8 shows examples of this process. Following this interrogation, a total of 157 supercells were confirmed; their paths are shown in Fig. 9.

Since minor cooling associated with the nocturnal transition occurs shortly before sunset, the start of the nocturnal transition was defined as sunset hour minus one (SS -1; Stull 1988). In order to better predict the how supercells will evolve during the nocturnal transition, the confirmed supercells then needed to be classified based on their evolution from SS -1 to SS +5. The ultimate purpose of this classification is to discover differences in the environments between the categories of dissipation, merging, upscaled and maintained supercells (Fig. 10), in order to increase forecasting skill during this time frame. Determining the evolution type for each supercell was done using the following criteria. A supercell was selected as a dissipation event if the cell remained isolated and ceased displaying supercellular characteristics before SS +5 (e.g., Fig. 10a). A supercell that lost the MDA flag for consecutive scans and ceased any mid-level rotation, or a supercell that no longer had discernable mid-level rotation or a bounded weak echo region, was considered to have dissipated. If the suspected dissipating supercell was positioned far from a radar, a combination of the above and any stop in hail reports was used to determine in the supercell dissipated. A cease in hail was used since it would represent a weakening of the updraft and elevated supercells generally cease damaging

wind or tornado production (e.g., Colman 1990; Horgan et al. 2007), but continue to produce hail. Maintained cases were chosen if the supercell remained isolated and continued to exhibit supercell characteristics through SS +5 (e.g., Fig. 10b). A merger type was selected if the isolated supercell collided with other supercells, or a larger convective feature, such as a squall line (e.g., Fig. 10c). Upscale cases were selected if the supercell grew into a larger form of convection that was not pre-existing (e.g., Fig. 10d). The distinguishing feature between upscale and merger categories is that merger was selected if the merged cells then dissipated or if the supercell interacted with a pre-existing feature. A total of 86 dissipation cases, 14 maintained cases, 12 merger and 45 upscale cases were identified.

3.2 RUC and RAP Sounding Collection

Once each supercell and its evolution type was confirmed, the associated environmental parameters were extracted using the Rapid Update Cycle (RUC) and the Rapid Refresh (RAP) numerical weather models (Benjamin et al. 2004; Benjamin et al. 2016). These models were chosen due to the both the time and spatial resolution they provide. The RUC uses an isentropic-sigma hybrid vertical coordinate of 50 levels and horizontal grid spacing of 40 km, 20 km or 13 km, as it has been upgraded over time. The 20 km horizontal grid spaced RUC was used for 2005-2008 and the 13 km spacing was used from January 2009-May 2012. The hour zero analysis from the RUC was used for each hour from SS -1 to SS +5. The RAP Model is used from May 2012-2016. Similar to the 13 km RUC model, the vertical coordinate system and grid spacing are the same.

Changes were made to the various physics parameterization schemes when the RAP replaced the RUC. The primary difference in the physics schemes is a change from the Burk Thompson (1989) 1.5 order PBL scheme in the RUC to the Mellor-Yamada-Janjic (MYJ; Janjic 1994) 1.5 order scheme in the RAP. Both of these schemes have a bias towards not properly mixing the BL but the introduction of the MYJ scheme was done to partially alleviate this issue, as the MYJ scheme generally outperforms the Burk Thompson method in this case (Cohen et al. 2015).

While both the RAP and RUC perform original calculations in the sigma vertical coordinate system with 50 levels, reanalysis output displays the vertical coordinates with pressure coordinates with 37 levels. The original sigma coordinate system is interpolated onto pressure levels from 1000 mb to 100 mb, with 25 mb spacing. This interpolation is always done regardless of what the original surface pressure was on the native grid. As noted in previous research (e.g., Thompson et al. 2003), this coarse grid spacing means there is a loss of precision when compared with balloon launched radiosondes. Importantly, any fine scale features in the profile are likely to be unresolved using these models.

For each hour from SS -1 to SS +5, a storm-relative upwind grid point in the inflow region of the supercell was selected based on the closest latitude and longitude point. Given that the spatial resolution of the models ranged from 13 km to 20 km, the grid point used varied from 10 to 30 km from the updraft signature (using either the hook echo or velocity couplet of the mesocyclone) of the supercell. The distance of the grid point from the updraft signature varied due to where the supercell was positioned on the

grid; no soundings were pulled when the grid point was within 10 km of the updraft signature to avoid contamination from convective adjustment in the model.

For upscaled and merged supercells, the grid point chosen was 10 to 40 km ahead of the direction of propagation of the squall line or MCS, in line with the portion of the system where the supercell interacted. At these grid points, a vertical profile was created using the 37 vertical pressure levels. However, since most locations in the Great Plains are well above sea level, and therefore have a surface pressure below 1000 mb, the vertical profiles had to be adjusted to remove the points that had a pressure greater than the original surface pressure resulting from the interpolation. The issue was also seen in other research involving the RUC and RAP models (Thompson et al. 2003; Benjamin et al. 2004; TME07). The RUC and RAP output a surface pressure, surface temperature, and surface height above sea level and surface wind speed values. Each vertical profile's lowest levels were then checked against the surface pressure; if the lowest pressure level was greater than the surface pressure, the lowest level on the level of the sounding was corrected to the surface values. For example, if the reported surface pressure at a grid point was 981.0 mb, the 1000 mb level would be removed and the first level in the sounding would be 981.0 mb. This correction created a more realistic view of the vertical structure by removing data points that did not physically exist.

Once the corrected soundings were created, numerous environmental parameters were derived. The python library SharpPy was used for the calculations of all the thermodynamic and kinematic variables (Halbert et al. 2015). The derived parameters included surface-based, mixed layer, and most unstable CAPE and CIN, 0-1 km SRH, 0-3 km SRH, 0-1 km bulk wind shear, 0-6 km bulk wind shear, effective SRH (ESRH),

effective bulk shear (EBS), the supercell composite parameter, Bulk Richardson Number (using MUCAPE; Equation 1) and the 700-500 mb lapse rate.

$$BRN = \frac{MUCAPE}{U^2}$$

Equation 1. Bulk Richardson Number, where U is the difference between the density weighted mean 0-6 km and the lowest 500 m mean wind (Weisman and Klemp 1982).

Using the wind profile, a test for the presence for the low-level jet was also performed. The criteria was having a meridional component wind speed at or below 1500 m AGL of 12 m/s or greater (Bonner 1968; Mead and Thompson 2011). The effective layer used for the ESRH and EBS was the same as in TME07, with parcels of 100 J/kg > CAPE and -250 J/kg > CIN constituting the inflow layer.

In order to determine how representative the RUC/RAP soundings were of the observed environments, the closest observed 0000 UTC sounding to the supercell was compared to a RUC/RAP sounding at the same location. Figures 11 and 12 show the error for various CAPE and SRH parameters calculated for all supercell case days. In general, the RUC and RAP both tended to overestimate the SB and MU CAPE, 0-3 km SRH (see Table 1, Figures 12 and 13). The overall errors fall in line with those seen in Thompson et al. (2003); thus, it is assumed that these errors are within reason and the RUC/RAP are sufficient representations of the environment parameters in question.

TABLE 1. RUC and RAP versus observed sounding errors. First value in a cell is total error, second value is solely RUC errors, third is solely RAP errors. Column from left to right: mean value, mean error, mean absolute error, standard deviation, and mean percent error.

Parameter Error (Total,RUC,RAP)	Mean	Mean Error	Mean Absolute Error	St. Dev.	Mean % Error
Surface Based CAPE ($J\ kg^{-1}$)	2077, 2174, 1905	-252, -190, -362	552, 528, 596	722, 768, 617	10.8, 8.0, 13.3
Mixed Layer CAPE ($J\ kg^{-1}$)	1711, 1757, 1629	103, 14, 263	443, 478, 381	635, 708, 436	6.5, 1.0, 21.7
Most Unstable CAPE($J\ kg^{-1}$)	2211, 2331, 1999	-214, -152, -326	562, 561, 565	767, 830, 622	8.8, 6.1, 11.6
Effective SRH (m^2s^{-2})	120, 129, 104	-14, -17, -7	57, 63, 48	83, 87, 76	10.4, 11.9, 6.7
0 - 1 km SRH (m^2s^{-2})	98, 108, 79	-11, -4, -22	49, 48, 49	67, 68, 64	10.2, 4.2, 22.
0 - 3 km SRH (m^2s^{-2})	176, 189, 153	-19, -13, -29	60, 62, 56	84, 89, 73	9.8, 6.5, 16.1

Once the parameters for each supercell were collected from SS -1 to SS +5, all the storms were divided into their respective evolution type. Statistical tests were then performed internally for each classification as well as tests between categories. The first type of statistical test was done internally for each classification, where a Student's T-test was performed to compare the distribution of each environmental parameter at hours at SS +0, SS +1, SS +2 , SS +3, SS +4, and SS +5 to SS -1, individually. The purpose of this test was to show if there was statistical difference between the starting environment and the subsequent hours. This was performed on the entire dataset (March – June) and for each individual month. Performing the tests on a monthly basis was done to avoid potential temporal bias since the timing of the evening transition is not constant.

In order to see if the differences in parameters have forecasting use, the next statistical tests performed were Kolmogorov-Smirnov (KS) test comparisons between the distributions of parameters between different storm evolutions (i.e., comparing the distribution of SBCAPE for the dissipating storms and surface based CAPE for the upscaled storms). The purpose of these tests was to check the likelihood that the two sample distributions in question were drawn from the same population distribution. This yields more information regarding the statistical strength in using some distributions for forecasting evolution type. The Student's T-test was not used solely, since the KS test accounts for differences in variances and shapes of each distribution that the T-test does not; the T-test assumes a Gaussian distribution. The KS tests were then performed comparing the hourly distributions for the same samples (i.e., comparing SBCAPE at hour SS +1 for dissipation cases to the SBCAPE at hour SS +1 for the upscale cases). The goal of these tests was to discover if a particular hour yielded a statistically significant difference, even if perhaps the total SS -1 to SS +5 distributions were not statistically significant for two samples in question. As with the Student's T-tests, all the KS tests were performed for the whole timeframe (March-June) and for each individual month.

3.3 Collection of the Environments and History of each Supercell

Beyond the statistical tests, information regarding the environment and history of each supercell was collected to assess differences between classifications not available through a single proximity sounding. These vary from large scale such as the general

synoptic environment (i.e. 300mb heights, 500mb heights, etc.) and proximity to frontal boundaries to smaller scale mesoscale spatial variations in the environment to microscale with tornado occurrences by case supercells.

Starting with the large scale features of each environment, synoptic-scale differences were assessed by plotting the average 300 mb, 500 mb and 925 mb heights 0000 UTC for each of the four evolution types; 0000 UTC was chosen since it is a proxy for sunset time and a standard time for numerical model output. The purpose of this methodology was to identify general differences among evolution types in the orientation of the jet stream, long and short wave trough patterns, and the height field gradient associated with the level low jet; this type of spatial data are not available through single proximity soundings. Using the RUC and RAP, the 300 mb, 500 mb, and 925 mb heights were extracted at 0000 UTC for each supercell; the mean for each classification was then calculated. As with the inflow grid, the RUC and RAP data needed to interpolated onto a consistent spacing in order to calculate the mean; the grids were all interpolated onto a 13 km spaced grid, keeping the boundaries at the same latitudes and longitudes.

In conjunction with the upper level flow patterns, assessing whether surface boundaries (such as warm fronts or stationary fronts) influenced the evolution of the supercell cases (e.g., Markowski et al. 1998; Bunkers et al. 2006b), was performed by comparing the longitude and latitude for each supercell to the Coded Surface Frontal Positions (CODSUS; NWS 2015) produced by the Meteorological Prediction Center (WPC) to measure distances to surface frontal boundaries. CODSUS files are produced with the WPC surface analysis data every three hours; these files contain a list of latitude and longitude corresponding to the location of cold, warm, occluded and stationary fronts

for the valid UTC time. The CODSUS data has been archived since 2009, so each supercell's coordinates were compared to the 0000 UTC and 0300 UTC CODSUS files from 2009 to 2016 to find the closest frontal boundaries to the supercell; cases from 2005-2008 were not included in this analysis due to lack of CODSUS files. The CODSUS front coordinates arrays were interpolated to 0.1^{o} latitude/longitude spacing for more accurate distance calculations. The distance from each point in each CODSUS front's coordinate array to the supercell's coordinate was then calculated; the minimum distance a supercell was from a front at a given time stamp was then recorded and binned based on evolution type (Figure 9). Since the supercells were originally identified as being located in the warm sector of mid-latitude low pressure systems and/or estimated to be far from boundaries, the majority of the supercells for this research occurred away from boundaries, presumably at a sufficient distance so as not to be influenced by enhanced vorticity or convergence (e.g., Markowski et al. 1998). No cases were removed if they occurred closer to a boundary, as there is no clear range at which boundaries are known to influence supercell intensity, organization, or evolution.

Along with synoptic scale variations in the environment, mesoscale variations were also assessed. The spatial distribution of parameters in the inflow of the supercell were calculated with the same RUC/RAP data as the original inflow soundings. A 160 km by 160 km grid of RUC/RAP data points was oriented so that the original grid point, used for all other calculation, was the most northwesterly point. This grid layout was used to assess how the typical inflow of the supercell changed as a whole through the nocturnal transition. Since the RAP and RUC data has grid spacing of 20km or 13km, all the data were linearly interpolated onto the same 160 km by 160 km grid. A sounding

profile was created at each grid point using the same method as the original sounding. To assess how the spatial distribution of variable changed with time, the grids were created at SS, SS +3, and SS +5. The spatial distribution in the inflow of several significant parameters were calculated using this method.

On the microscale level, potential distinguishing characteristics among evolution categories include the total storm lifetime and history of producing tornadoes; proximity soundings are unable identify these differences in these characteristics. The storm lifetime is defined as the time from the supercell first formed to when the supercell underwent its aforementioned evolution. The beginning of the supercell's lifetime was defined by using the same criteria as the initial supercell confirmation mentioned previously; each supercell was analyzed to see when it became a sustained supercell. The end of the lifetime was defined by when the supercell either dissipated, grew upscale, merged or maintained; the same criteria were used for this as discussed previously. Each supercell's total lifetime was recorded. Collection of whether or not a supercell produced a tornado during its entire lifetime was then performed. Using the full 1950-2016 tornado archive from the SPC, each supercell was compared to the historical record. To check if a supercell produced a tornado, the supercell's date and hour of occurrence were cross checked with the database; within this archive is the date, and the start and end latitude and longitude for each tornado. If the tornado occurred during that supercell's lifetime, then the spatial location relative to the supercell was verified. If the tornado occurred within 20 km of the inflow grid point for the given date and hour, it was inferred that the tornado resulted from that supercell. 20 km was used as the cutoff since this would

account for distance between the grid point chosen and where the tornado associated with the supercell would generally occur.

CHAPTER 4. RESULTS

In order to maintain a persistent rotating updraft, it is hypothesized that increases in SRH via the LLJ and the existence of MUCAPE will provide the necessary support for supercells to be maintained (either as surface-based or elevated) through SS +5, independent of surface based CIN. This result would follow suit with Nowotarski et al. (2011) and Coffer and Parker (2015), which showed that a strong updraft would still be able maintain a supercell despite surface layer stabilization. It is expected that the major distinguishing characteristic between upscaled and maintained supercells will be a difference in SRH, where upscaled storms will have a statistically lower amount as upscaled cases are expected to develop more unidirectional shear to promote the linear convective feature. Due to expected weakening of updraft speed and rotation, the dissipating storms are anticipated to have the smallest amount of MUCAPE and SRH, accelerating their demise once CIN increases, since the VPPGF in the updraft will fail to continue lifting moist parcels from the surface layer.

4.1 General characteristics of each classification

A total of 157 nocturnally transitioning supercells were investigated for this research, with 86 dissipating, 14 maintaining through SS +5, 12 merging with preexisting squall lines and 45 growing upscale.

The geographic distribution of the cases shows the expected bias towards the higher population regions of Texas and Oklahoma, compared to the Dakotas (Fig. 8). The spatial distribution of each classification type shows possible geographic correlation; all maintained and merger cases were all located south of 40^{0} N, while upscale and merger occurred throughout the domain (Fig. 13). This correlation could be a result of population bias but may be related to the stronger presence of the low level jet in the southern plains; this connection will be assessed in the discussion section. The month of occurrence for each classification showed only minor correlation. Total cases were highest in May (41%) followed by April (27%), June (20%) and March (11%); the temporal distribution follows the expected supercell climatology of the geographic domain (Fig. 14). The individual classifications followed the same temporal pattern as the total distribution, with all the evolution types having the maximum in occurrence in May and minimum in March.

4.2 Synoptic Environments

The mean 300 mb, 500 mb and 925 mb heights were calculated for each evolution type as a means to assess the extent to which large-scale differences could explain the classification categories. The mean 300 mb heights (Fig. 15) show some expected features associated with severe weather outbreaks in the Great Plains. A low amplitude 300 mb trough centered over the Great Plains is evident in dissipation environments; progressively increasing amplitudes are present for the upscale, merger, and maintained cases. High amplitude troughs at 300 mb centered over the Southern Rockies indicate the

presence of a strong low pressure system in the Central Plains due to enhanced divergence aloft. Merger and maintained cases are associated with the higher amplitude 300 mb trough and therefore stronger synoptic forcing in general. Domain wide, maintained cases were associated with the lowest 300 mb heights. However, this could be a result of the varying geographic distribution of cases (Fig. 13). For example, a supercell in the Northern Plains would likely be associated with a more northerly 300mb trough, compared to a supercell in Oklahoma (where maintained cases tended to cluster); a direct comparison of mean 300 mb heights is thus somewhat limited. To compensate for the spatial differences (all maintained and merger cases occurred south of 40^{o} N), the 300 mb mean heights were calculated only using supercells that occurred south of 40^{o} N (Fig. 16). However, limiting the domain to less than 40^{o} N had no appreciable change on the mean heights; merger and maintain cases still showed the most amplified trough.

The 500 mb mean heights for each evolution type contained similar patterns as at 300 mb; dissipation cases showed the most zonal flow with increasing amplitude troughs over the Western Plains for the other supercell classifications (Fig. 17). The meridional height gradient was also greatest in the maintained cases, while merger cases tended to have weaker gradients. As with the 300 mb heights, focusing on supercells that occurred south of 40^{o} N had little impact when compared with the full domain; each evolution category had approximately the same pattern at 500 mb (Fig. 18).

The mean 925 mb heights (Fig. 19) show the expected trough and associated southerly flow in the Western Plains for each evolution type; maintained and merger cases however show a deeper trough and thus larger height gradients. With a 925 mb trough centered over the Southwestern Plains, the associated cyclonic flow yields

southerly flow over the Texas and into the Plains. The large zonal height gradient seen in the Southern Plains is likely associated with frontogenesis and possibly nocturnal cooling on the sloping Plains. Since the mean plot was created at SS for each case, only modest cooling has occurred by that time. This implies that the majority of the height gradient seen is a result of baroclinicity from synoptic features; forcing for the LLJ by nocturnal cooling would only supplement the expected wind speeds. The southerly flow, amplified by the low level jet, is weakest in the dissipation cases; large zonal gradients in the height field across the Southern Plains are seen in every other evolution type but are strongest in merger and maintain cases. A region of diffluence in the heights is seen over the Central Plains, where wind speeds are expected to decrease; this diffluence could imply an area of convergence as the faster wind to the south (LLJ) converge into the slower winds. This convergence would suggest an area of general low level lift in the exit region of the LLJ. Confirming the influence of the LLJ on evolution type will be addressed later in this section. As with the other height fields, the average 925 mb heights were also calculated with a restricted (less than 40^{o} N) domain (Fig. 20). Similarly, the smaller domain showed no appreciable influence when compared to the full domain.

In conjuncture with the isobaric maps, the average distance to the nearest front was checked. As noted in the methods section, the CODSUS data were used to roughly estimate the distance to nearest front at 0000, 0300, and 0600 UTC. The distributions of these distances show that the majority of the supercells occurred greater than 200 km from a front (Fig. 21). Merger cases had a more cases that occurred within 200 km primarily due to the nature of these case types; merger cases collided with a squall line that was frontally induced. Only a small minority of cases occurred within 100 km, which

is likely a result of the chaotic nature of frontal placement; the NWS may place a weak warm front at 0300 UTC only which may or not have any impact on the storm system. Since there is no scientific consensus on what distance from fronts may cause supercell modifications, this small minority of cases was included in the study.

4.3 Mesoscale Environments

To assess the mesoscale environment the supercell exists within, a 160km by 160km grid of RAP and RUC soundings was created in the inflow of the supercells; the grid contained 12 by 12 interpolated grid points (see Methods section). The grid point located in the upper left (northwest) of the grid, is the nearest grid point to the supercell. The grid is then 160 km south and 160 km east of that point; this constitutes the inflow of the supercell. Using this grid, various parameters were derived from each sounding: MU CAPE, Effective SRH, MU CIN, and temperature advection; these parameters were selected as being the most likely to illustrate differences among the evolution types according to the expectations outlined at the beginning of this section. Low level temperature advection has been shown to be a contributor to the upscale growth of supercells and thus a possible discriminator between classifications (Peters and Eure 2016). The mean of each of these parameters was calculated at each grid point, binned by respective evolution type. To assess the temporal change through the nocturnal transition, an individual grid was created at SS, SS +3, and SS +5 for each of these parameters with their respective evolution type.

The local variations in MU CAPE within the inflow (Fig. 22) of the supercell immediately highlight the amount of heterogeneity in these environments, as expected from previous studies (e.g., Markowski and Richardson 2007; Parker 2014). The spatial variability in MU CAPE at SS is largest in the merger cases, where decreasing zonal MU CAPE gradient of ~1000 J/kg is present. All four evolution types see a similar gradient in MU CAPE, albeit not as large in magnitude. At SS +3, MU CAPE gradients in merger cases has decreased dramatically, while zonal gradients are still seen in the other three evolution types; maintained and upscale see a much larger gradient relative to dissipation (Fig. 23). A similar pattern is seen by SS +5, but upscale and maintain cases do see a general decrease in MU CAPE domain wide (Fig. 24). The most notable feature of the MU CAPE inflow grid is the large spatial variation, with the highest magnitudes existing near the supercell. This implies that nearest inflow air being ingested into the supercell is the most unstable within the inflow.

Inflow grids of MU CIN further support the notion that the most unstable air is closest to the supercell (Figs. 25-27). Upscale and maintained cases show domain wide low MU CIN (< ~ -50 J/kg) at SS, while dissipation cases are more stable in general; merger cases show low MU CIN near the supercell, but very stable air away from the supercell. By SS +3, MU CIN increases domain wide for all cases except maintained. This trend continues by SS +5, where maintained show no domain wide difference in MU CIN, compared to SS. Upscale cases show the least MU CIN along the northern portion of the domain; the gradient is normal to the mean surface wind vector. This distribution of CIN could allow for a linear band of convection to form if a source of lift is introduced along this MU CIN gradient. The general trend of the MU CIN inflow grids shows that

maintained cases are far and away the least stable, followed by upscale, merger, and dissipation.

Effective SRH inflow grids show a discernible trend between maintained and all other cases (Figs. 28-30). At each time step, effective SRH has a local maximum in the nearest grid points to the maintained supercells. All other cases see a similar pattern, but effective SRH magnitudes are less than half of those seen in the maintained cases. The magnitudes of the near storm maxima in maintained cases is nearly steady from SS to SS +5, with a slight increase at SS +3. A combination of the favorable MU CAPE and MU CIN near the supercell is likely increasing the depth of the effective layer in the near storm grid points. A deeper effective layer allows for more turning and speed shear within the inflow layer; increasing mean southeasterly low level winds are also present, thus increasing SRH.

The temperature advection in the inflow has been shown as a possible cause for upscale growth of supercells (Peters and Kure 2016). The temperature advection in the inflow (Figs. 31-33), show large meso and microscale variations. At SS, there is a meridional gradient in temperature advection, with warm air advection (WAA) to the north and cold to the south, in all four evolution types. WAA rates of ~1° C/hour are seen in the each evolution; cold advection rates are an order of magnitude smaller. By SS +3, the organization of warm advection in dissipation cases is null, while stronger WAA exists across the northern portion of the domain in the other three classifications; magnitudes are a similar to those at SS. By SS +5, WAA in dissipation cases is still unorganized. Upscale and merger cases see strong WAA concentrated from the supercell and to the east. Physically, rising motion can be expected in the regions of strongest low

level warm advection as heights rise. Rising motion will also be a function of CIN; warm advection may not lead to rising motion in the presence of large CIN. From Figs. 25-27, the most favorable MU CIN is located across the northern portion of the inflow domain; this is collocated with the strongest warm advection in the upscale, merger, and maintained cases. Thus, rising motion will be most likely in regions with strong WAA and low MU CIN. This rising motion could explain the development of linear system in upscale and merger cases, especially in the presence of outflow boundary where forced uplift would amplify the vertical motion.

4.4 Storm Scale Characteristics - Storm Lifetimes and Tornadic vs non-Tornadic

The storm lifetime and tornado production are two additional measures for assessing broad differences among evolution categories. The lifetime of a supercell was defined by when it first attained supercell characteristics (e.g., mid-level rotation) to when the supercell underwent its evolution during the nocturnal transition or until SS +5 for maintained cases. Maintained cases were the longest lived supercells as expected with a mean lifetime of 7 hours, followed by merger cases (~5 hours), then dissipation and upscale (both ~4 hours). The average start times of the supercells show that maintained, dissipating, and upscale supercells formed on average at SS -2 (standard deviation of plus or minus one hour); merger cases formed on average at roughly SS -3 with the same standard deviation (Fig. 47). The start times of maintained and dissipation cases are nearly identical, indicating that formation time may not play a role in determining the maintenance through the nocturnal transition. Dissipating supercells have a mean total lifetime of ~4 hours and dissipate, on average, nearly 2 hours after sunset. Merger,

upscale, and dissipation cases all undergo their transition at roughly SS +2; physically, this implies that the forcing mechanism for each of these transitions is linked directly to the nocturnal transition. What this forcing mechanism is will be explored later in this section; some likely candidates include increasing stability and variations in the formation of the LLJ.

Tornado production during the nocturnal transition (SS -1 to SS +5) was assessed as another metric for determining differences among evolution types. Using the criteria outlined in the Methods section, each supercell was analyzed for tornado frequency and then binned into their respective classification. A total of 45 tornadoes out of the 157 supercells occurred; 29% (4) of maintained, 58% (7) of merger, 40% (18) of upscale, and 19% (16) of dissipation cases produced a tornado during the nocturnal transition. As expected, a minority of supercells produced tornadoes overall, given the relative infrequency of nighttime tornadoes (Kis and Straka 2010). Since tornado production is correlated with high low-level shear and SRH (Rasmussen and Blanchard 1998), it is expected that merger, upscale, and maintained supercells (with the highest frequency of tornadoes) might exist in higher regimes of these parameters based on nocturnal tornado production. Even so, due to the stable nature of the nocturnal boundary layer, tornado occurrence may be an unreliable proxy for these parameters (Mead and Thompson 2011).

4.41 Storm Scale Characteristics - Average Sounding and Hodograph

To broadly assess differences in the inflow environment, a mean sounding was created for each evolution category on the 38 mb vertically spaced grid from the

RUC/RAP. The average sounding was computed between the 975 and 100 mb levels; the 975 mb level was chosen as the base since the majority of cases had a surface pressure closest to this value. Profiles containing mean temperature, mean dew point, the MU parcel trace, and effective layer base and top at SS -1 and SS +5 were created for each classification (Fig. 35). Environmental changes associated with the nocturnal transition tend to be focused in the low-levels; thus, unsurprisingly, nocturnal cooling is evident in the lowest levels from SS -1 to SS +5 in each classification. Additionally, dew points increased slightly from SS -1 to SS +5 for maintained cases within the effective layer, while small low-level decreases were seen in the merger, dissipation, and upscale cases. In comparison, temperature and dew point above 800 mb remained essentially unchanged in each category (Fig. 35).

Focusing on the MU parcel trace, the nocturnal transition is associated with decreases in MU CAPE between SS -1 and SS +5 for all supercell categories (Fig. 35). On average, MU CAPE decreased by 1282 J/kg (48%), 1615 J/kg (68%), 1045 J/kg (45%), and 1620 J/kg (55%) for dissipation, merger, maintained, and upscale cases, respectively. Mean MU CIN increased by -76 J/kg (176%), -42 J/kg (98%), -5 J/kg (9%), and -35 J/kg (95%) for dissipation, merger, maintained, and upscale, respectively. Notably, the percent decreases in MUCAPE were fairly similar among evolution types, but the changes in MUCIN were quite different, indicating that MUCIN is potentially a discriminatory parameter.

Another trend evident in the average sounding profiles is a decrease in the depth of the effective layer from SS -1 to SS +5 for merger, dissipation, and upscale cases. Merger cases saw a 596 m (23%) decrease, upscale cases saw a 290 m (14%) decrease,

and dissipation cases saw a 560 m (27%) decrease. Maintained cases conversely only saw a 15 m decrease (< 1%) through SS +5. A consistent effective layer depth indicates that the inflow of the supercell remained relatively unperturbed. Since only maintained cases retained their effective layer depth, this could be a potentially useful distinguishing factor. Physically, this consistency appears to be tied to the subtle increases in dew point during the nocturnal transition; cooling temperatures but increases relative humidity would allow more stable CIN (as noted earlier with regards to average MUCIN in maintained cases) and thus a stable effective layer.

In tandem with the mean thermodynamic profiles, the SS -1 to SS +5 cumulative mean thermodynamic variables were calculated for each supercell. The distributions of mean CAPE values for each parcel (SB, ML, and MU) show subtle differences between classifications, with merger cases tending towards the lowest overall values (Fig. 36). Maintained cases also show the smallest overall range; no cases had a mean CAPE less than 1000 J/kg, contrary to all other evolutions. Cumulative mean CIN distributions are also fairly similar among evolution types, though the dissipation cases tended to have larger values. As with CAPE, maintained do show the smallest range for MU CIN, with no mean values greater than -100 J/kg. Despite these differences, cumulative averages of environmental parameters may be misleading, given the strong evolution that occurs in the environment during the transition.

Thus, the temporal changes of each of these cumulative parameters is assessed by taking the parameter average from SS -1 to SS +1 minus the average from SS +3 to SS +5; these multi-hour bins were used rather than individual hour subtractions to avoid possible hourly data noise. CAPE changes during the transition were generally negative,

as expected (Fig. 37). Dissipation, merger, and upscale cases show similar rates of decrease for SB, ML, and MU CAPE; conversely, maintained cases show large decreases in SB CAPE, but markedly lower rates for ML and MU CAPE. This result implies that the surface and elevated layers are not coupled in maintained cases, as it appears they are in all other classifications. Mean CIN distributions changes show that SB CIN tended to be large for all classifications as a result of surface cooling, particularly for dissipate and upscale cases. In contrast, MU CIN tended to change less over time (Fig. 37). Dissipation cases showed the largest decrease in MU CIN as expected; maintained exhibited the smallest decreases with no overlap of its interquartile range with other cases. Maintained cases saw a median *positive change* in MU CIN implying that some parcels are becoming less stable with time. MU CIN changes being largest in dissipation cases physically implies that all parcels are becoming more difficult to lift; other evolutions show more modest change allowing for sustained lift and convection.

Composite 0-6 km wind profiles were also created for each classification at SS -1, SS +2 and SS +5 (Fig. 51). The hodograph shape in all cases was conducive for right moving supercells, given the strongly veering wind profile at all times. The most significant changes in the shape of the hodograph are evident from SS +2 to SS +5, likely due to the strengthening of the LLJ. In all four storm evolution types, increases in low and mid-level wind speeds are seen from SS -1 to SS +5; the increasing southerly wind speed with time in all cases results in increasing low-level shear and increasing SRH. Overall, the strongest kinematic difference among evolution types is evident by SS +5: maintained cases see large increases in 0-3 km SRH while dissipation and merger cases experienced comparatively smaller increases or decreases. From SS -1 to SS +5, the

average 0-3 km SRH changed by 24%, -7%, 39% and 48% for dissipation, merger, upscale, and maintained cases, respectively. These differences are likely related to LLJs of varying intensity, a feature that will be discussed later. Visual support for merger cases observing a decrease in 0-3 km SRH is seen in the average hodograph where the low level southeasterly winds shift towards southerly by SS +5, decreasing the total area of the hodograph. Synoptic scale changes associated with the front the supercell merges with is likely the cause.

Evidenced in the evolution of the mean hodographs, the LLJ plays a major role in each supercell classification; the main difference is the varying intensity. Using the original inflow proximity sounding, an assessment of the low level jet was performed each hour from SS -1 to SS +5, using the criteria outlined in the Methods section (using a threshold of the meridional component of wind > 12 m/s at or below 1500 m AGL). At each hour for each case, the supercell was flagged as either meeting this threshold or not. Of the total 157 supercells, 132 of those cases were identified as having a LLJ present for at least one hour, consisting of 69 (80%) dissipating supercells, 13 (93%) maintained, 38 (84%) upscaled, and 12 (100%) merger cases. The mean meridional velocity of the each case's LLJ was 16, 19, 17, and 20 m/s for dissipating, maintained, upscaled and mergers, respectively. These results are consistent with the composite hodographs; for example, dissipation cases contained the fewest and weakest LLJs, aligned with the overall weaker SRH during the nocturnal transition (Fig. 38). Based on the mean 925 mb height fields discussed previously, the forcing mechanism behind the LLJs seen in merger and maintained cases is a combination of baroclinicity (indicated from the strong height

gradients) and nocturnal cooling; upscale and dissipation cases LLJs appears to more cooling induced, as the baroclinicity is not as prevalent in these cases.

The mid- and upper-level winds show some noticeable changes with time when comparing supercell classifications. The 6 km wind direction for the upscale and merger cases stayed roughly constant from SS -1 to SS +5; the magnitude of this wind decreased slightly by SS +5 for both classifications (Fig. 38). Dissipation and maintained supercells contained increasingly westerly 6 km winds, veering over time. Similar to upscale and merger cases, dissipation cases experienced a slight weakening in the 6 km wind by SS +5. Such changes in the speed and direction of the mid- and upper-level winds suggests that the synoptic environment is evolving around the supercell. The extent to which this would positively or negatively impact a supercell will be explored further in a subsequent section.

Cumulative mean SS -1 to SS +5 distributions of SRH values show maintained cases exist in the highest SRH environment; merger, upscale, and dissipation cases contain noticeably smaller values of 0-1 km, 0-3 km, and effective layer SRH (Fig. 39). The high SRH environment was expected for maintained supercells, since sustaining an updraft with surface cooling will require strong vertical accelerations to lift parcels, particularly as stability increases. Mean shear distributions show 0-3 km shear as the highest in magnitude across the time frame for each evolution type. As with SRH, the shear values show differences across the different classifications, primarily in the 0-3 km shear for maintained cases.

Changes in cumulative average SRH values over time yield interesting results; 0-1 km SRH shows the largest increase across classification types with effective SRH

generally seeing the smallest increase (Fig. 40). The low level jet's impact on the 0-1 km layer and the surface cooling decreasing the depth of the effective layer are likely the causes of this. Maintained cases are the only evolution type to not follow this pattern entirely; the 0-1 km, 0-3 km, effective SRH show similar rates of increase. The rates of change for the wind shear are highest in the 0-1km level, followed 0-3 km, and then the effective bulk layer. This pattern is consistent across each classification; the LLJ will have the largest impact on the 0-1 km layer, hence the largest increase. Despite finding that the dissipation cases have the weakest mean LLJ, the 0-1 km shear increases seen here are of the same order as all other classifications. Effective bulk shear is seen to decrease with time for all cases, albeit minimally. As with the total mean distributions, the mean changes from SS -1 to SS +5 for each supercell may also over smooth how parameters are changing with time.

4.42 Storm Scale Characteristics - Time Series Analysis

Given the overall thermodynamic and kinematic changes present for each supercell classification, a finer-scale temporal assessment is needed to determine how these classifications arose in response to environmental modifications. Evidence of the nocturnal transition is seen in SS -1 to SS +5 time series of mean surface temperatures (Fig. 41). Each evolution classification experienced decreases in mean temperature throughout the transition: -5.3° C, -4.0° C, -4.2° C, and -3.6° C for dissipation, merger, upscale and maintain cases, respectively. Differences in the temperature advection or cloud debris could be the driving force behind these different rates of change. Dew points remained quasi-steady with SS -1 to SS +5 of less than 1° C in all cases. As a result of the

temperature and dew point time series, relative humidity is increasing with time at the surface.

These temperature and dew point changes are tied into the modification of CAPE over time; as the boundary layer cools, SB, ML, and MU CAPE all generally decrease over time (Figs. 42-44). In comparison to starting values at SS -1, SB CAPE for dissipation and upscale cases contain a statistically significant decrease by sunset (SS 0), while merger and maintain cases see a significant decrease by SS +2 and SS +1, respectively (Fig. 42). A significant change occurring at a later hour implies that the environment is remaining favorable for longer, thus the updraft is likely to remain steady longer. Considering that merger and maintain cases have convection present through SS +5, it is not surprising to see the strongest decrease in SB CAPE with dissipating supercells; upscale cases seeing a similar rate of decrease is somewhat unexpected. However, transition to an MCS or squall line implies that the system is now cold pool driven; cold pool driven systems generally do not rely on high CAPE to drive an updraft that will then lift parcels as with a supercell.

ML CAPE in dissipation and upscale cases also decreased with time, becoming significantly lower (compared to SS -1) by SS +2, two hours later compared to SB CAPE (Fig. 43). As with SB CAPE, merger cases see significant decrease at later times (~SS +4) than for dissipation cases. Maintained cases see a significant decrease in ML CAPE but only by SS +5, with a mean value at SS -1 of 2059 J/kg and SS +5 mean value of 1314 J/kg. Since ML CAPE is not entirely a function of the surface layer, its magnitude is less impacted by surface cooling; maintained cases therefore tend to have more favorable conditions above the surface layer relative to other classifications. As evident in the mean

hodographs (Fig. 38), warm air and moisture advection from the enhanced southerly flow in the merger and maintained cases is likely helping offset the surface cooling and sustained ML CAPE for merger and maintenance cases.

The temporal evolution of MU CAPE (Fig. 44) illustrates that dissipating and upscale cases again see the earliest significant decrease (by SS +2). Merger cases also contain significant changes, but by SS +3; in contrast, as with ML CAPE, the maintained cases do not significantly change until SS +5, indicating comparatively steady elevated instability to maintain convection. Upscale and merger cases both see decreases in ML CAPE of over 1100 J/kg. MU CAPE decreases are more modest for maintained and dissipation events highlighting that MU CAPE likely plays little role in distinguishing evolutions, since dissipaters still retain their MU CAPE.

Environmental changes associated with the nocturnal transition prompted significant decreases in instability (SB, ML, and MU parcels) over time in each evolution category. The key difference was that merger and maintained cases contained a statistically significant decrease at later hours relative to upscale and dissipation, suggesting that their long-lived natures is due at least in part to sustained instability, particularly elevated instability. However, on average, the CAPE values for each supercell classification were large enough to support convection. This finding implies that while decreasing CAPE may be of some importance in predicting the evolutionary response of a supercell, that criteria is not a primary driver in determining the exact classification.

SB CIN values, as expected, notably increase over time; these increases were statistically significant for maintained, upscale and dissipation cases by SS +1, SS -0, and

SS -0, respectively (Fig. 45). Merger cases also experienced large increases in SB CIN, though the changes were not statistically significant; even so, the average SB CIN value in merger cases was greater than -100 J/kg from SS -1 to SS +5. MU CIN also generally increased over time, though these changes did not have as clear of a statistically significant trend; only dissipation cases had significant increases in MU CIN by SS -0, while upscale cases showed significant increases only at SS +5 (Fig. 46). In contrast, the merger cases show discernible (but not significant) increases over time; on average, MUCIN increased from roughly -50 J/kg to approximately -100 J/kg. Notably, maintained cases showed very little changes in MU CIN over time, remaining nearly steady on average around -60 J/kg. It was expected that MU CIN would be generally more favorable for convection in the maintain, upscale, and merger cases versus dissipation cases, since high MU CIN values in dissipation would completely inhibit lifting of parcels into the updraft. Between CAPE and CIN, the time series analysis suggest that MU CIN is most influential in distinguishing among evolution types; for these data only, the distinguishing capability is primarily between maintain, upscale, and merger versus dissipation cases. Physically, greater MU CIN (particularly evident in the dissipation cases) implies that all parcels in a profile have difficulty reaching their LFC; this is consistent with the dissipation category losing all convection during the nocturnal transition. The other storm classifications with lower MU CIN (or at least not statistically greater MU CIN) have comparatively more favorable elevated profiles, given that SB CIN was high for all cases.

The hourly evolution of kinematic parameters is expected to expose notable difference among evolution types, based on the differences depicted earlier in the LLJ

frequency and the mean hodographs. Storm-relative helicity in the 0-3 km and 0-1 km generally increased over time, consistent with the evolution in the mean hodographs and frequency of the LLJ (Fig. 38); however, large differences between classifications were evident (Figs. 47-49). Dissipation, upscale, and maintained cases all saw significant increases in 0-3 km SRH (Fig. 47), occurring at SS +1 in all three classifications, increasing by greater than 70 m^2s^{-2} in each case. In contrast, merger cases never saw a significant change from SS -1 to SS +5, decreasing by 6% (-24 m^2s^{-2}) by SS +5. Similarly, 0-1 km SRH shows increasing values for all evolutions (Fig. 48). Maintained cases increased by twofold, with progressively smaller increases for upscale, dissipation, and merger cases. All of the classification types had sufficient 0-3 km SRH to allow for the single rotating updraft to be maintained through SS +5; even, surprisingly, in the dissipation cases. Notably, the largest increase in both 0-1 km and 0-3 km SRH was associated with the maintained cases, suggesting that a strong, sustained VPPGF was at work to maintain the updraft. Despite increasing in value, dissipation cases still had the smallest time averaged value for both 0-1 km SRH and 0-3 km SRH. These results raise the question of how important kinematic changes are relative to thermodynamic changes due to the similar trends observed between classifications. Additional discussion of this result will be presented in the Discussion section.

Interestingly, in contrast to 0-1 and 0-3 km SRH, effective SRH *decreased* on average over time for dissipation, upscale, and merger cases; only maintained cases illustrated increases in mean effective SRH (Fig. 49). The decreases in the upscale cases was significant between SS +1 and SS +3, while merger cases decreased significantly only at SS +1; the decreasing trend in dissipation cases was not statistically

significant. Between SS -1 and SS +5, mean effective SRH decreased by 6% (11 m^2s^{-2}), 4% (8 m^2s^{-2}) and 43% (76 m^2s^{-2}) for dissipation, upscale and merger cases, respectively, but increased 22% (50 m^2s^{-2}) in maintained cases. While only statistically significant for a single hour (SS +4), the fact that it was the only category of storms to have any kind of upward trend in the parameter indicates its ability to discriminate among evolution classifications.

The temporal evolution of 0-6 km shear was not expected to be statistically significant, since the development of the nocturnal LLJ does not modify the mid- and upper-levels of the atmosphere. However, 0-6 km shear was found to decrease significantly for all supercell classifications except maintained cases (Fig. 50). Even so, the magnitude of the changes were relatively small. A decreasing 0-6 km shear vector implies either a changing synoptic environment or increasing surface wind speeds. Increasing surface winds are not expected based on surface cooling and associated increases in stability (e.g., Fig. 38). Thus, the decreases in 0-6 km shear is connected to changes in the synoptic environment; specifically, the motion of the 500 mb trough (Fig. 17). As the trough propagates eastward, the large height gradient associated with the leading edge of the trough will also move eastward, decreasing the upper level winds. Since this seen in each case other the maintained cases, this could imply that the motion of 500 mb trough is slower in maintained cases, allowing the supercell to remain under the region of largest 500 mb height gradient.

In contrast to 0-6 km shear, the mean values for 0-3 km shear generally changed little over time in each classification; only merger and dissipation cases saw a statistical decrease by SS +4 (Fig. 51). However, significant increases in 0-1 km shear were evident

in each classification type, occurring at SS +1 for merger and maintained cases, SS -0 for dissipation, and SS +2 for upscale cases (Fig. 52). Between SS -1 and SS +5, 0-1 km wind shear increased by 74% (6 m/s), 43% (5 m/s), 63% (6 m/s), 94% (9 m/s), for dissipation, merger, upscale, and maintained cases, respectively. As with SRH, these increases in low-level shear are attributed to the LLJ, present in every supercell evolution type.

Effective layer bulk shear magnitudes were generally flat over time and changes were not statistically significant, with the exception of decreases evident in dissipating cases, significant starting at SS +2 (Fig. 53). However, it is important to note that the overall average decrease from SS -1 to SS +5 was relatively small, approximately 3 m/s. Unlike effective SRH or 0-1 km shear, mean effective shear did not increase with time for any classification. Since effective SRH is calculated by integrating over the depth of the layer, the LLJ's impact is included; the shear magnitude only measures the difference in wind between the top and bottom of the layer (50% of the equilibrium level and the top of the effective layer). Given that the top of mean effective layer at SS +5 for maintained cases was 1755 m AGL and the LLJ maximum occurs at roughly 1 km (Bonner 1968), the effective layer shear magnitude does measure the LLJ directly. Notably, the larger shear depths (0-6 km and effective bulk) showed significantly decreasing dissipating cases, while maintained cases showed no such decrease.

Bulk Richardson Number (BRN; Equation 1) is a common composite parameter utilized in forecasting convective mode. BRN values between 10-50 generally indicate supercellular convection is likely, while environments with BRN > 50 tend to support more linear or multi-cellular convection (Weisman and Klemp 1982). Supercellular BRN

values imply that there is an ideal balance between the velocity and vorticity associated with the updraft and the environmental deep layer shear, while high BRN values imply that there is not enough shear for a given CAPE. The BRN time series (Fig. 54) shows mean values within the expected supercellular range. Percent changes for BRN from SS -1 to SS +5 were: -34% (-10.6), -45% (-7), -0.1% (-0.1), -87% (-16.7), for dissipation, merger, upscale, and maintained, respectively; these decreases indicate the environment becoming more favorable for supercellular convection. Dissipation and upscale cases showed statistically significant decreases at different points in time, occurring at SS +4 and SS +1, respectively. Upscale supercells saw the largest BRN values overall, which was expected as higher BRN values tend to favor linear convection. Merger cases see small BRN values indicating a higher shear, low CAPE environment. Given that many merger cases involved a supercell merging with a synoptically-driven squall line, the mean BRN values is somewhat surprising and could be result of the extremely high shear that is baroclinically generated by the cold front.

Another commonly-used composite parameter in forecasting is the Supercell Composite Parameter (SCP; Equation 2). The effective SRH, effective bulk shear and MU CAPE were the parameters used to calculate the SCP for this study (Thompson et al. 2004); the higher the SCP the more likely supercellular convection will be produced when convection initiates.

$$SCP = (\frac{MUCAPE}{1000 J/kg}) * (\frac{Eff.SRH}{50 m^2 \bar{s}^2}) * (\frac{Eff.Shear}{20 m/s})$$

Equation 2. The Supercell Composite Parameter (SCP) equation using the MU CAPE, Effective SRH, and Effective Shear. Each term is divided by a respective scaling factor.

Thompson et al. (2004) shows the interquartile range of SCP for supercell thunderstorms ranges from 2.0 to 11.0. The time series of average SCP shows that each evolution type contained sufficient, but decreasing, SCP values between SS -1 and SS +5. These decreases are primarily a result of decreasing MU CAPE, as effective SRH and shear remain fairly steady (Fig. 44; Fig. 49; Fig. 53). A 32% (3.3), 60% (8.1), 37% (4), and 8% (1) decrease through SS +5 was observed for dissipation, merger, upscale, maintained cases. Maintained cases retained the highest SCP values, consistent with the nature of their classification; dissipate, merger, and upscaled cases were associated with stronger decreases, their categories of weakening or increasingly linear convection. Since this composite parameter takes into account multiple effective and MU variables, the trends seen in here likely play an important role in evolution. When compared to the other time series variables, the mean SCP values show strong distinguishing capability among evolution types. The SCP is able to quantify respective balances between kinematic parameters and thermodynamic instability; supercells can exist with only moderate MU CAPE if SRH and shear are strong and vice versa. The SCP does not account for CIN in any manner, however, which appears to be discriminatory among storm classifications (e.g., Fig. 46).

Several important themes arise from the time series analysis of numerous environmental parameters. Notably, dissipation cases tend to have the least favorable environments for supercell maintenance, including the largest increase MU CIN, the quickest occurring significant decrease in MU CAPE, no significant increase in effective SRH, and a significant decrease in effective shear. Physically, this implies that

dissipating supercells have weakening updraft velocities due to a combination of increasing MU CIN and decreasing MU CAPE. Decreasing MU CAPE would weaken stretching and velocity of the updraft; with CIN increasing and no increase in SRH to balance this, dynamically lifted parcels are not able to attain their CAPE. The VPPGF from the updraft would also weaken as result and the supercell would quickly dissipate. In contrast, maintained supercell environments tend to experience increasing effective SRH, constant MU CIN and MU CAPE. This implies that the VPPGF should remain steady from continuing updraft stretching and rotation.

4.43 Storm Scale Characteristics - Cumulative Statistical Comparisons between each Evolution

The previous significance tests assessed whether environmental parameter changes were significant over time within a given evolution category; the extent to which the distribution of parameter values are statistically different among classification types still needs to be determined. To achieve this, two statistical tests were performed. The two-way KS test was utilized to compare each parameter's total distribution (i.e., the cumulative SS -1 to SS +5 distribution), while the Student's T-test was utilized to compare the means of the cumulative distributions between each pair of classification types. A total of six comparisons were performed between the four classifications to test for significance at the 95% level; all environmental parameters were tested. Results of these tests are shown in Table 2. The listed parameters were those that were significant at the 95% level for both the KS Test and T test.

Comparing the cumulative distributions of dissipation and upscale cases revealed statistically significant differences among many parameters, both thermodynamic and kinematic, including MU CIN, supercell composite parameter (SCP), effective SRH, and effective bulk shear (Table 2). The mean values for these parameters are more favorable for supercell maintenance in the upscale cases compared to the dissipating cases; BRN suggests upscale cases are closer to a multicellular linear convective environment. The transition to upscale implies an evolution towards cold pool driven lifting (Coniglio et al. 2010), where a balance between environmental shear and cold pool intensity produces the most intense, upright updraft (e.g., Rotunno et al. 1988). The more favorable MU CIN values also allow for ample lifting to the LFC and thus utilizing the elevated CAPE. Dissipation cases see no significant increase in effective shear or effective SRH relative to upscale cases, and along with more unfavorable MU CIN, this implies that dissipation cases fail to reach a balance between inhibition and updraft strength.

TABLE 2. Comparisons between each evolution type for each parameter combining all hours (SS -1 to SS +5) together. Parameters column shows only those that were statistically significant at 95% confidence level for both the KS-test and Student's T-test. Mean cumulative values for each of the parameters are shown in column three, in the same order as the parameters column.

Comparison	**Significant Parameters at 0.05**	**Mean Value Comparison**	
		Dissipate	Upscale
Dissipate to Upscale	MU CIN (J kg^{-1}) 0-1 km SRH (m^2s^{-2}) 0-1 km Shear (m s^{-1}) Effective SRH (m^2s^{-2}) Supercell Composite Parameter Bulk Richardson Number	-85 204 11 173 8.6 35	-56 227 13 228 11 49

Dissipate to Merger		Dissipate	Merger
	SB CAPE (J kg^{-1})	1940	1403
	ML CAPE (J kg^{-1})	1902	1374
	MU CAPE (J kg^{-1})	2555	1941
	0-1 km SRH (m^{2}s^{-2})	204	304
	0-3 km SRH (m^{2}s^{-2})	282	413
	0-1 km Shear (m s^{-1})	11	16
	0-3 km Shear (m s^{-1})	16	18
	Effective SRH (m^{2}s^{-2})	173	252
	Bulk Richardson Number	35	22
Dissipate to Maintain		Dissipate	Maintain
	SB CIN	-187	-150
	0-3 km Shear (m s^{-1})	16	18
	0-3 km SRH (m^{2}s^{-2})	282	404
	0-1 km SRH (m^{2}s^{-2})	204	299
	0-1 km Shear (m s^{-1})	11	14
	Effective Bulk Shear (m s^{-1})	24	27
	Effective SRH (m^{2}s^{-2})	173	318
	Supercell Composite Parameter	8.6	15
	Bulk Richardson Number	35	27
Upscale to Merger		Upscale	Merger
	SB CAPE (J kg^{-1})	1949	1404
	ML CAPE (J kg^{-1})	2004	1375
	MU CAPE (J kg^{-1})	2615	1941
	0-3 km SRH (m^{2}s^{-2})	-54.9	-88.1
	0-1 km SRH (m^{2}s^{-2})	227	304
	0-3 km Shear (ms^{-1})	16	18
	0-1 km Shear (ms^{-1})	13	16
	Bulk Richardson Number	49	22
Upscale to Maintain		Upscale	Maintain
	ML CAPE (J kg^{-1})	2004	1788
	0-3 km Shear (m s^{-1})	16	18
	0-3 km SRH (m^{2}s^{-2})	296	404
	0-1 km SRH (m^{2}s^{-2})	227	299
	0-1 km Shear (m s^{-1})	13	14
	Effective SRH (m^{2}s^{-2})	228	318
	Bulk Richardson Number	49	27
	Supercell Composite Parameter	11.2	15.3
Maintain to Merger		Maintain	Merger
	SB CAPE (J kg^{-1})	1893	1403
	ML CAPE (J kg^{-1})	1788	1375
	MU CAPE (J kg^{-1})	2496	1941
	Effective SRH (m^{2}s^{-2})	318	252
	Bulk Richardson Number	27	22
	Supercell Composite Parameter	15.	10.3

Dissipation versus merger cases show more differences in thermodynamic quantities, with all three CAPE values being significantly different (Table 2). Interestingly, dissipation cases have on average at least 500 J/kg *more* SB, ML and MU CAPE than merger cases. However, merger cases tend to have more favorable kinematic

parameter values; 0-1 km, 0-3 km SRH and 0-1 km shear had mean values that were 100 m^2s^{-2}, 130 m^2s^{-2}, and 5 m/s greater, respectively. The synoptic level forcing associated with the merging front likely contributes to this, as the thermal gradient across the frontal zone yields a LLJ on the warm side of the front.

Dissipation versus maintain cases are primarily distinguishable via their kinematic quantities, as well as SCP and BRN; the only statistically significant thermodynamic quantity was SB CIN, indicating the importance of strong kinematics in sustaining supercells during the nocturnal transition. The maintained cases contained larger mean values for all kinematic parameters, with the largest difference in means for effective SRH; on average, maintained cases had 144 m^2s^{-2} more SRH. Surprisingly, given the differences seen in MU CIN for the time series data (Fig. 46), MU CIN was not statistically significant when comparing the total distributions; this result will be addressed in more detail in the Discussion section.

Since both upscale and merger cases both exhibit linear convection in their environments, the environments were expected to be similar. However, there were significant differences in all CAPE values; on average, more favorable values were present in upscale environments, as SB, ML and MU CAPE were larger by 545 J/kg, 629 J/kg, and 674 J/kg, respectively (Table 2). In contrast, the significant kinematic parameters were slightly more favorable for merger cases. A difference in means of 77 m^2s^{-2} for 0-1 km SRH could be physically significant, and useful when using RUC/RAP data to forecast lifetime. Comparing BRN values reveals lower average BRN in merger cases and higher BRN in upscale cases, indicating that upscale environments tend to be on the multicellular side of the spectrum. While both upscale and merger events have

linear convection, the differences in BRNs suggest two different forcing mechanisms; merger cases being synoptically driven via a high shear frontal environment while upscale cases utilize a balance between shear and CAPE to lift parcels. Upscale cases are therefore outflow driven, where shear and the upward acceleration from CAPE balance along the leading edge to continually lift parcels to the LFC. Merger type linear convection is not in this type of balance; small CAPE implies that the vertical forcing is not entirely thermodynamic and is therefore a combination of the weak CAPE, frontal lift, and other kinematics (i.e. frontal circulation, upper level divergence etc.)

Upscale versus maintain cases show significant differences in ML CAPE; ML CAPE was larger in upscale cases, though the difference of only ~200 J/kg is likely not physically important or discriminatory (Table 2). Kinematically, maintained cases contained statistically larger values for 0-3 km shear and SRH compared to upscale; however, only SRH is likely physically significant, as the mean difference in shear was only 3 m/s but the mean difference in SRH was 107 m^2s^{-2}. BRN mean values were statistically smaller for maintained events; smaller BRN values indicate a greater balance between shear and CAPE, which then suggests that the upscale cases are being influenced by the larger CAPE values and smaller 0-3 km and effective shear.

Maintained versus merger cases show statistical differences in both thermodynamic and kinematic parameters, with maintain cases showing smaller MU CIN and SB CIN but greater SCP values (Table 2). Since merger events require the presence of a linear convective feature, it was expected that maintained events would have would generally more favorable supercellular environments. SB CIN and MU CIN both were significantly smaller for maintained cases and no significant differences in any CAPE

parameters were found. Merger cases did see a slightly larger mean 0-1 km shear value of 14.3 m/s versus 12.0 m/s for maintained; this is not quite large enough to make a physical difference.

4.44 Storm Scale Characteristics - Hourly Statistical Comparisons between each Evolution

Evolution types that have large statistical differences among various parameters were then examined further, comparing distributions at each hour among the categories (Tables 3 and 4), rather than comparing the cumulative SS -1 to SS +5 distributions. Overall, fewer parameters were significantly different, potentially due to the smaller sample size. Table 3 shows hourly parameters that were statistically significant under both the KS and Student's T-test; Table 4 shows the hourly parameters that were only significant under the Student's T-test. These two different tests were run due to the small sample size, which was borderline for the KS test (30 data points are recommended, maintained and merger cases will not meet this requirement at an hourly level) when looking at an hourly comparison. Since dissipation and upscale cases will meet the 30 point criteria at each hour, the combination of T and KS tests will be trusted more so than the T test only. The opposite is true with maintained and merger events (14 and 12 data points per hourly comparison), where the sample is too small and thus the T test will be trusted more. To confirm that the small sample size in these hourly tests was not impacting the results, the distributions from SS -1 to SS +1 and the distributions from SS +3 to SS+5 were compared for the same parameters as the hourly tests; using a three time period increased the sample to be more robust for the KS and Students T-test. The

results of the three hour tests supported the results in Tables 3 and 4; thus the hourly statistical tests yield reasonable results despite the small sample.

TABLE 3. Hourly tests for significance for entire dataset. Listed parameter was significant at 95% confidence level for both the KS test and T test for the corresponding comparison, a dash (-) indicates that no parameters were significant for that hour.

	SS -1	SS	SS +1	SS +2	SS +3	SS +4	SS +5
Dissipate to Upscale	-	-	-	SCP Eff. SRH	SCP Eff. SRH MU CIN	-	-
Dissipate to Maintain	-	-	- Eff. SRH	- 0-3km SRH Eff. SRH SCP	MU CIN 0-1km SRH 0-3km SRH Eff. SRH SCP	MU CIN 0-1km SRH 0-3km SRH Eff. SRH	MU CIN 0-1km SRH 0-3km SRH Eff. SRH
Dissipate to Merger	0-1km Shear 0-3km SRH 0-1km SRH	0-1km Shear 0-3km SRH 0-1km SRH	0-1km Shear 0-3km SRH 0-1km SRH	0-1km Shear 0-3km SRH 0-1km SRH	0-1km Shear 0-1km SRH	0-1km Shear 0-3km SRH	0-1km Shear
Maintain to Upscale	-	-	BRN	-	0-1km SRH	0-1km SRH Eff. SRH SCP	-
Maintain to Merger	-	-	-	-	ML CAPE SCP	ML CAPE Eff. SRH SCP	SCP
Upscale to Merger	SB CAPE 0-1km SRH 0-3km SRH 0-3km Shear BRN	0-1km SRH 0-3km SRH 0-1km Shear BRN	0-1km SRH 0-3km SRH 0-1km Shear BRN	SB CAPE 0-3km SRH 0-1km Shear	MU CAPE SCP	MU CAPE	-

TABLE 4. Hourly tests for significance for entire dataset. Listed parameter was significant at 95% confidence level for only the Student's T test for the corresponding comparison, a dash (-) indicates that no parameters were significant for that hour.

	SS -1	SS	SS +1	SS +2	SS +3	SS +4	SS +5
Dissipate to Upscale	-	-	SCP Eff. SRH	SCP Eff. SRH	SCP Eff. SRH MU CIN	BRN Eff. SRH MU CIN	SB CAPE MU CIN
Dissipate to Maintain	-	-	0-3km SRH Eff. SRH	0-1km SRH 0-3km SRH Eff. SRH SCP	MU CIN 0-1km SRH 0-3km SRH Eff. SRH SCP	MU CIN SB CIN 0-1km SRH 0-3km SRH Eff. SRH SCP	MU CIN 0-1km SRH 0-3km SRH BRN
Dissipate to Merger	0-1km SRH 0-3km SRH Eff. SRH 0-3km Shear 0-1km Shear BRN	0-1km SRH 0-3km SRH 0-1km Shear BRN	MU CAPE 0-1km SRH 0-3km SRH Eff. SRH 0-1km Shear Eff. Shear	SBCAPE 0-1km SRH 0-3km SRH 0-1km Shear	MU CAPE 0-1km Shear	SB CAPE MU CAPE 0-3km SRH 0-1km Shear BRN	SB CAPE MU CAPE 0-3km SRH 0-1km Shear BRN
Maintain to Upscale	-	-	0-3km SRH 0-3km Shear BRN	0-3km SRH 0-3km Shear	0-3km SRH	0-3km SRH SCP	BRN
Maintain to Merger	-	-	-	SFC CAPE	ML CAPE MU CAPE SCP	SB CAPE ML CAPE MU CAPE Eff. SRH SCP	MU CAPE SCP
Upscale to Merger	BRN 0-3km Shear 0-3km SRH MU CAPE SB CAPE	BRN 0-1km Shear 0-3km SRH MU CAPE	BRN 0-1km Shear 0-3km SRH 0-1km SRH MU CAPE	0-1km Shear 0-3km SRH	SCP MU CAPE	SCP BRN MU CAPE	BRN

When comparing dissipated versus upscaled supercells at every hour during the nocturnal transition, effective SRH, SCP, and effective shear are significantly different under the KS and T-test starting at SS +2; unlike with the cumulative comparison, BRN, 0-1 km SRH and 0-1 km shear differences are not significant at the hourly level (Table 3). Effective shear and SRH tends to be larger for upscaled supercells (Figs. 49 and 40), and thus is more conducive for sustaining severe convection. In fact, both effective SRH and effective shear increase from SS -1 through SS +3 in upscaled supercells, indicating that they are able to remain in balance with increasing surface stability; this balance allows for stable updrafts. The SCP showing significance across multiple hours suggests that upscaled supercells exist in more favorable environment for supercells overall, despite the change from supercellular to linear convection. Effective SRH, effective shear, and MU CIN values for dissipation cases are also significantly lower for multiple hours under only the T-test (Table 4). The T-test results note the importance of both effective layer and thermodynamic variables. Of note is the lack of purely kinematic variables (i.e. 0-1 km SRH, etc.), with only thermodynamic and effective layer kinematics showing significant differences. Physically, the higher effective SRH and effective shear seen in the KS and T tests results was expected in upscale due to the more favorable low level thermodynamic setup and lengthened hodograph.

SRH in the 0-1 km, 0-3 km, and effective layers, as well as SCP are all identified as significantly different between dissipation and maintained cases under both statistical tests, especially starting at SS +2 (Tables 3-4); this is consistent with the cumulative tests previously shown (Table 2). This result further enforces the importance of strong kinematics in sustaining rotating convection during the nocturnal transition. Additionally,

MU CIN is also revealed as a statistically significant discriminatory parameter, providing further support for sustained convection. The combination of relatively consistent MUCIN and increasing shear and SRH over time in maintained supercells is in line with the need for strong dynamic lifting to promote supercell maintenance.

Dissipation and merger events see a large number of significantly different parameters on an hourly scale. Pure kinematic variables show the largest differences during the majority of the nocturnal transition in 0-1 km shear and 0-1 km and 0-3 km SRH (Table 3). Using only the T-test more differences arise; dissipation cases surprisingly show significantly *larger* SB and MU CAPE from SS +1 to SS +5 (Table 4). These results suggest that merger cases exist in a high shear/low CAPE environment relative to dissipation cases; high low-level shear and SRH from synoptic level forcing is able to amend for the lack of strong instability.

Only a few significant differences are present when comparing maintained and upscaled events when both statistical tests were applied, suggesting that the environments for these evolution types are somewhat similar (Table 3). Given that BRN should increase as convection evolves into a multicellular form, it was expected that BRN would be larger and significantly different for upscale cases; however, BRN only showed a difference at SS +1. Using only the T-test, 0-3 km SRH is significantly larger in merger cases as time progresses (Table 4). Further analysis of maintained versus upscale supercells will be discussed in a subsequent section.

Maintained versus merger events show differences in SCP, ML CAPE and effective SRH (Tables 3-4); this was expected based on the results of the cumulative comparisons, since maintained supercells would likely retain a higher SCP. The

difference in SCP at later hours arises from small differences between ML CAPE and effective SRH; when included in the SCP equation, these differences become more apparent. Under only the T-test, more differences are seen but only in thermodynamics parameters (Table 4) with maintained cases having larger CAPE values. In general, these two environments appear fairly similar from a parameter perspective, with maintained cases having a more unstable profile; the larger SCP and effective layer SRH (both functions of CAPE) in maintained cases support this as well.

A variety of parameters show hourly differences in all tests between upscale and merger cases; this was surprising given the similar nature of their convection (e.g., Fig. 10). BRN and MU CAPE is significantly lower at multiple hours for merger cases; however, shear and SRH in the 0-3 km are larger across multiple hours. The nature of the synoptically forced squall lines in the merger cases appears in these comparisons with low CAPE and high shear still providing a conducive environment for strong sustained convection; upscale cases show the more typical moderate/high CAPE and moderate/high shear environments associated with MCSs.

4.45 Storm Scale Characteristics - Parameter Correlation to Lifetime

From a forecasting perspective, estimation of the how long the supercell will persist into the nocturnal transition would be beneficial. To accomplish this, supercells were binned based on their hour of dissipation, merger or upscale growth; maintained cases were assumed to ‘dissipate’ at SS +5. The bins used ran from SS to SS +5; each supercell’s SS -1 to SS +5 mean was then included in the bin for when that supercell

evolved. Effective SRH, MU CIN, 0-1 km shear, and SCP were the parameters chosen for this test as these parameters showed the strongest significance when comparing maintained to dissipation cases. The time of dissipation was found to qualitatively trend well with effective SRH, MU CIN, and SCP; 0-1 km shear showed a weakly discernible trend (Fig. 56). High shear merger cases, which tended to merge between SS +2 and SS +4, increased the frequency of extreme 0-1 km values giving reason for the lack of trend in those hours. Despite this, these results further support the previous statistical tests that effective SRH, MU CIN, and SCP provide strong distinguishing power for maintained and dissipation cases; they will also act as a forecasting tool with high effective SRH and SCP implying longer lifetime for supercellular convection during the nocturnal transition.

4.5 Development of Supercell Composite Parameter with CIN and LLJ shear

Due to the unique nature of the nocturnal transition, parameters that are useful in the daytime may lose skill as the nocturnal boundary layer developments; the introduction of strong CIN may negate the use of certain parameters. To account for this and the significant differences observed in the time series and statistical tests, two new parameters are proposed: the Supercell Composite Parameter with CIN and the Low Level Jet shear. The CSCP (CIN Supercell Composite Parameter) uses the same formula (equation 2) as the SCP but includes a scaling term based on the amount of MU CIN present (equation 3). The purpose of the scaling term is to lower the SCP when MU CIN is present; a SCP of 18 with -100 J/kg of MU CIN will result in a SCP of 4. A similar CIN based scaling term is seen in the Significant Tornado Parameter (Thompson et al.

2004). For the CSCP, any MU CIN with value between zero and -25 J/kg, the MU CIN is set to -25 J/kg; the CIN term is thus equal to one. This accounts for the limited impact that small amounts of CIN will have.

$$CSCP = \frac{MUCAPE}{1000J/kg} * \frac{Eff.SRH}{50m^2s^2} * \frac{EB.Shear}{20m/s} * \frac{-25J/kg}{MUCIN}$$

Equation 3. CIN Supercell Composite Parameter, same as equation 2 but includes CIN scaling term.

The utility of this parameter is seen by further separating maintained supercells from the other evolution types, relative to the SCP alone (Fig. 57). Comparing the SCP to the CSCP, a general decrease in magnitude is seen in each evolution type. Maintain cases see a significantly different distribution from all other cases (p value < 0.05); unlike in the SCP, maintained and dissipation cases are different enough that the interquartile ranges do not overlap in the CSCP. This parameter suggests that dissipation predominantly occur with CSCPs of less than 5. Given the statistical differences seen in the CSCP, it may provide use in a forecasting sense. Each term in the CSCP equation was then assessed to quantify the relative contribution to the total CSCP value (Fig. 58). The magnitude of each term's contribution can be measured by how much the median values shift between each evolution type. Clearly, MU CAPE and Effective Bulk Shear play little role in the differences seen in CSCP (Fig. 58); this was expected since these parameters showed no significance in the previous tests. Effective SRH and MU CIN show the largest differences with the clear trend in favorability from maintained to dissipation cases. However, a much more rigorous assessment of the CSCP's utility will need to be undergone first, which is beyond the scope of this study.

The second new parameter used in this study is the low level jet shear. The LLJ shear is calculated from difference in meridional wind speed at the level of maximum wind below 2 km (i.e. the low level jet) and the surface meridional wind speed. 0-1 km shear does not universally measure the LLJ since the LLJ can vary in height AGL. The LLJ shear therefore always measures the maximum shear associated with the LLJ in the lowest levels. A comparison between the 0-1 km shear and LLJ shear shows subtle but significant differences (Fig. 59). Maintained versus dissipation distribution comparisons show a T test p value of 3.08×10^{-9} for LLJ shear compared to 2.2×10^{-6} for 0-1km shear. The range of both merger and maintain cases show that only LLJ shear of 20 knots or more yields these evolutions. While statistical differences are seen, these are insignificantly small and use of this parameter is likely unnecessary from a statistical perspective. However, given the more robust physical nature of the parameter (dynamically measuring the LLJ rather than a static layer), continuation of its use seems reasonable. As with CSCP, a more thorough assessment is necessary.

CHAPTER 5: DISCUSSION

Statistical comparisons among the four different evolution categories yielded a fairly unique set of distinguishing factors; the set of for each comparison has a physical implication and thus forecasting use. Dissipation versus maintained cases by far are the most statistically distinct storm classifications. MU CIN and effective SRH are the primary distinguishers with the lowest and physically significant p values, along with composite parameters SCP and CSCP (Table 3; Fig. 57). With lower MU CIN in maintained cases, parcels are readily lifted, thus utilizing MU CAPE to increase the velocity of updraft, allowing for further stretching and lifting. Due to the favorable MU CIN, the effective layer is able to remain steady with time while dissipating supercells saw a 34% decrease in effective layer depth. The low MU CIN maintains the inflow layer and thus allows for the ingestion of increasing SRH in the effective layer during the transition. The updraft is then able to maintain both vertical velocity and vertical vorticity. The VPPGF from the stable updraft then can induce further vertical accelerations, sustaining the supercell. Dissipation cases, due to high MU CIN and lower effective SRH are not able to able to overcome the stabilization and thus dissipate.

Theoretically and based on the analyses conducted, a balance between effective SRH, MU CAPE and MU CIN is necessary for supercells to persist deep into nocturnal transition; at least one of the three above parameters was found to be unfavorable in dissipating events. Effective SRH quantifies potential updraft rotation and dynamic lift, MU CAPE represents the stretching term of the vorticity equation, and MU CIN acts as a

cap on lift. With increasingly unfavorable SB and ML CIN during the nocturnal transition, a supercell will need enhanced effective SRH and MU CAPE in order to maintain the updraft by dynamically lifting parcels. Since MU CAPE was not found to be significantly different between maintained and dissipating cases, effective SRH's impact on lifting is balancing the enhanced MU CIN; while the stretching from MU CAPE is present, it is not the distinguishing factor. In dissipating cases, the increasingly unfavorable MU CIN is not balanced by an increase in effective SRH, resulting in weakened lifting and no updraft maintenance. Increasing MU CIN and relatively low effective SRH, contribute in some manner to updraft weakening in dissipation cases. Exactly which set of values for these parameters are necessary to create this balance is not clear. For example, could high MU CAPE and moderate effective SRH compensate for unfavorable MU CIN development? The CSCP appears to be fairly universal in describing the general ratio between these different parameters and thus is the best distinguisher. The specifics of how this balance develops is a point for future numerical modeling research that could assess the individual and cumulative impact of these changes.

With dissipation and upscale cases, effective SRH and MU CIN were found to be both physically and statistically different, with upscale being more favorable for supercells in both parameters. Since no static layer SRH parameters were significant, larger effective SRH in upscale cases implies a deeper effective layer with more favorable thermodynamic parameters (i.e., lower CIN and higher CAPE; Thompson et al. 2007) for maintenance. The effective layer in upscale cases saw a 20% decrease in height AGL versus a 34% in height for dissipation cases from SS -1 to SS +5. This decrease is

evident by the significant differences in MU CIN, where upscale cases show notably weaker stability (Table 4) in both the proximity soundings and inflow grids; MU CIN is more favorable across the northern portion of the of the grid at all times (Figs. 25-27). Enhanced MU CIN (as observed in the dissipation cases) tends to limit the effective layer depth, thus inhibiting the amount of streamwise vorticity (i.e. effective SRH) that the storm can ingest. This results in weakening updraft velocities as more unstable parcels are not ingested, a weaker VPPGF, and eventual dissipation of the supercell.

The retention of strong convection in upscale cases is likely related to favorable MU CIN during the nocturnal transition. However, upscale convective growth can be caused by external forcing, such as convergence of boundaries and the low level jet or gravity wave development in the stable boundary layer; in a favorable low MU CIN environment, these external forcings could be the trigger of upscale growth. The external forcing could prevent the enhanced effective SRH from sustaining isolated supercellular convection. These external features are not identifiable from a single proximity sounding, as assessed in this study. However, the distribution of CIN in the inflow grids suggests that such external forcing could be a factor (Figs. 27 and 33). The most favorable area of MU CIN is located across the northern portion of the inflow, collocated with the region of maximum temperature advection. Since the MU CIN in this region is not inhibiting vertical motion, lift from the low level warm air advection would provide forcing across a broad region, thus triggering linear convection. Isentropic lift from the warm advection would only be amplified given the presence of an outflow boundary. In dissipating cases, uplift is inhibited by stronger MU CIN and weaker warm advection.

Comparisons between merging and dissipating supercells show an interesting group of significant parameters; thermodynamic parameters tended to be higher in dissipation cases, while kinematic parameters were more favorable for merger cases, particularly the static-layer parameters (0-1 km shear and 0-3 km SRH; Table 3). Notably, both classification types exhibited large MU CIN, but only dissipation cases ceased convection; this further implies the importance and discriminatory power of shear and SRH, as they seem to be large enough in merger cases to overcome the unfavorable MU CIN. Interestingly, unlike dissipation and maintained cases, the SCP and CSCP do not show any skill in distinguishing merging and dissipating supercells; this is likely tied to the large MU CIN in both cases types, since SCP and CSCP include CIN (either directly, or indirectly via an effective layer parameter; cf. Equations 2 and 3). In merger events, a squall line envelops the supercell of interest prior to SS +5, so it is impossible to know if these supercells would have sustained themselves or dissipated had they not merged. Even so, as in the upscale events, focusing on the presence of external forcing (such as a frontal boundary, initiating an associated squall line) would be useful for forecasting. This, in combination with large SRH and shear downstream of the front suggests an environment supportive of a merger. Dissipation cases could exist in a similar synoptic environment but would likely see much weaker SRH and thus not be able maintain the updraft when MU CIN increases.

Merger versus upscale supercells show many of the same characteristic as merger compared to dissipation; merger cases tend to be observed in a higher shear, lower CAPE environment relative to upscale events (Table 4). Bulk Richardson Number provided the most hourly comparison differences, with mean upscale BRNs approaching 50; merger

cases averaged below 25. Since both cases exhibit quasi-linear convection, the BRN were expected to both be on the high end for supercells (~50). As previously discussed, merger cases do not see high BRN values due to the 'over sheared' nature of the merger cases due to the associated baroclinic forcing; the CAPE in merger cases tends to be too weak relative to low level shear. Upscale cases exhibit large BRNs as expected, since shear and CAPE balance to create an outflow driven system (i.e., Rotunno et al. 1988). Thus, forecasters are more likely to observe upscale events in environments with weak synoptic forcing, steady moderate to high CAPE, shear, SRH, and BRN through the nocturnal transition.

Maintained and merger cases both exist in strongly sheared environments; maintained cases exhibit higher CAPE and lower CIN, especially at later hours (Tables 2 and 4). For this reason, the SCP and CSCP distinguished the best between these cases. Since both the SCP and CSCP show significant differences, MU CIN is not the only difference in these environments; larger CAPE and SRH in maintained cases appear to be as influential as increasing MU CIN. As with previous merger comparisons, the presence of a synoptically forced squall line and the storm motion vector may be more important. If a squall line is present and the storm motion vector is more northerly, a merger is probably more likely. The amount of CAPE and CIN could also play a role in storm motion; with higher CAPE and less CIN, stronger updraft velocities can be inferred. Large updraft velocities will cause the downshear pressure perturbation to increase, resulting in a storm propagation that is more easterly as well. So even if a merging and maintained supercell as identical storm motion vectors, the maintained case would still propagate more easterly due to the higher CAPE and thus updraft velocities. In summary,

merger cases will be more thermodynamically stable, tend to move more northerly, and have a nearby synoptically forced squall line; maintained have favorable CAPE and CIN, strong SRH and may or may not have squall line present.

Lastly, upscale and maintained cases show differences across several parameters; BRN and effective SRH showed large differences as time progressed (Table 4). Large BRN, indicating linear and outflow-driven convection, was thus expected to be larger in supercells that grew upscale. Higher effective SRH in maintained cases indicates greater streamwise vorticity ingestion and thus greater propensity for a rotating updraft. The decreasing effective SRH in upscale cases is a result of enhanced CIN in these cases, creating a more shallow effective layer. With less streamwise vorticity being ingested into the upscale cases, the transition from supercellular to linear convection is not surprising. This study finds that upscale growth tends to occur in moderate to high CAPE environments with moderate SRH, but only small increases in SRH fail to sustain an isolated supercell. Since the environment switches from supercellular to linear convection, new lifting mechanisms must be present; these lifting mechanisms are not 'available' through a proximity sounding.

As noted previously, upscale growth can be caused by several features not available through a proximity sounding. For example, the orientation of the deep layer shear with respect to the cold pools and triggering mechanisms. Deep layer shear perpendicular with the initiating boundary of the supercell tends to keep cold pools discrete, in the case of multi-cell convection. A more parallel component of the deep layer shear vector can cause merging of these cold pools and therefore force a more linear system along the gust front (Bluestein and Weisman 2000), thus promoting upscale

growth of supercells. The inflow grids shows favorable MU CIN and low level winds to potentially force convection linearly; the effective SRH in upscale events is also seen to be orientated across the northern portion of the inflow grid rather than concentrated near the supercell, as in the maintained cases (Fig. 30). Warm air advection and MU CIN are also collocated linearly across the northern portion of the inflow, suggesting an area of uplift (Figs. 27 and 33); when in conjunction with some sort of boundary or outflow, isentropic lift could cause a band of parcels to reach their LFCs and help initiate an MCS.

To generalize these results for forecasting use, phase space diagrams of CSCP and the LLJ shear were developed (Figs. 60-62). These two parameters were chosen for the phase space since they encapsulate all major categories of parameters in this study: CAPE, CIN, SRH, deep layer shear, and low level shear. Ideally, this phase diagram would show four separate boxes, indicating that each evolution type exists within its own regime of CSCP and LLJ shear. The SS -1 to SS +5 plots (Fig. 60) show little to no overlap for maintained cases, compared to merger or dissipate; upscale cases overlaps all three storm classifications. From SS-1 to SS+2, the differences in median and distribution between each class is small; all four parameters overlap at ~25 knots LLJ shear and ~ 3 CSCP. However, from SS+3 to SS+5, differences between evolution types become much more apparent. This change in overlap with time is likely due to the increase effective SRH in maintained cases and increasing MU CIN for merger, upscale and dissipation cases; the influence of SRH and CIN were seen in the individual contribution plots (Fig. 58). The forecasting use of this plot therefore becomes more skillful at later hours, when the environmental differences are more significant. For example, using a RAP forecast for SS + 4 and SS +5 combined with this phase-space

diagram, a forecaster could predict, based on high CSCP (~7) and large LLJ shear (~ 35), that maintained supercells are likely. Conversely, low CSCP and LLJ shear would suggest a forecaster can lower the risks associated with nocturnal supercells. However, if the RAP forecast predicts values that fall within overlaid areas on the phase space diagram, further assessment of factors beyond a proximity sounding is necessary (e.g. synoptic setup, frontal positions, outflow boundaries etc.).

The overlap between some evolution types highlights the importance of these larger scale features, which need to be assessed separately. The key findings of this study allow for general assumptions to be made about the lifetime of a supercell in the nocturnal transition; the differences found between maintained and dissipated supercells are the most robust and exhibit the highest confidence.

CHAPTER 6: CONCLUSIONS

To assess how the environmental changes associated with the nocturnal transition impact supercell thunderstorm evolution and lifetime, inflow proximity soundings from the RUC/RAP were collected at sunset relative hours -1 to +5 for 157 Great Plains supercells occurring over a span of 11 years. Each supercell was classified based on its evolution from SS -1 to SS +5 as either: dissipating, merging with another convective feature, growing upscale or maintained (Fig. 10). A plethora of environmental parameters were calculated from the proximity soundings and then statistical differences between the classifications were assessed. Along with the proximity soundings, various synoptic, mesoscale, and storm scale characteristics were assessed.

Mean upper level flow patterns for each evolution type reveal that merger and maintain cases are associated with more amplified 300 mb, 500 mb and 925 mb troughs over the western Plains; upscale and dissipation cases show lower amplitude troughs and weaker height gradients each level (Figs. 16 and 18). Evidence of the LLJ jet is also seen in the 925 mb mean heights, with merger and maintained cases showing the largest height gradients.

The proximity soundings showed the expected increases in SB CIN and decreases in SB CAPE with time for all four evolution types. All evolutions also saw increases in low level shear and SRH with time from the development of the low level jet; however, maintained and merger cases saw the highest magnitude kinematic parameters (Fig 39). MU and effective layer parameters began to elucidate more notable differences, where

proximity soundings show that maintained cases are the most favorable for supercell development and thus maintenance. Only maintained cases exhibited increases in effective SRH throughout the nocturnal transition. MU CIN also remained steady and favorable for maintained cases. The exact opposite was found for dissipation cases, where effective SRH decreased and MU CIN increased significantly. These results were the most physically and statistically significant among all parameters for the comparisons. This suggests a balance between increasing stability and updraft rotation (SRH serves as a proxy) is necessary to maintain the VPPGF; stronger updraft rotation will allow dynamic lifting of parcels despite low level stability in maintained cases.

The largest difference across the various comparisons were in effective SRH, MU CIN, and low level shear. To account for these, two composite parameters were developed: a MU CIN scaled Supercell Composite Parameter (CSCP) and the Low Level Jet Shear. The combination of these parameters showed significant skill in differentiated the various cases (Figs. 57 and 59) and allow for forecasting the evolution type and lifetime of nocturnal supercells; phase space diagrams using these two parameters show this forecasting skill (Figs. 60-62). From a forecasting perspective, supercells associated with deep short or long wave troughs, stable MU CIN values, and increasing effective SRH are those most likely to persist well into the nighttime hours even with strong SB CIN; dissipating supercells see the opposite with no increase in effective SRH and high MU CIN. Importantly, static layer SRH (e.g. 0-1 km, 0-3 km SRH) and SB parameters show less impact on evolution than effective layer and MU CIN.

To verify these findings, expanding the dataset to include more cases would provide more robust statistical conclusions. Numerical modeling using base state

substitution would be the ideal method for as an assessment of each individual environmental change's impact (i.e. varying the MU CIN, MU CAPE, and effective SRH with time). To remove possible small scale boundary interactions or other external phenomenon, microscale case studies of individual supercells could also help verify these results.

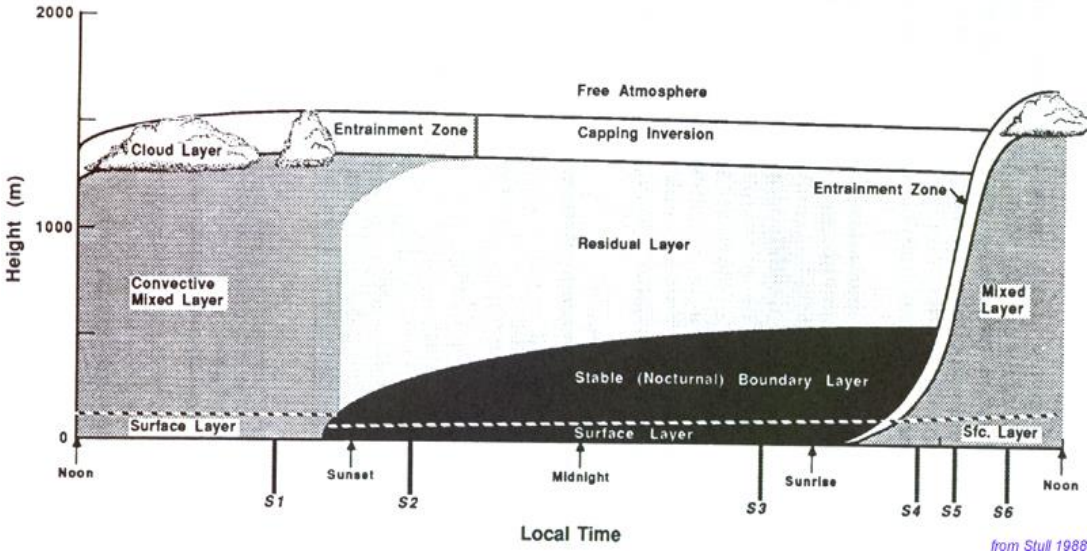

FIGURE 1: Diurnal variation in the boundary layer structure. Figure from Stull (1988).

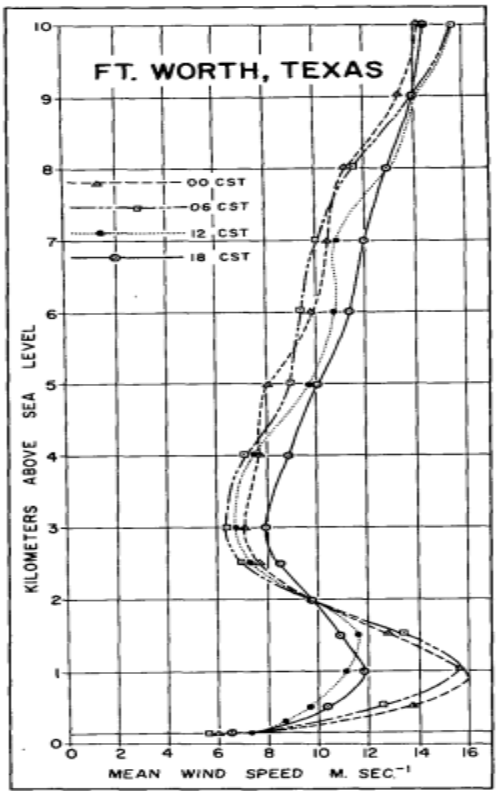

FIGURE 2: Vertical profile of mean wind over Fort Worth, Texas showing the presence of the low-level jet at 1 km AGL and corresponding minimum at ~3 km AGL. Figure from Bonner (1968).

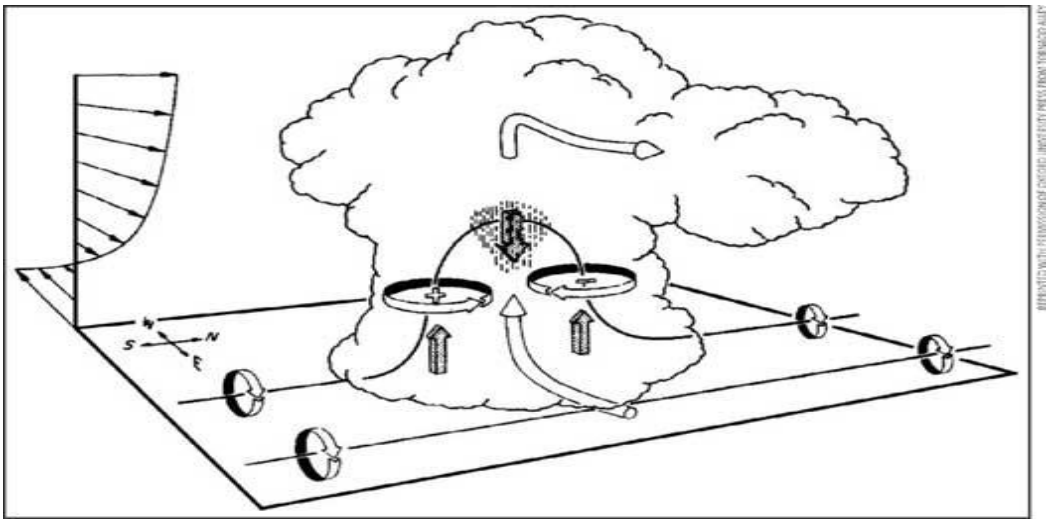

FIGURE 3: Updraft tilting of horizontal unidirectional environmental shear into vertical vorticity. CAPE in the updraft stretches the vertical vorticity as parcels increase velocity. Figure from Bluestein (1999).

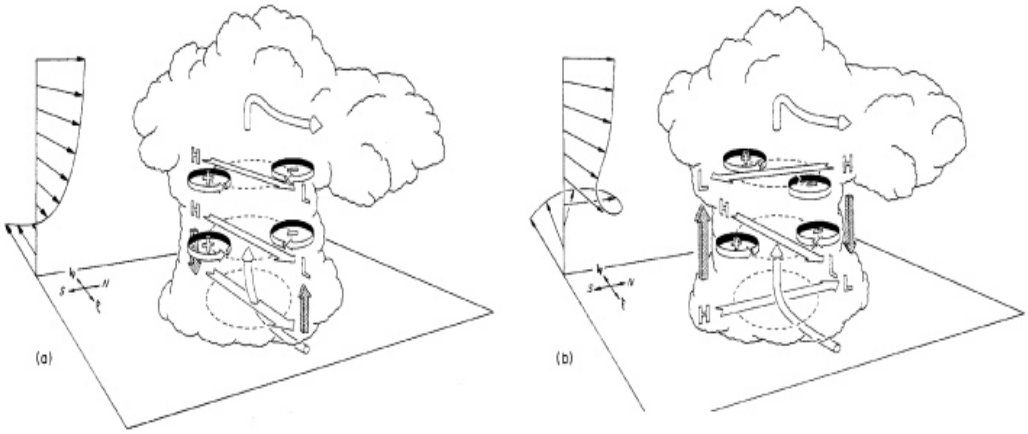

FIGURE 4: Upshear and downshear pressure perturbations associated with a) a unidirectional wind profile and b) a veering wind profile. Figure from Markowski and Richardson (2010).

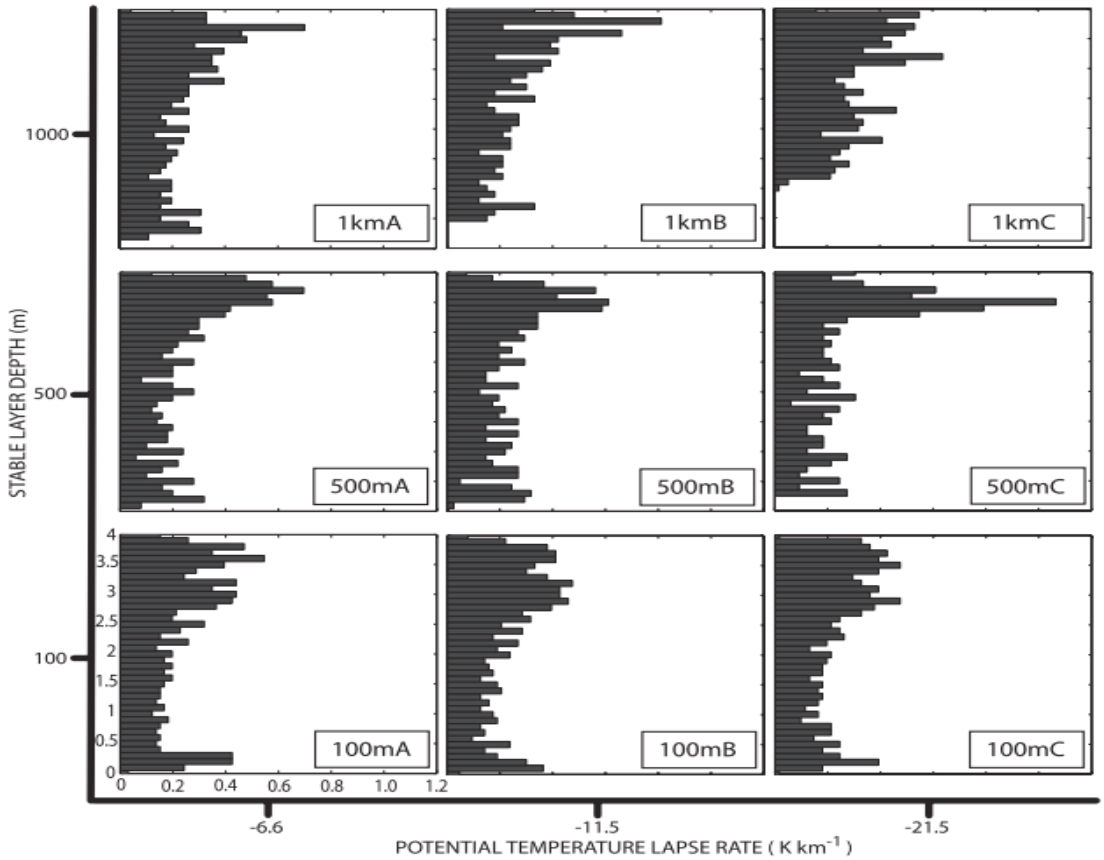

FIGURE 5: From Nowotarski et al. (2011), a matrix of simulation setups with the most stable low level profile in the upper right and least stable in the lower left. Histograms show the normalized number of parcels that originated from that level and were ingested into the updraft.

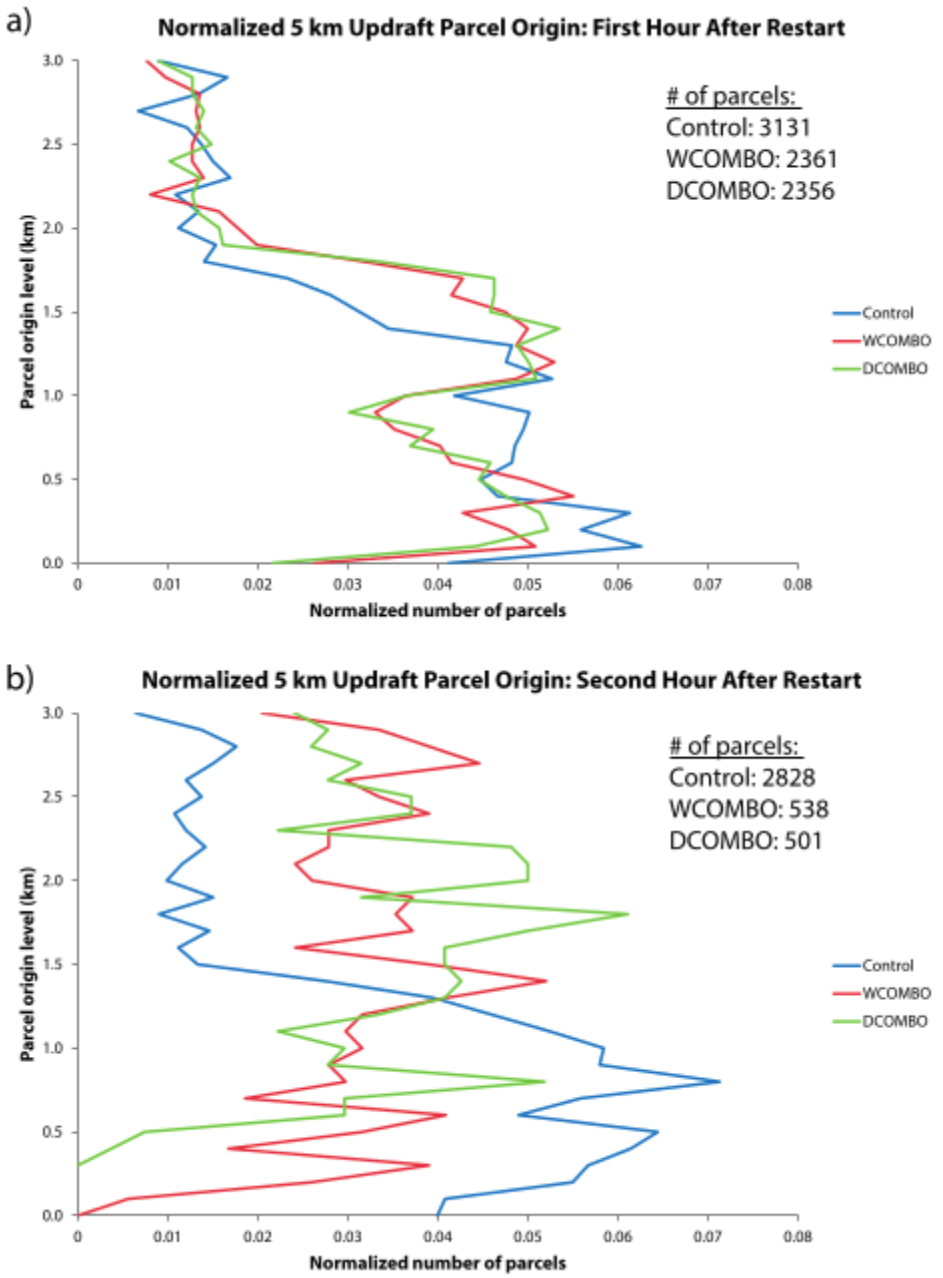

FIGURE 6: From Davenport and Parker (2015b). Parcel origin levels for three different base state substitution (BSS) simulations, starting from the same mature supercell homogenous environment. Control was initiated and let run, WCOMBO used BSS to mimic the change from the mature environment to when the original supercell was weakening. DCOMBO used BSS to mimic the environment changes from the mature environment to when the supercell dissipated. Note that parcels are still ingested from the surface one hour after restart for all cases, while by hour two the little to no parcels originate from the surface for the WCOMBO or DCOMBO supercells.

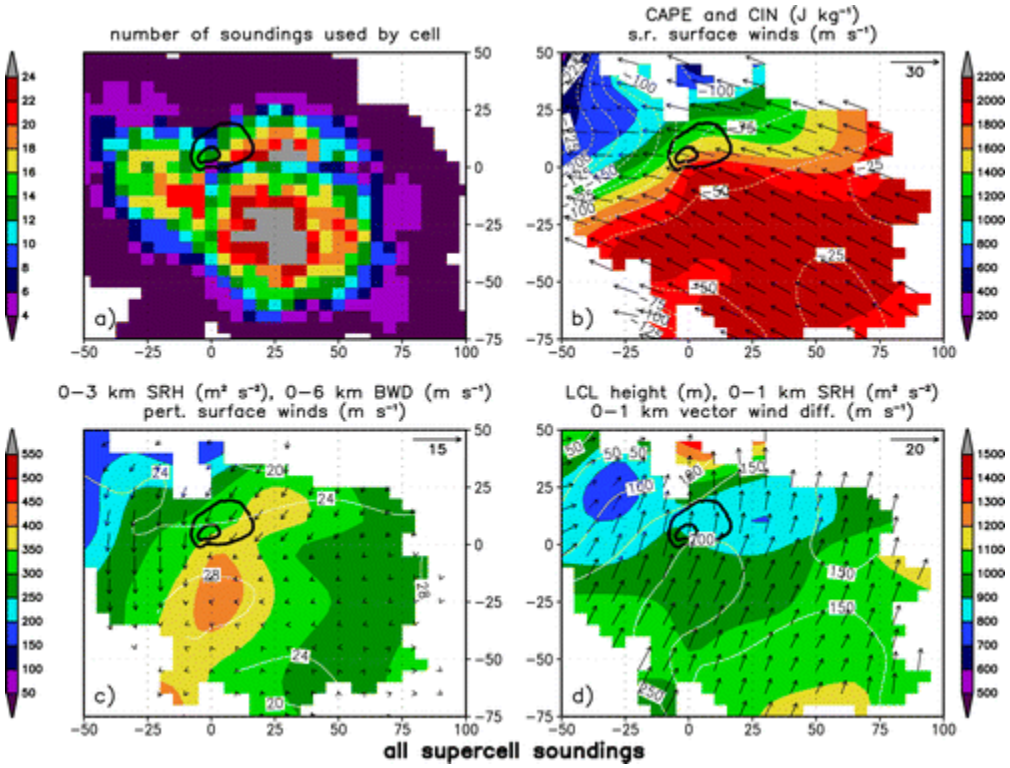

FIGURE 7: Environmental heterogeneity in proximity to supercells. From Parker (2014)

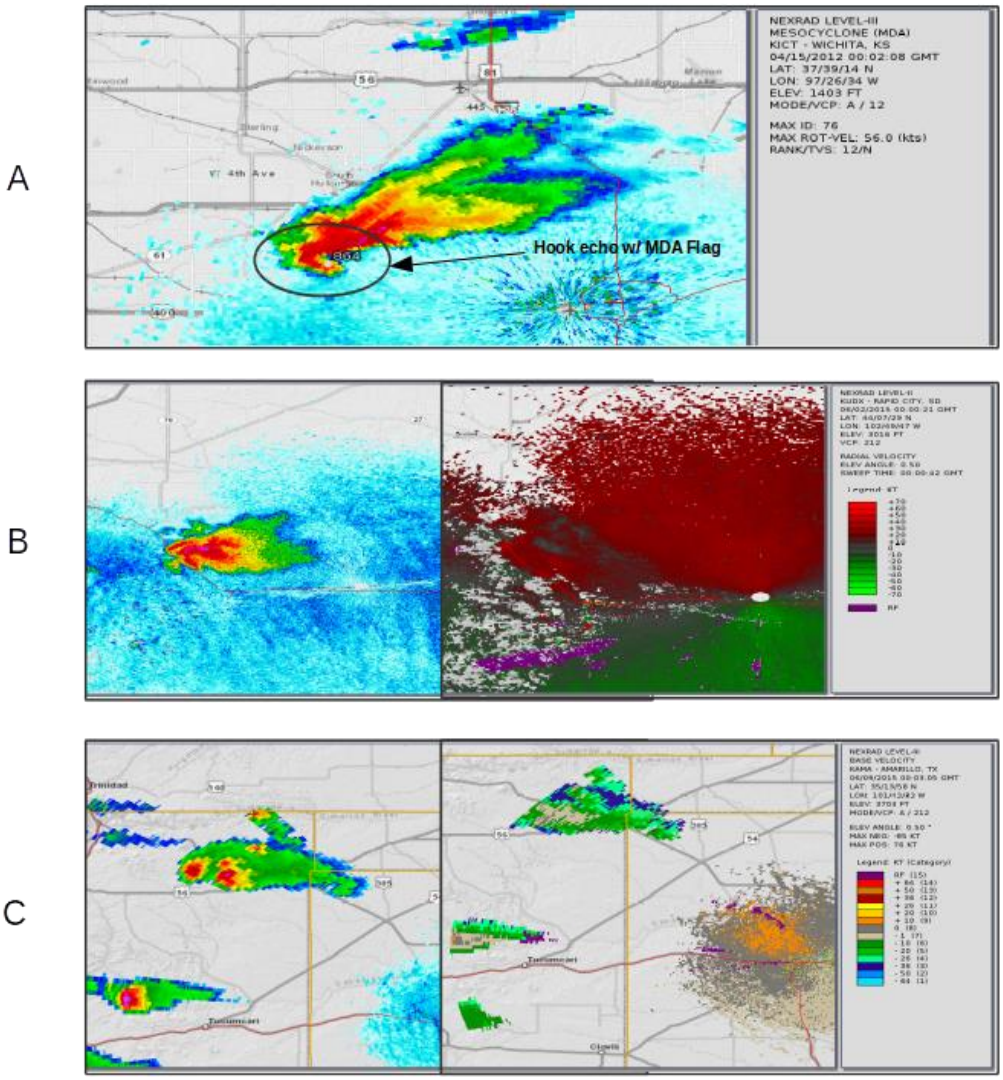

FIGURE 8: Example of the supercell confirmation process. Panel a) illustrates a well-defined isolated supercell with a weak echo region, and MDA flag where expected. Panel b) shows an isolated thunderstorm without the MDA flag, but is confirmed as a supercell due to the identifiable hook echo and rotation. Panel c) illustrates a discarded case where the potential cell was too far from the radar for reflectivity or velocity data to be useful.

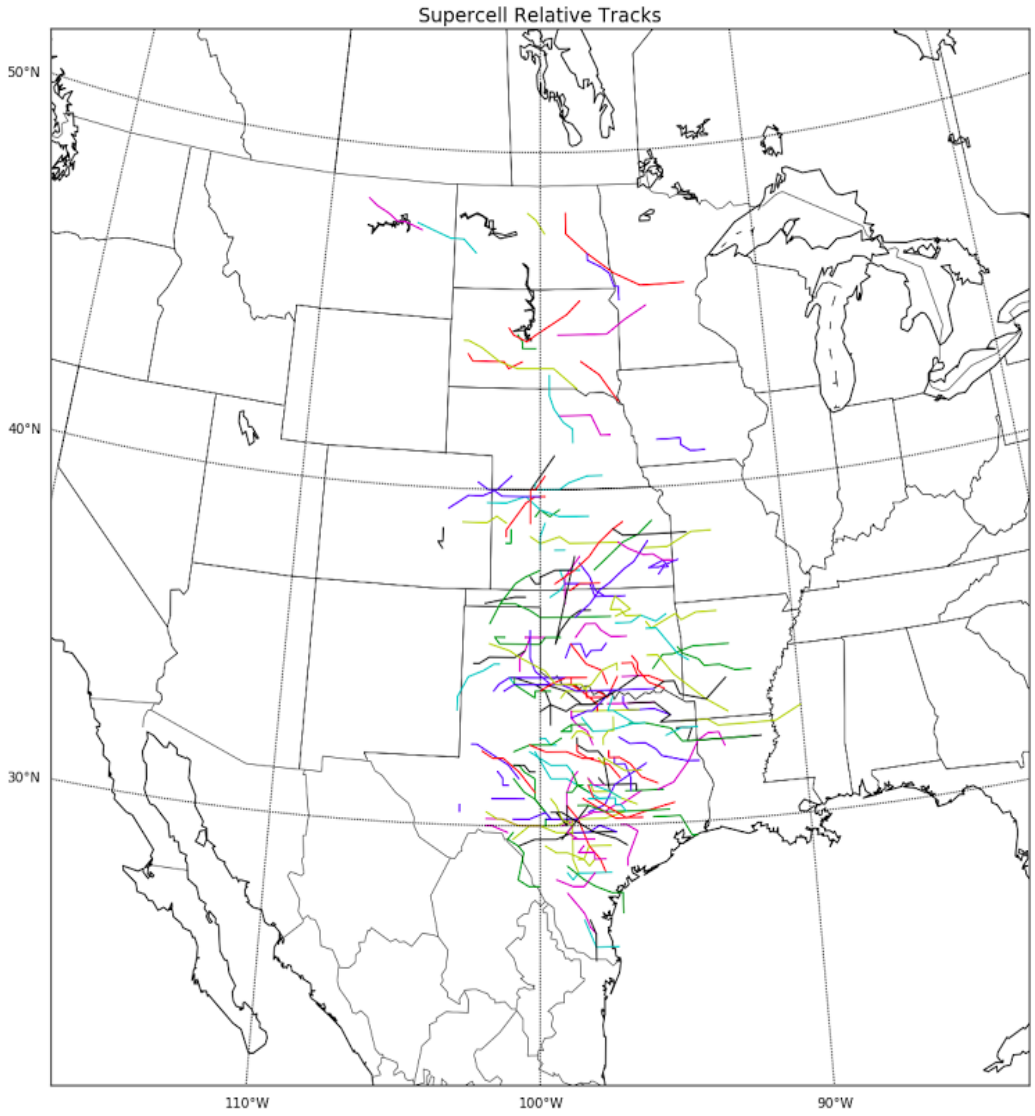

FIGURE 9: Locations of where each RUC/RAP model sounding was drawn from in the inflow for each confirmed supercell used in this study.

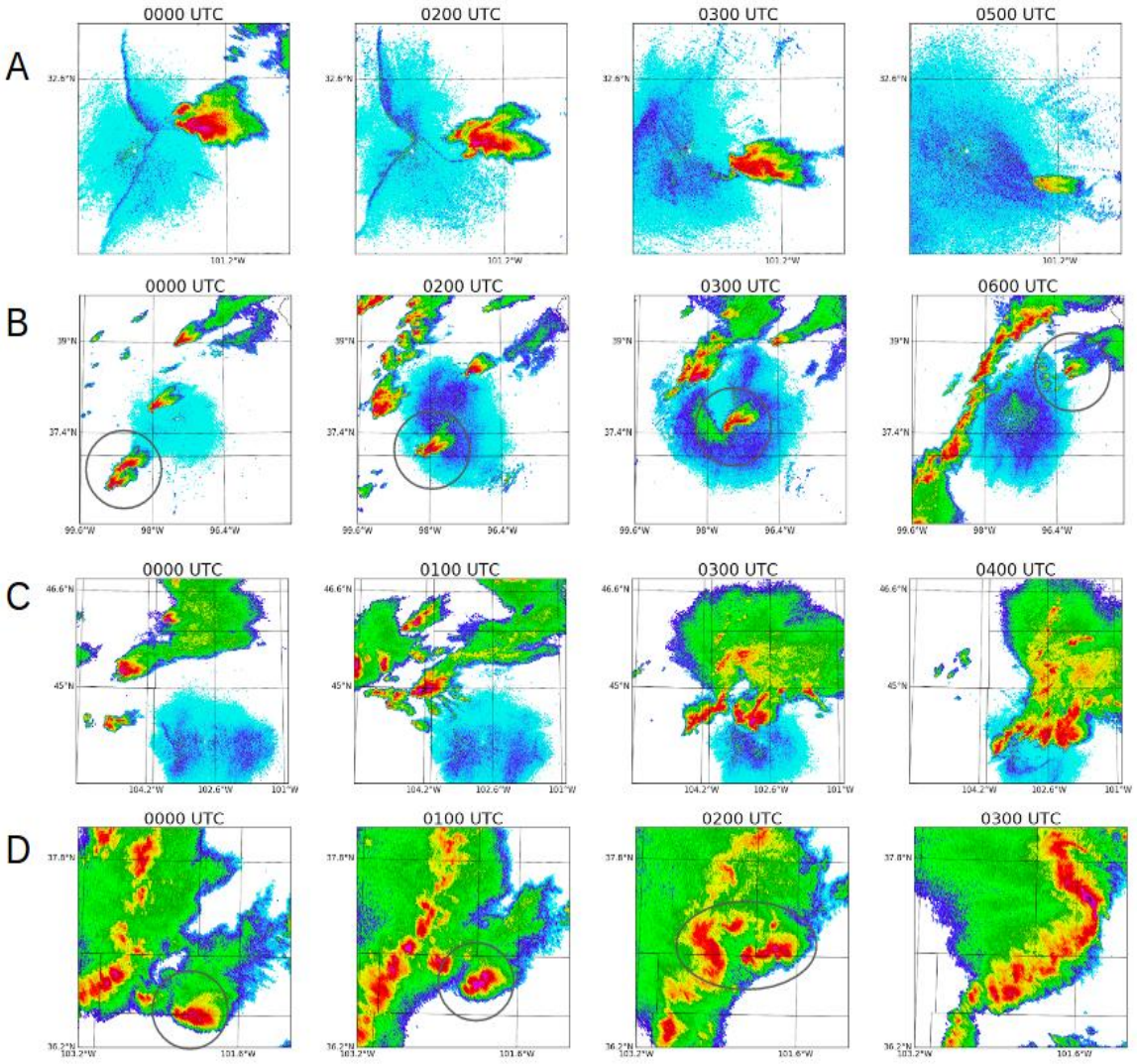

FIGURE 10: Panel a) shows an example dissipating supercell case from 0000 UTC to 0500 UTC. Panel b) shows an example of a maintained case from 0000 UTC to 0600 UTC. Panel c) shows an upscale case from 0000 UTC to 0400 UTC. Panel d) shows a merger case from 0000 UTC to 0300 UTC. The supercell in question is circled for each evolution type. Python library Pyart was used to create these images (Heistermann et al. 2015)

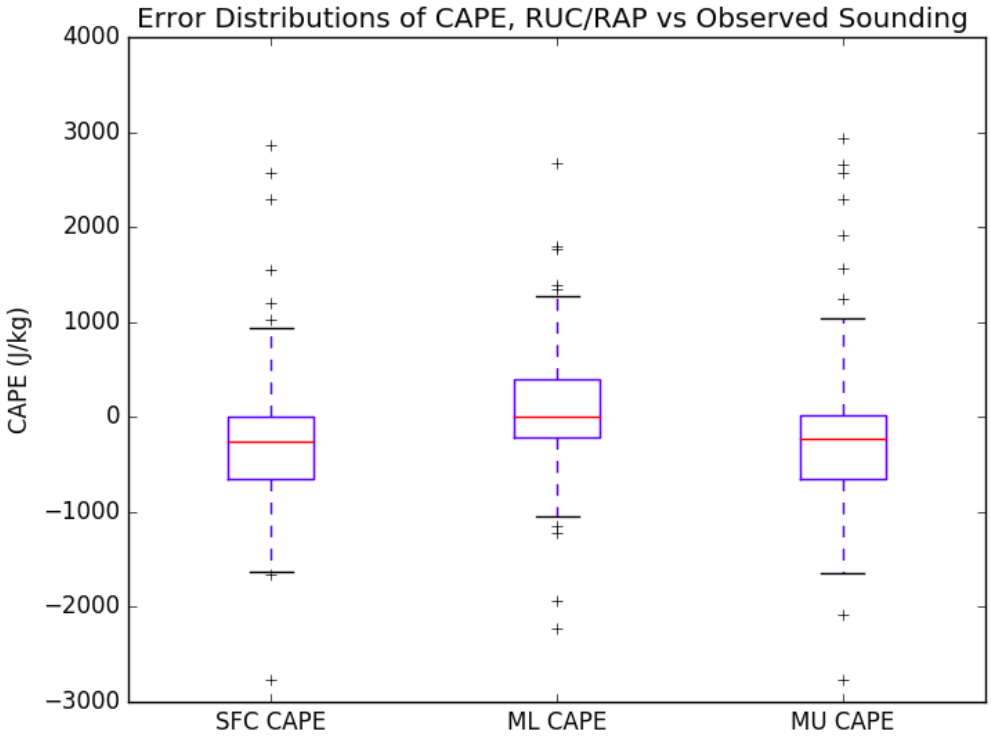

FIGURE 11: Box and whisker plot of average RUC/RAP CAPE errors versus observed soundings. Red line is median, outer blue box 75% and 25% percentiles and black line 90% and 10% percentiles. Positive values indicate the observed sounding value was greater than the RUC/RAP sounding.

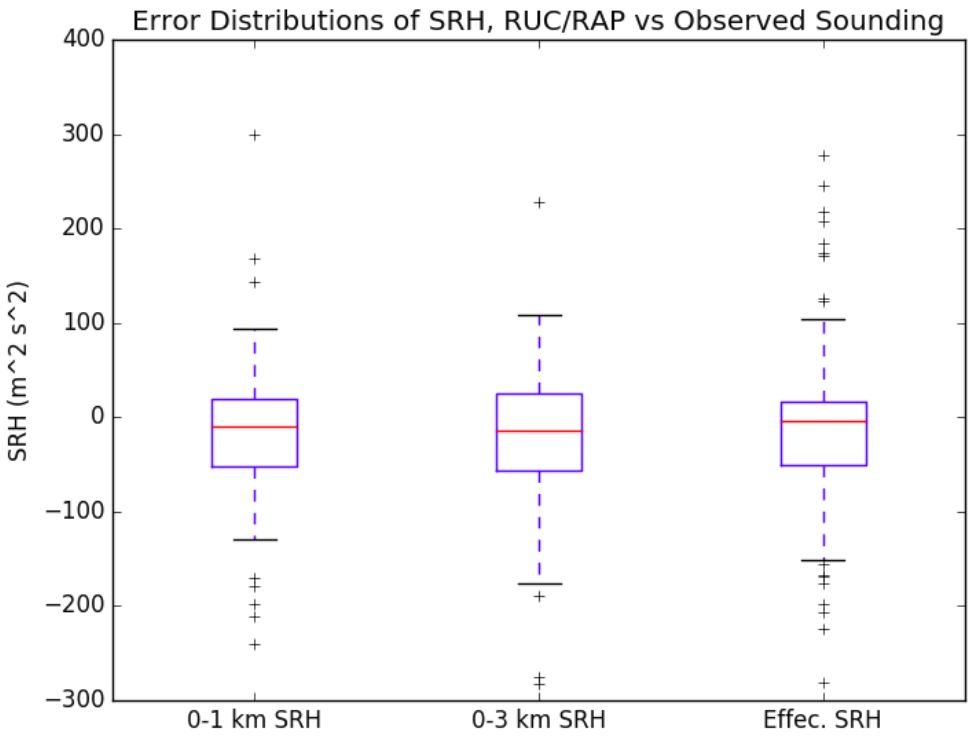

FIGURE 12: As in Fig. 8, but for RUC/RAP errors of SRH.

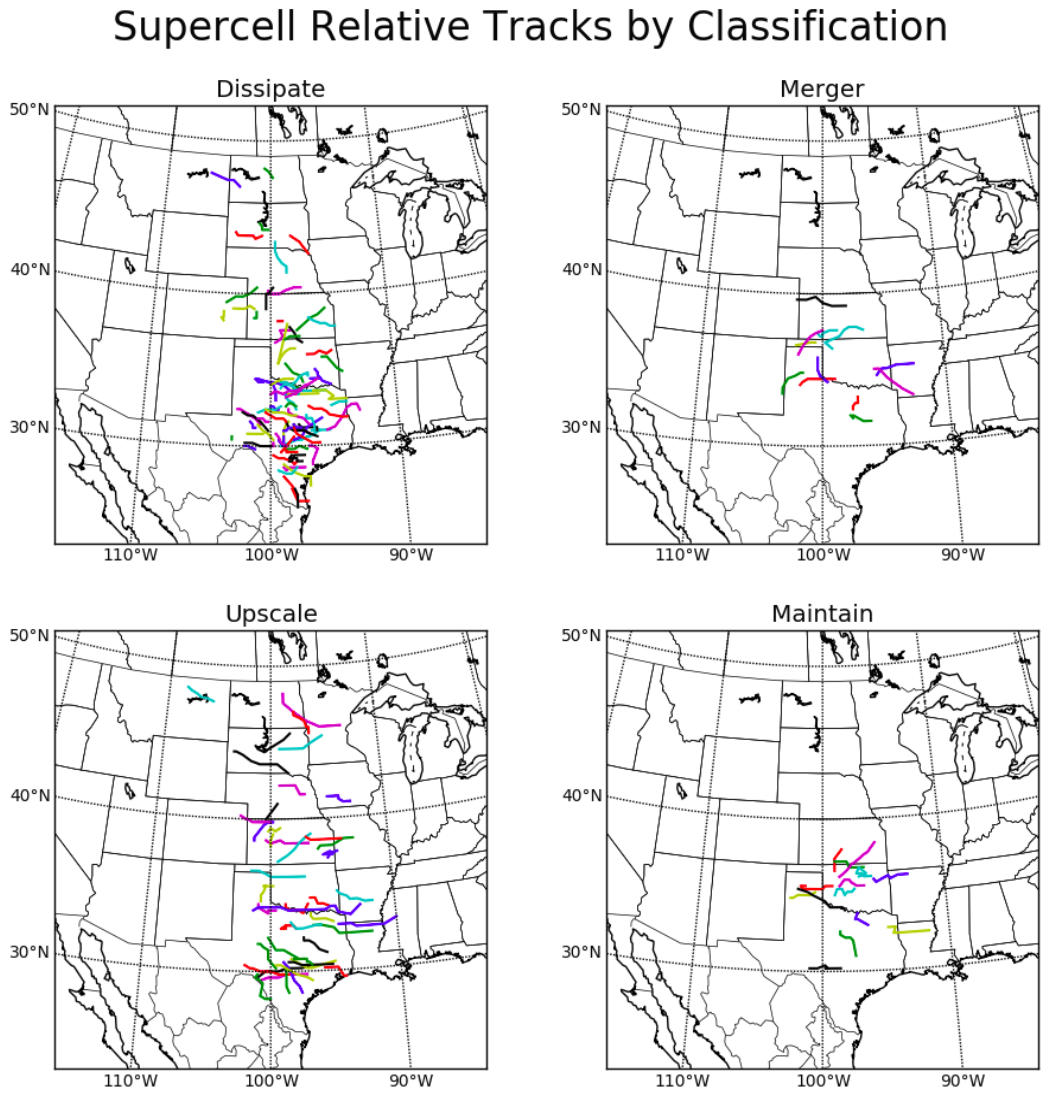

FIGURE 13: Tracks of each supercell by classification type.

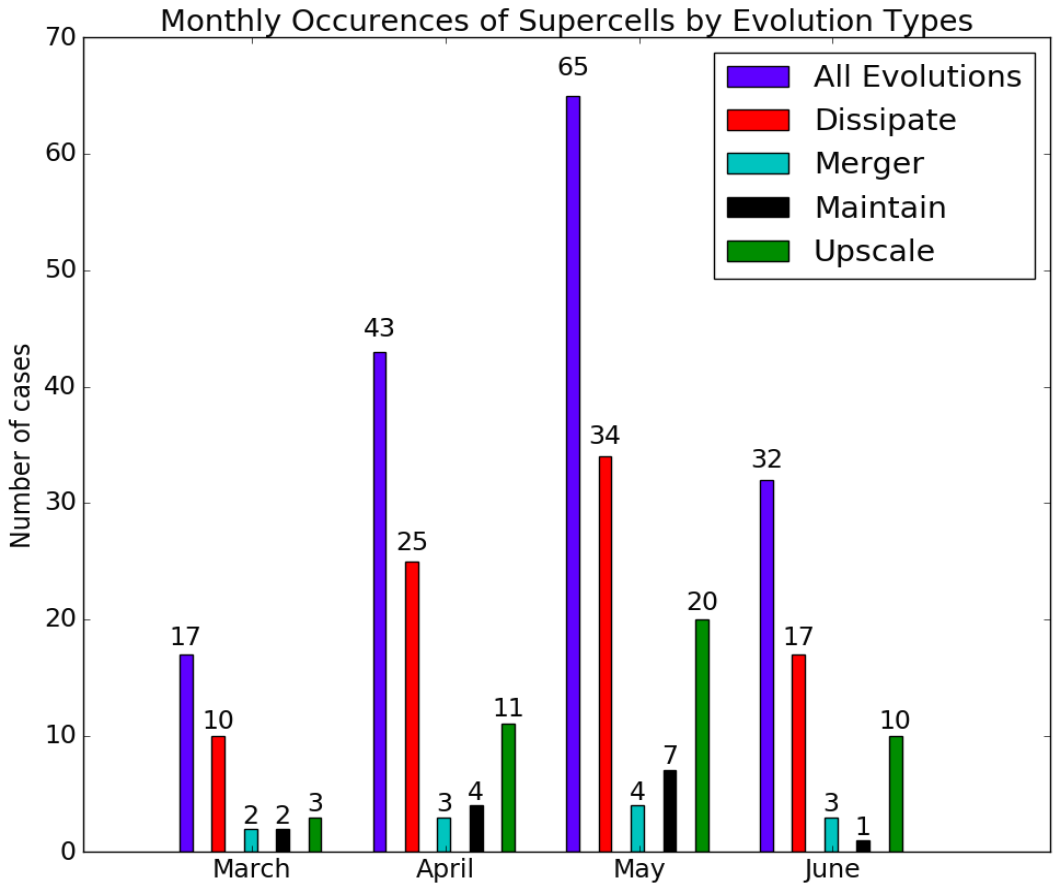

FIGURE 14: Temporal distributions for each supercell based on the month and by each evolution type.

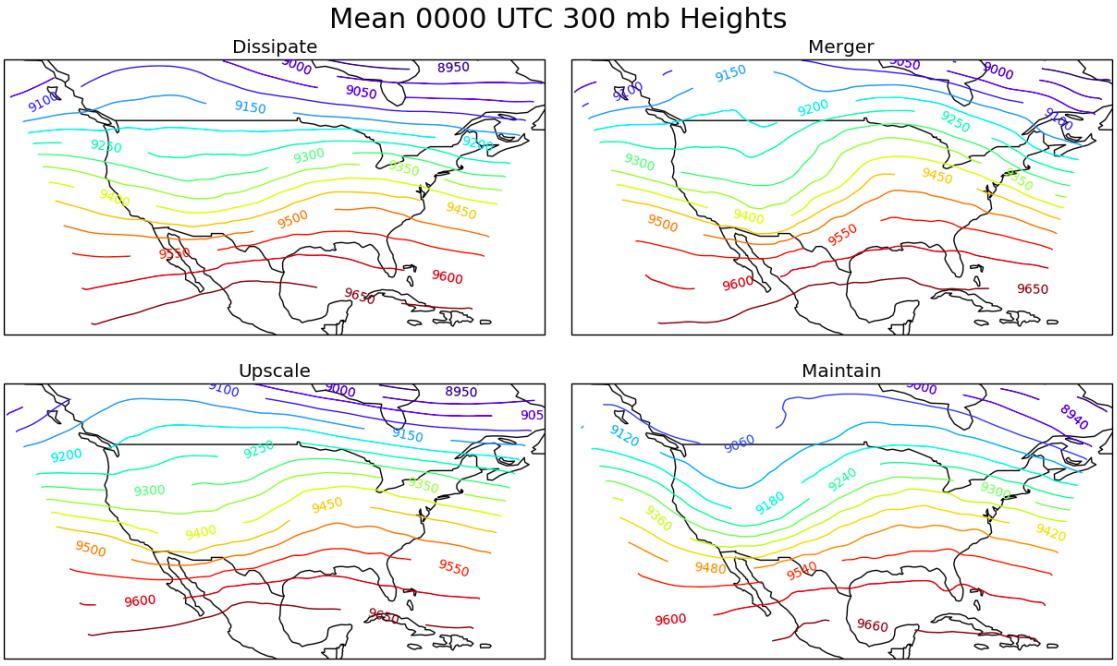

FIGURE 15: Mean 300 mb heights (meters) for each classification interpolated onto the 13 km spaced grid.

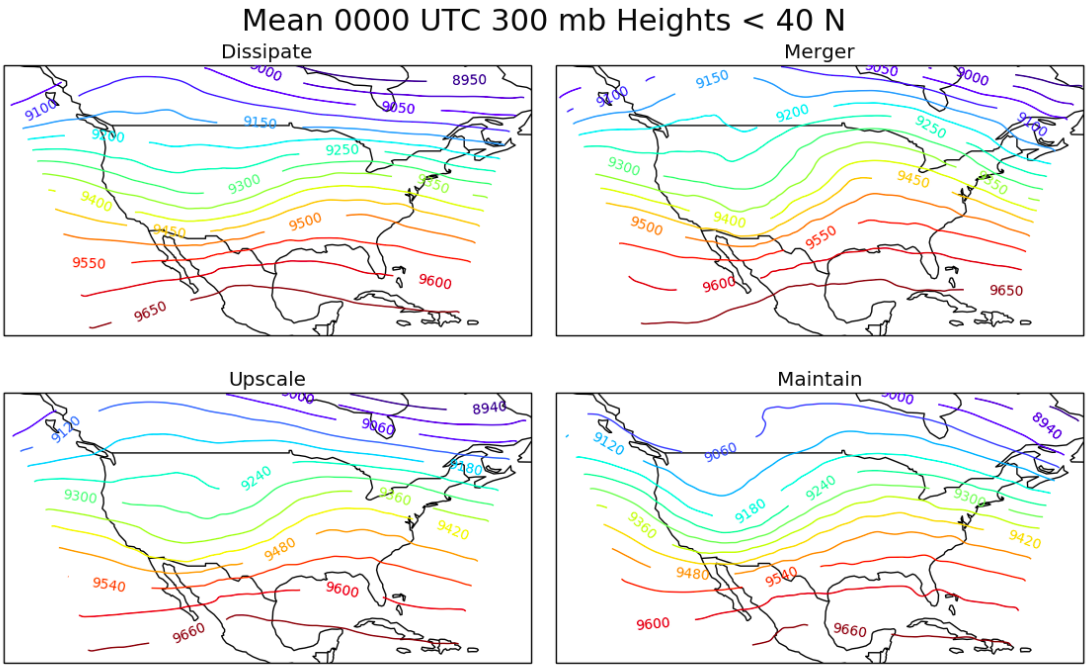

FIGURE 16: Same as Fig. 15, but limiting to the domain of supercells including to those that occurred south of 40 N.

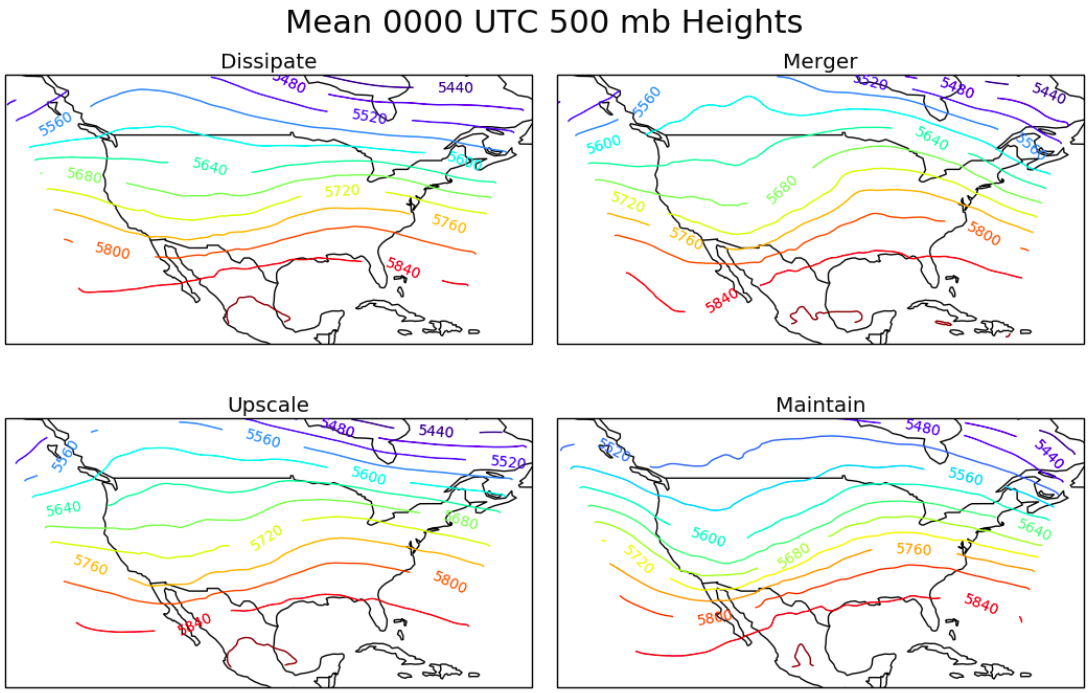

FIGURE 17: Same as Fig. 15, but for 500 mb heights.

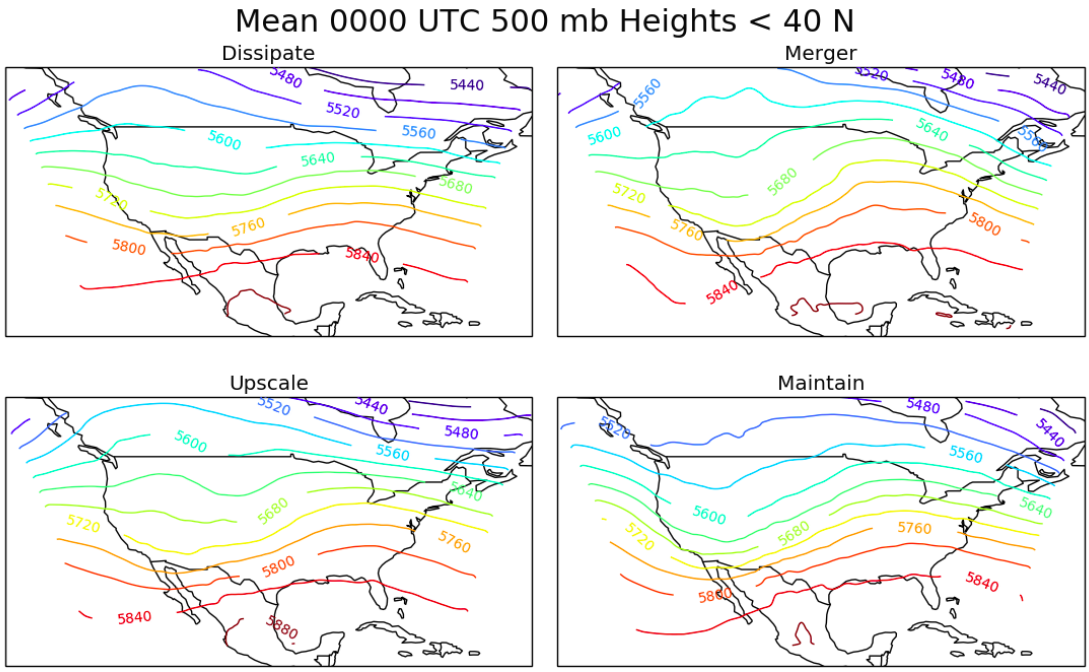

FIGURE 18: Same as Fig. 16, but for 500 mb heights

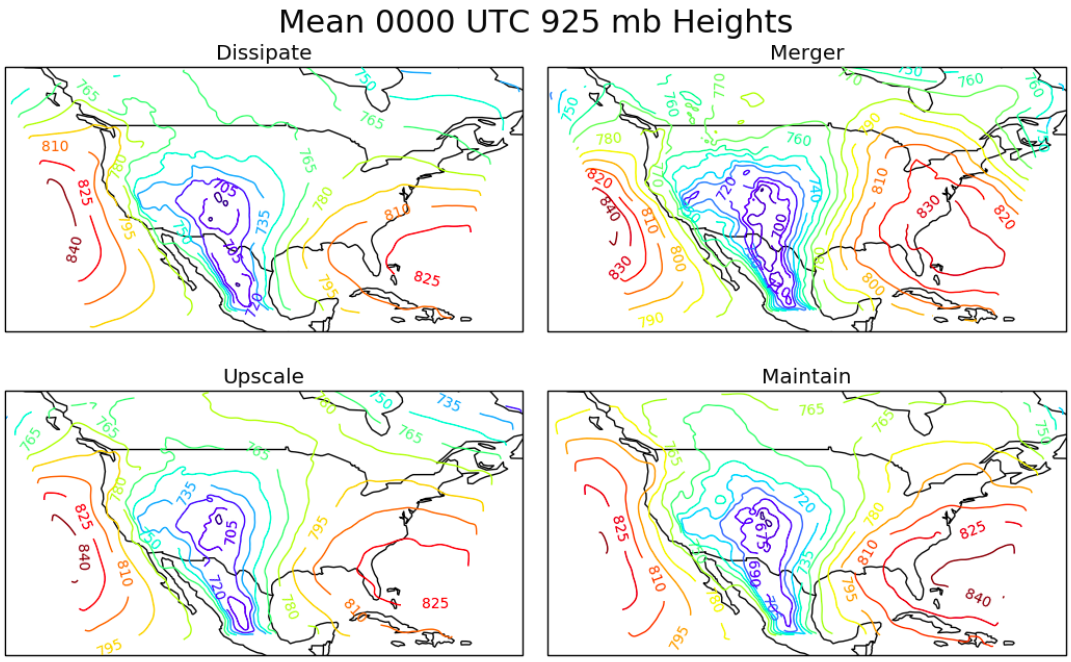

FIGURE 19: Same as Fig. 15, but for 925 mb heights

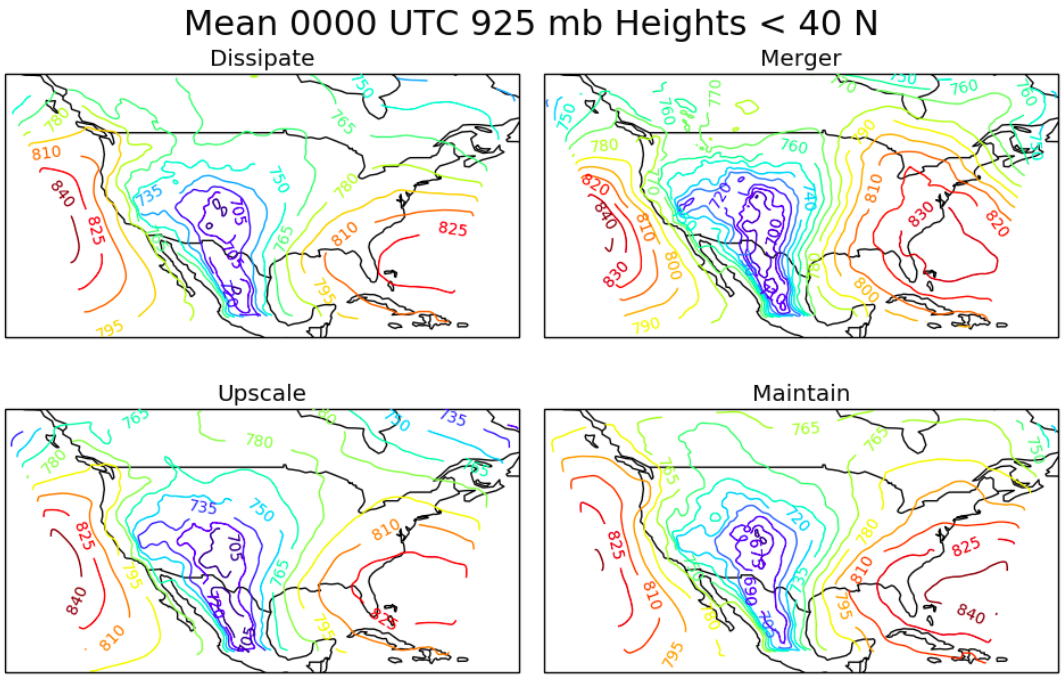

FIGURE 20: Same as Fig. 16, but for 925 mb heights

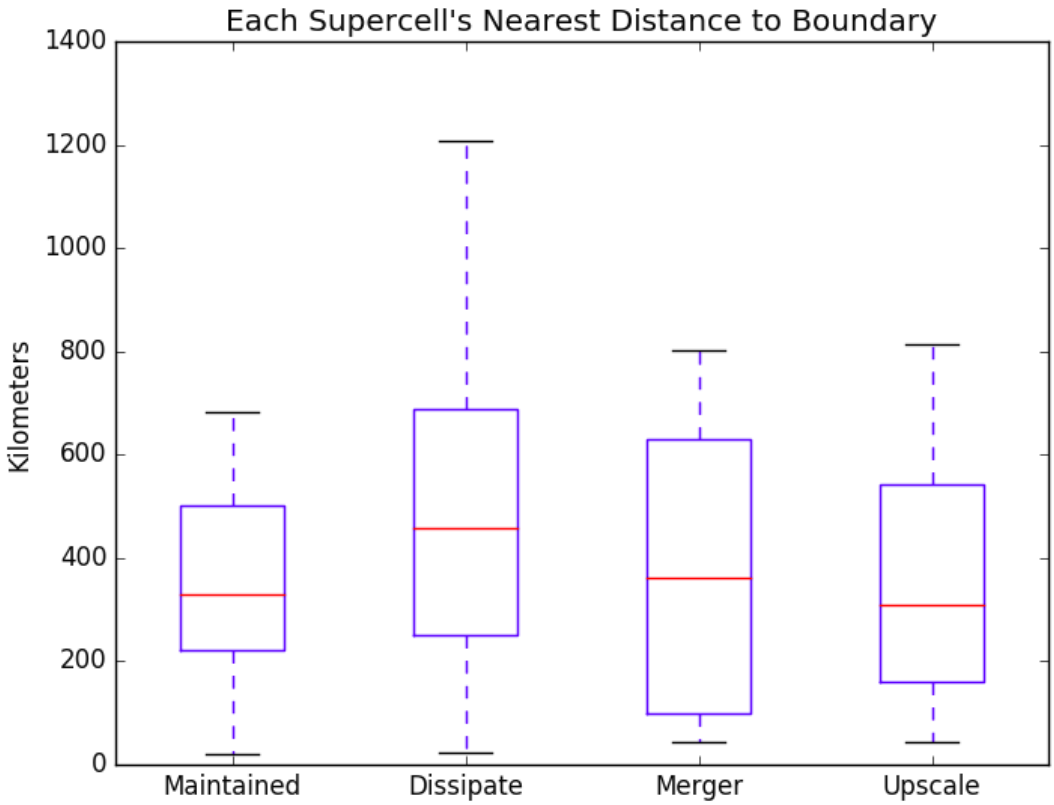

FIGURE 21: The average nearest distance front to the closest cold, warm or stationary front for each evolution type.

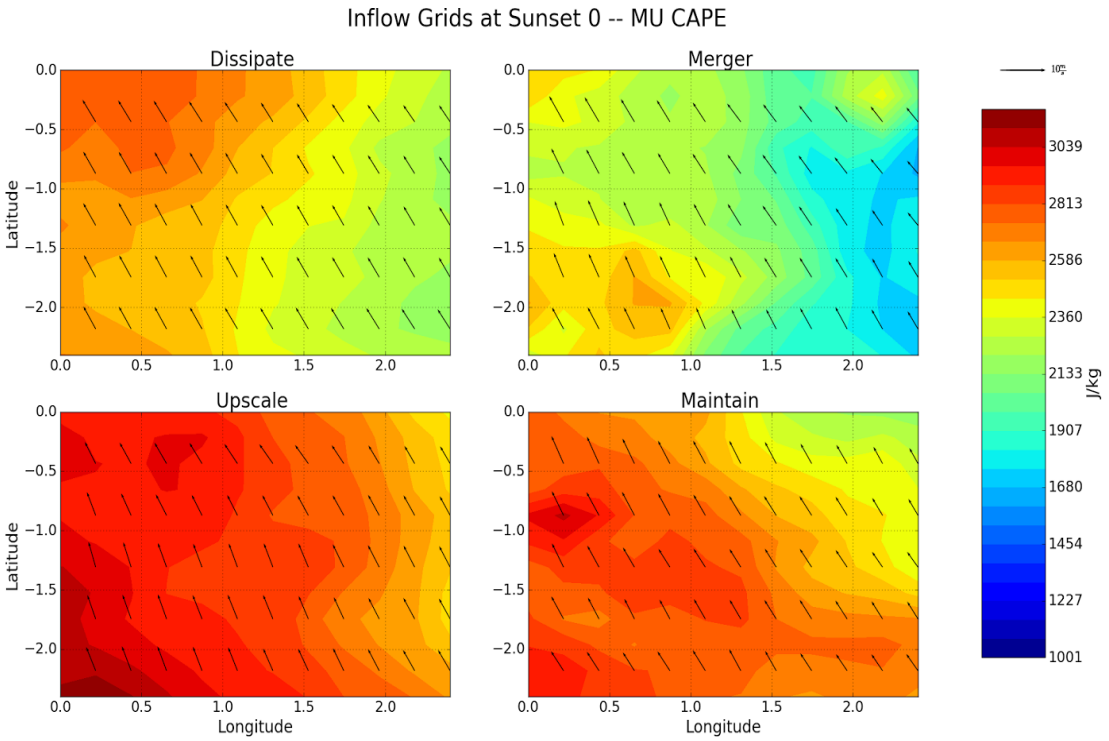

FIGURE 22: 160 km by 160 km inflow grid of MU CAPE at SS and overlaid surface wind vectors. Northwest corner represent the closest grid point to the supercell. Vector above the colorbar is scaled at 10 m/s.

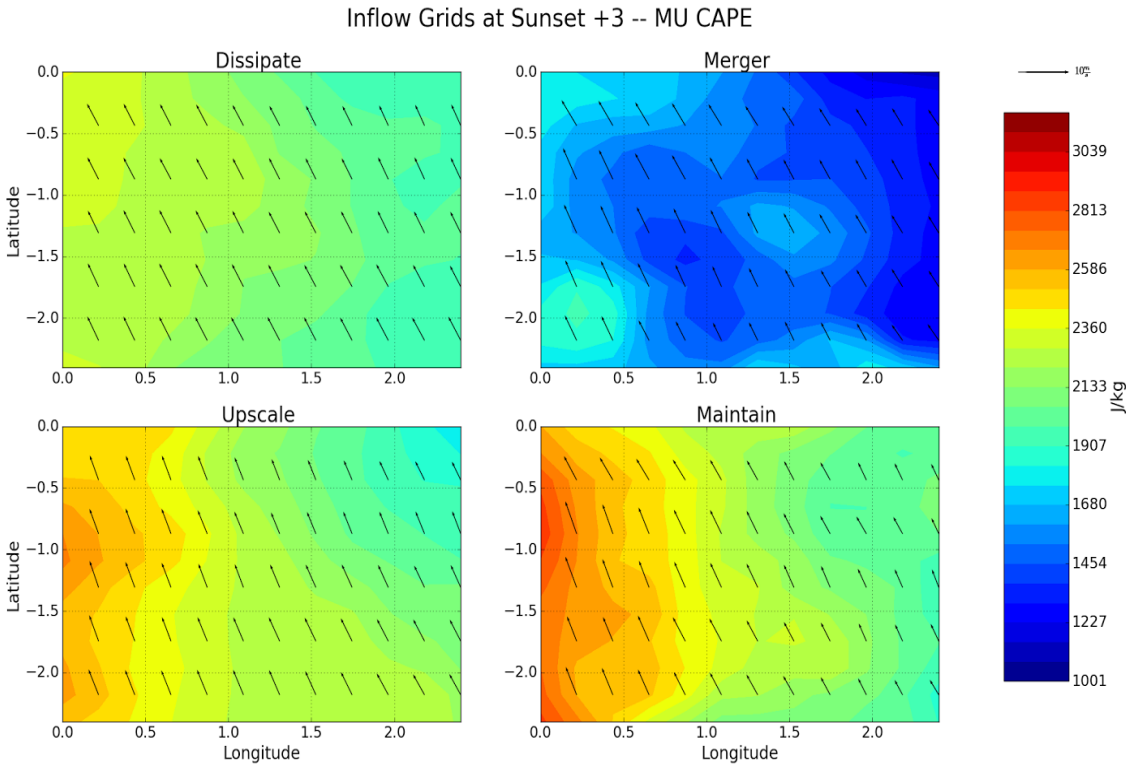

FIGURE 23: As in figure 22, but at SS +3

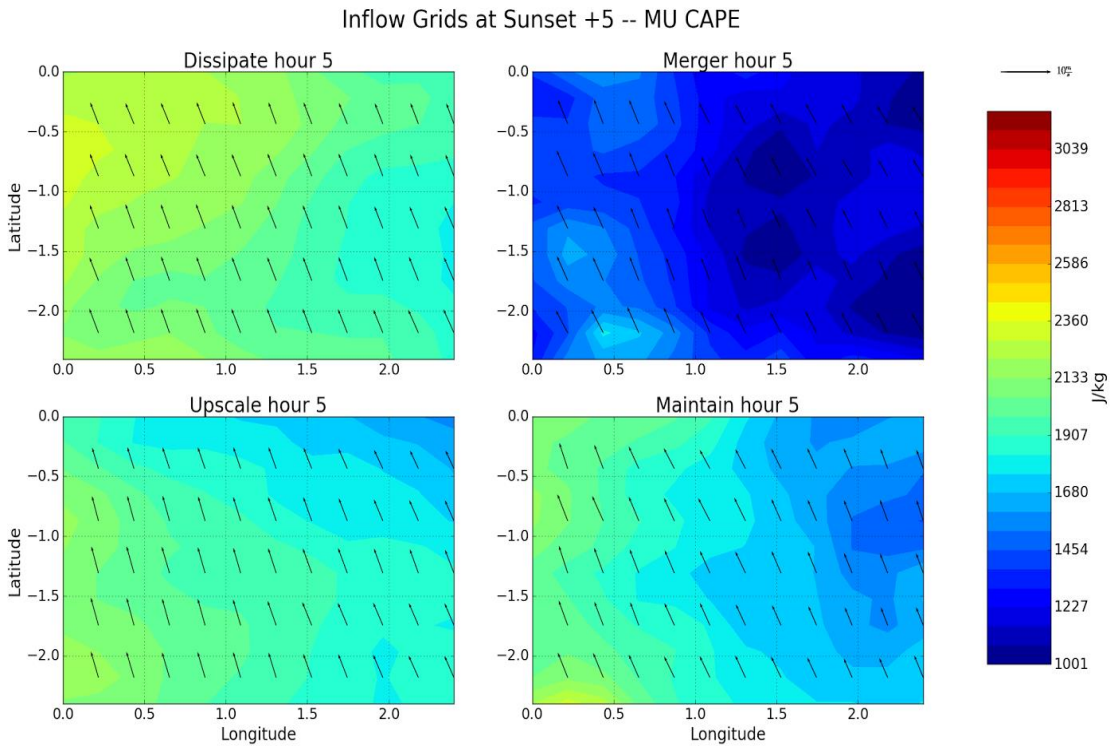

FIGURE 24: As in figure 22, but SS +5

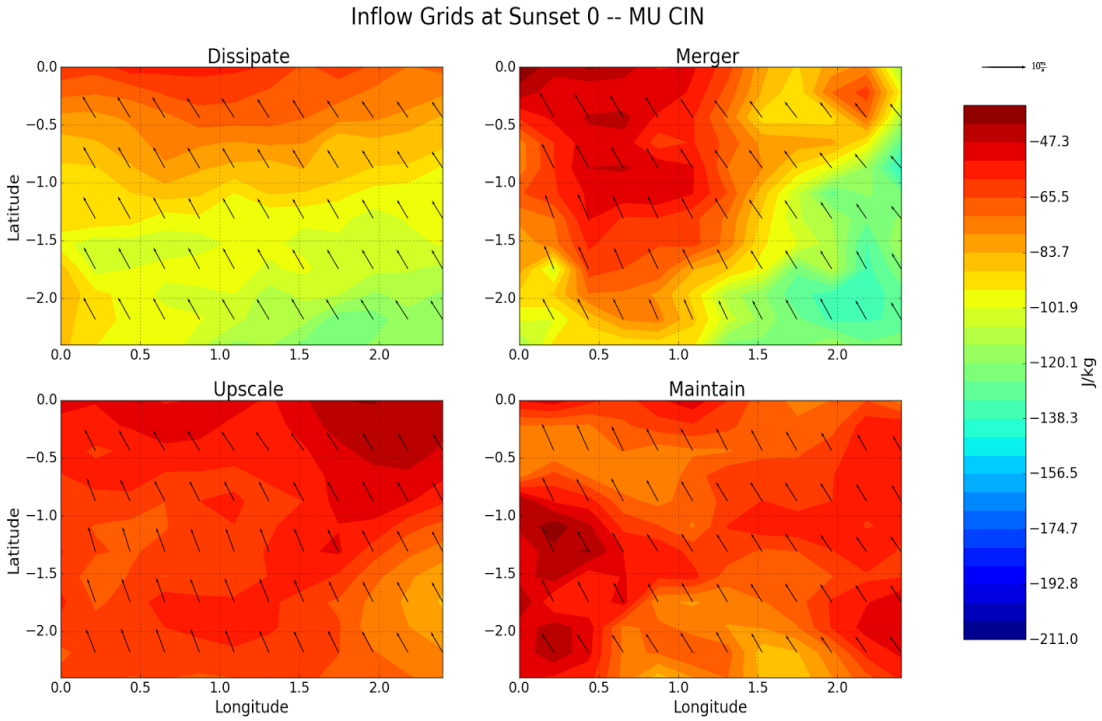

FIGURE 25: As in figure 22, but for MU CIN

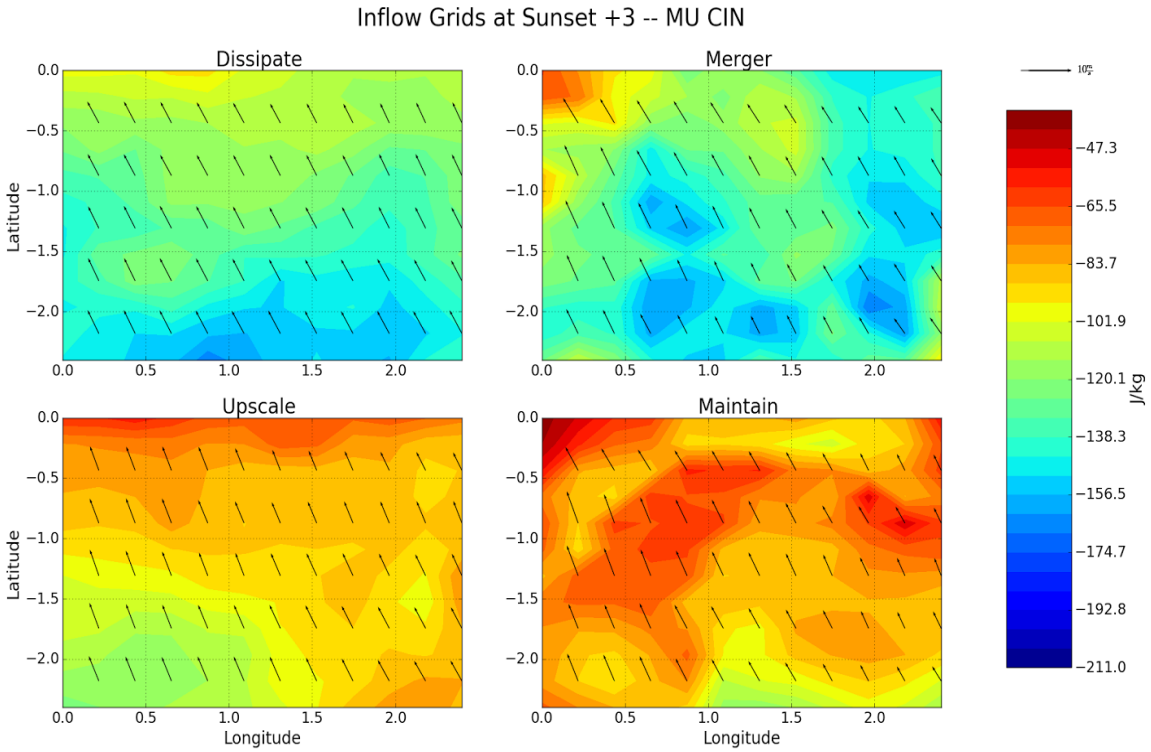

FIGURE 26: As in figure 25, but at SS +3

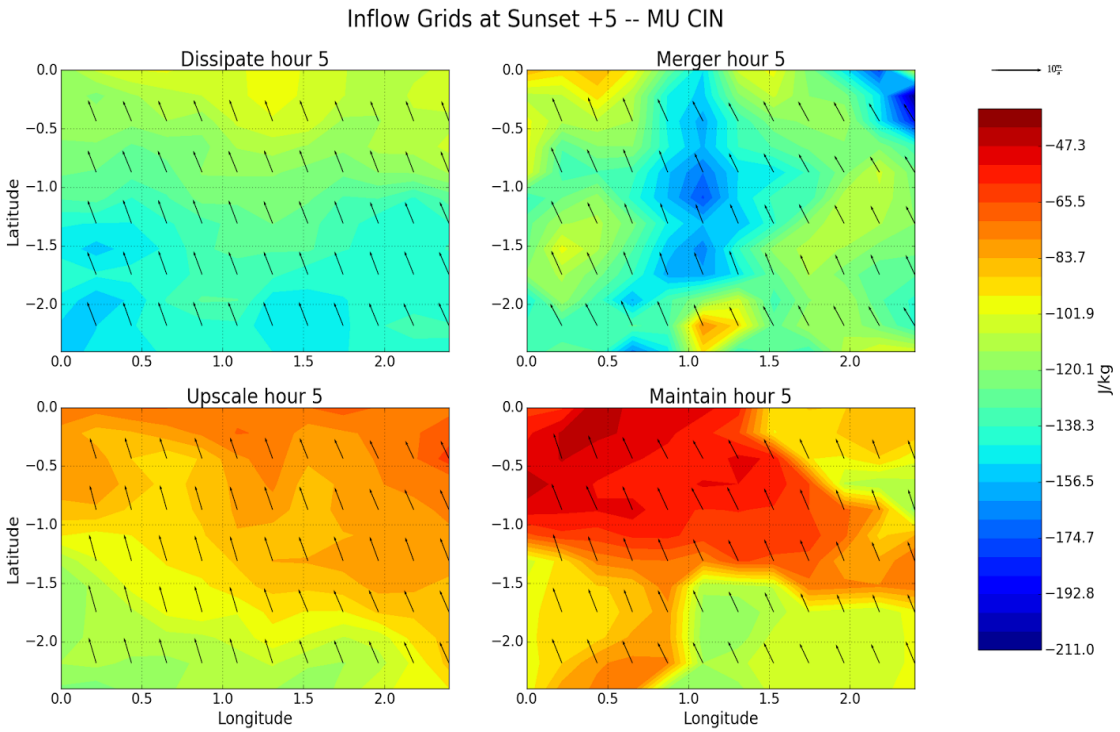

FIGURE 27: As in figure 25, but at SS +5

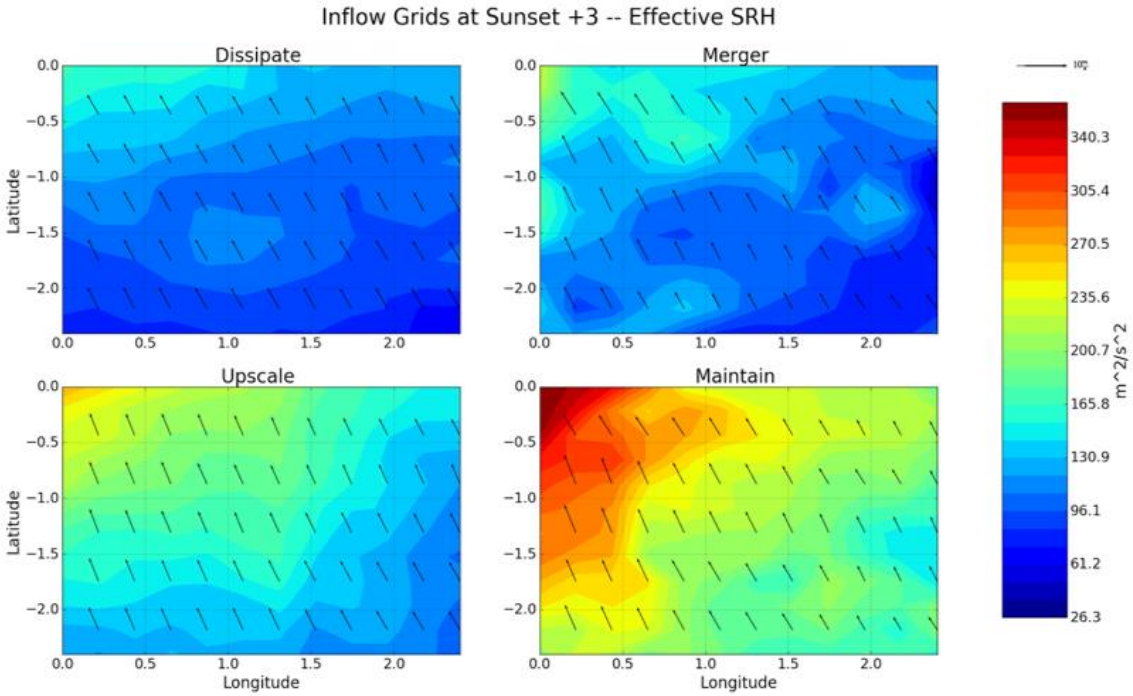

FIGURE 28: As in figure 22, but for Effective SRH.

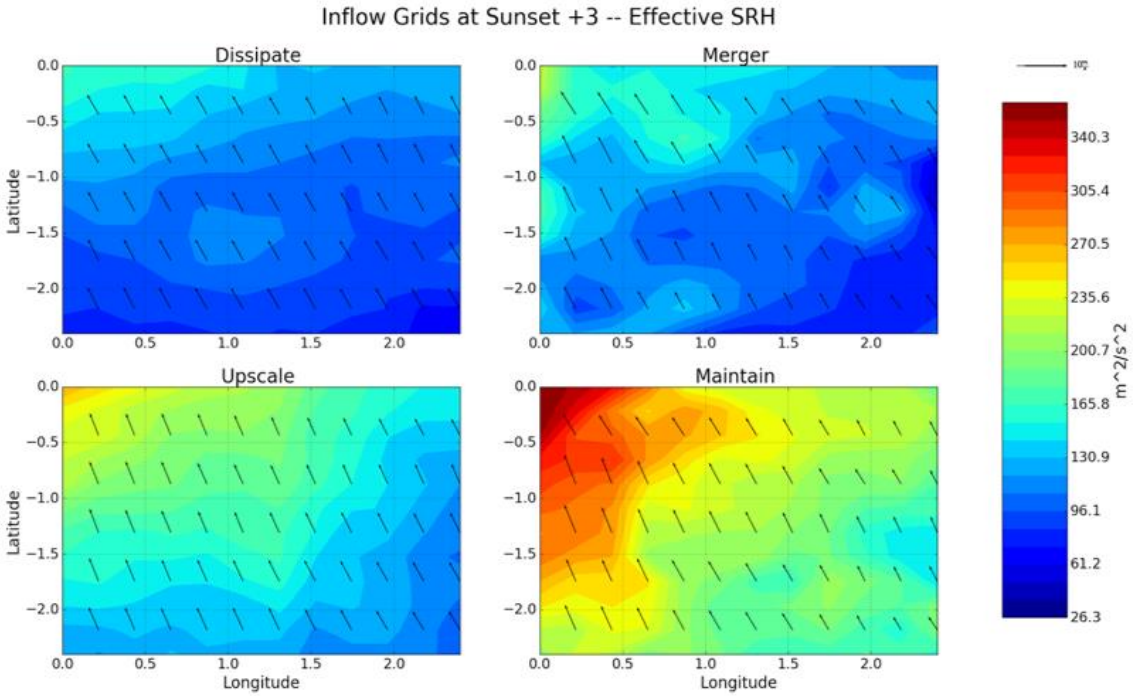

FIGURE 29: As in figure 28, but at SS +3

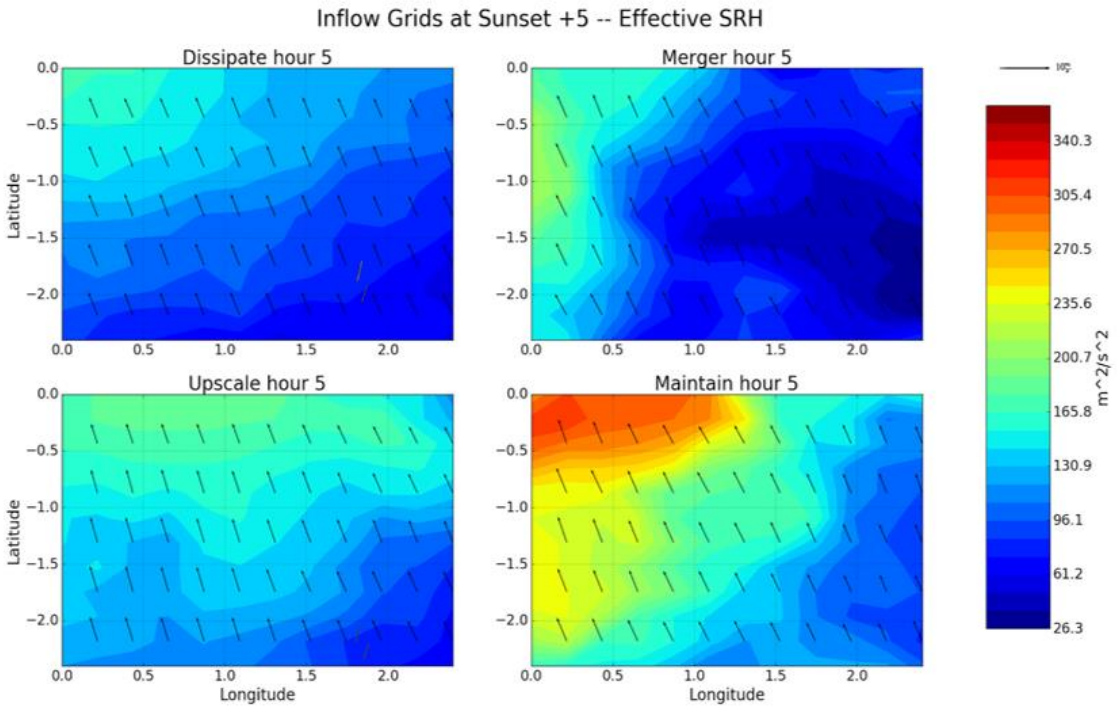

FIGURE 30: As in figure 28, but at SS +5

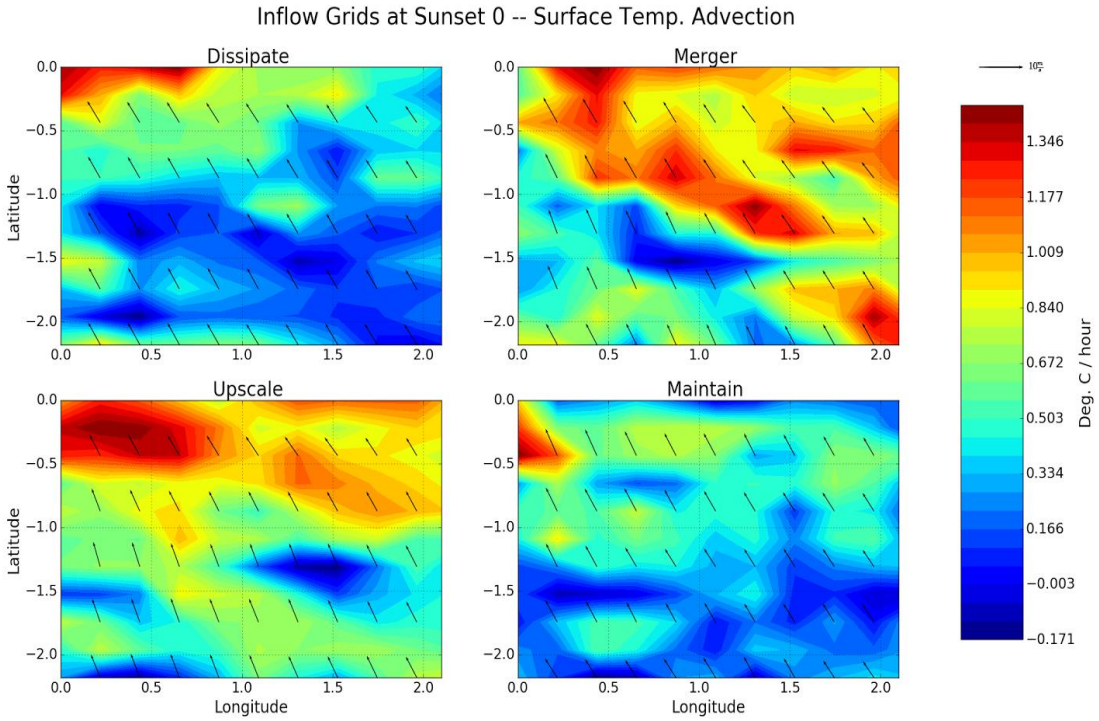

FIGURE 31: As in figure 22, but for surface temperature advection.

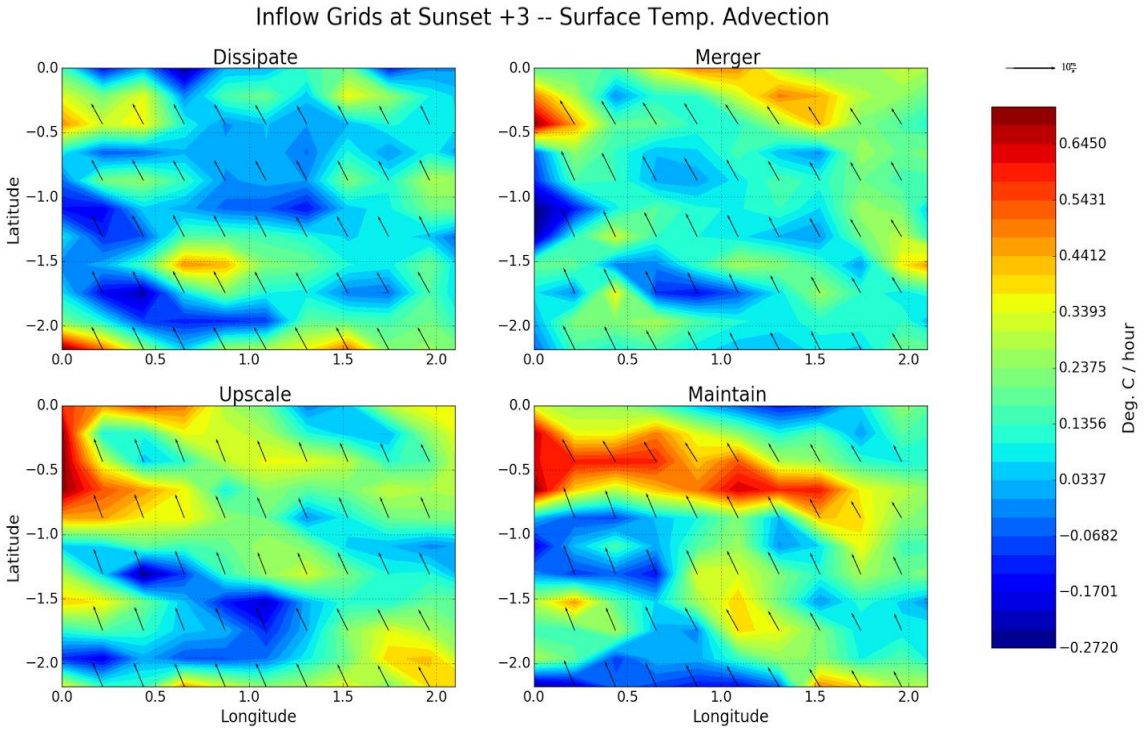

FIGURE 32: As in figure 31, but at SS +3

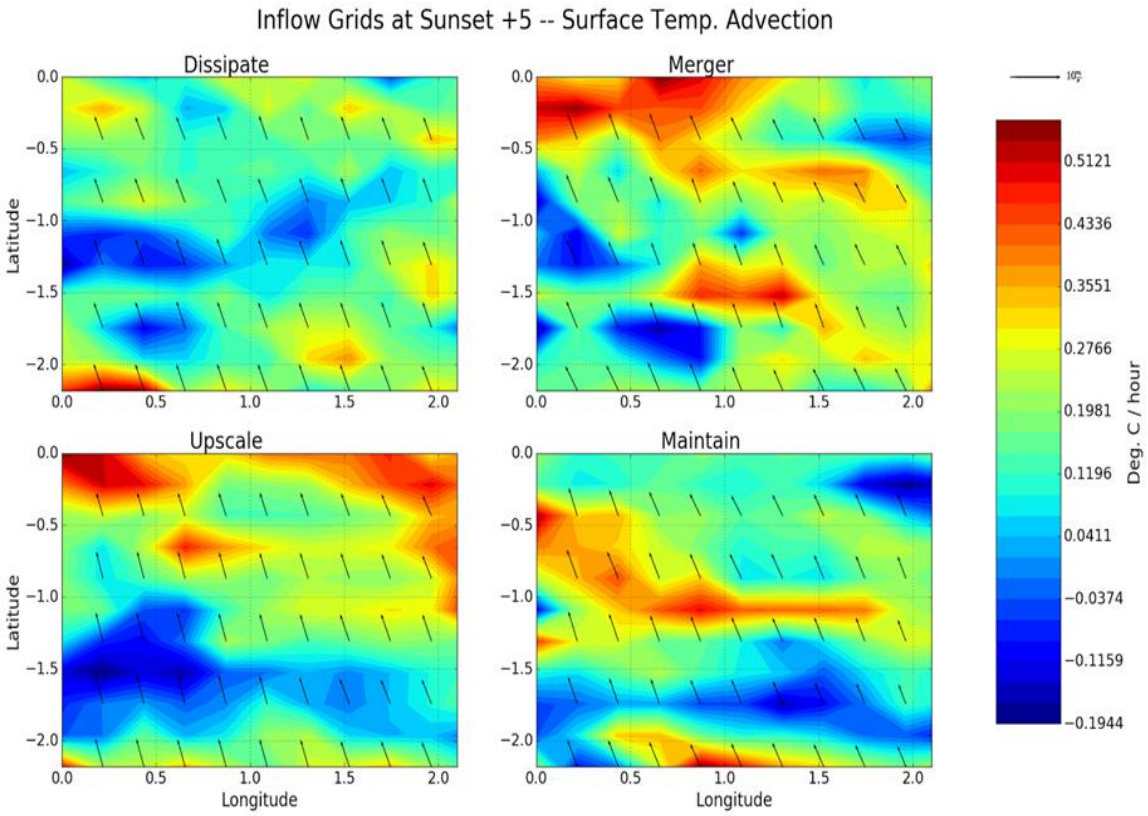

FIGURE 33: As in figure 31, but at SS +5

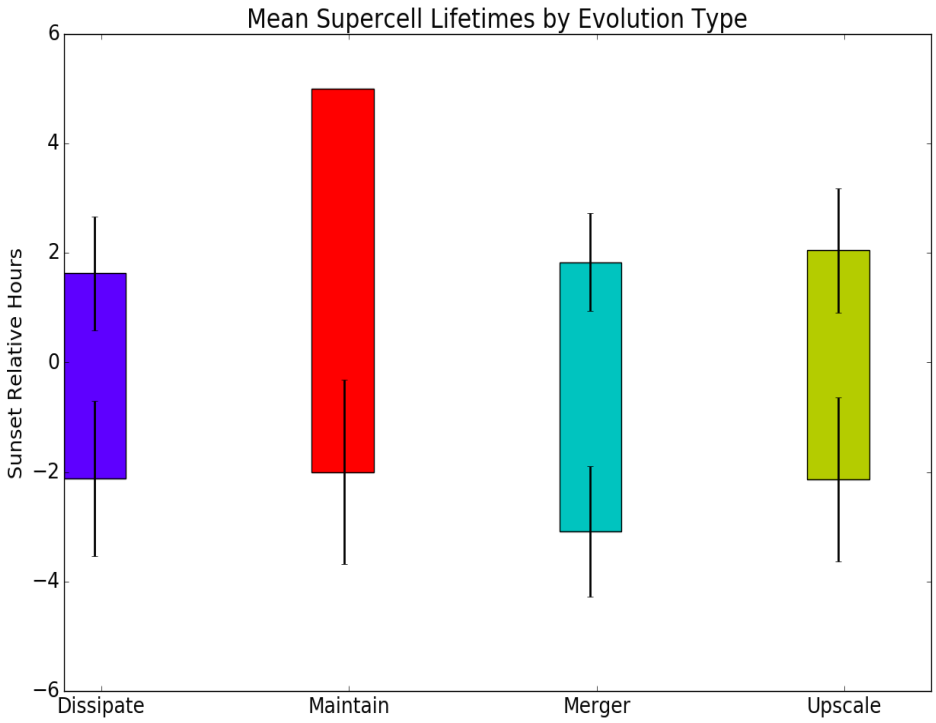

FIGURE 34: Mean lifetime of each supercell classification (bar), with one standard deviation (black line) shown for the mean start and end times. Bottom of the bar indicates mean start time and top indicates mean time of evolution. For example, dissipating supercells averaged a start and end time of ~ SS-2 and ~SS+2, respectively.

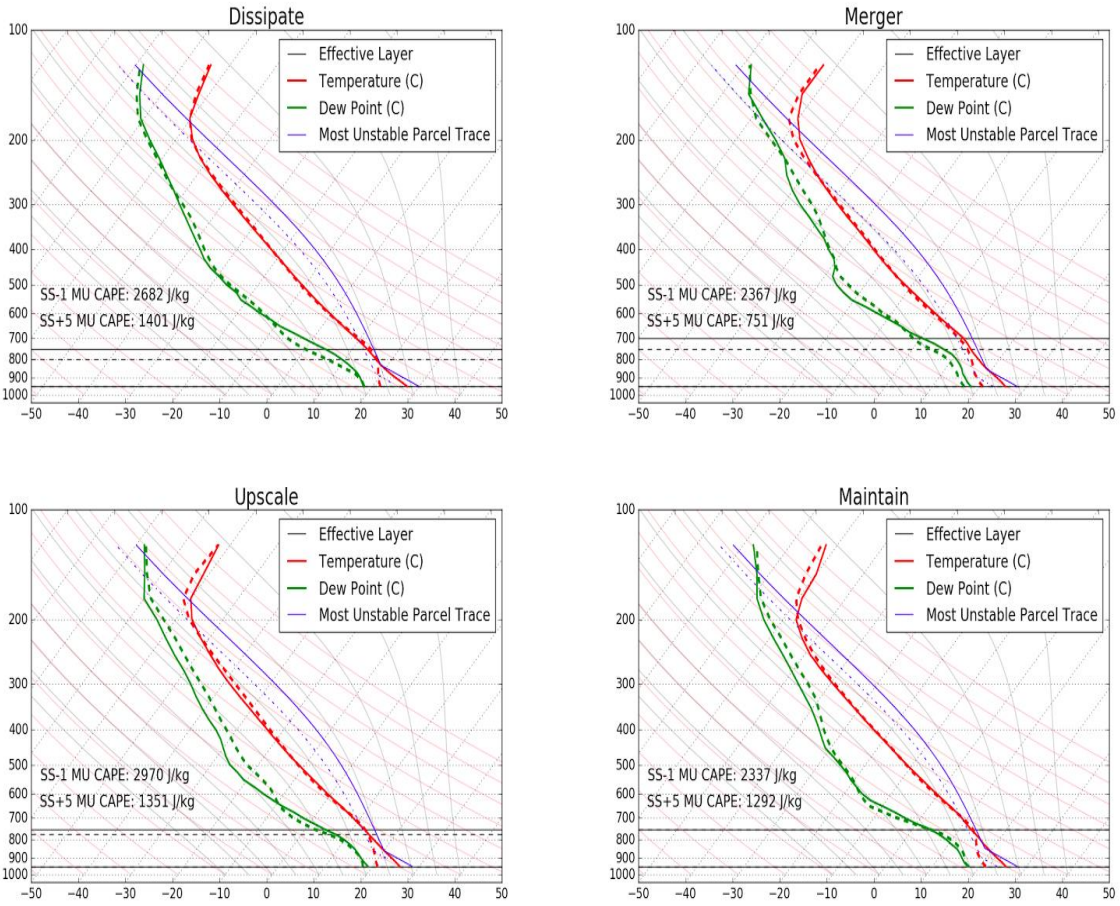

FIGURE 35: Composite soundings for each evolution type. Solid line represents the profile at SS -1, the dashed at SS +5. Temperature (red), dew point (green), MU parcel trace (blue), and effective inflow layer bounds (black) are shown.

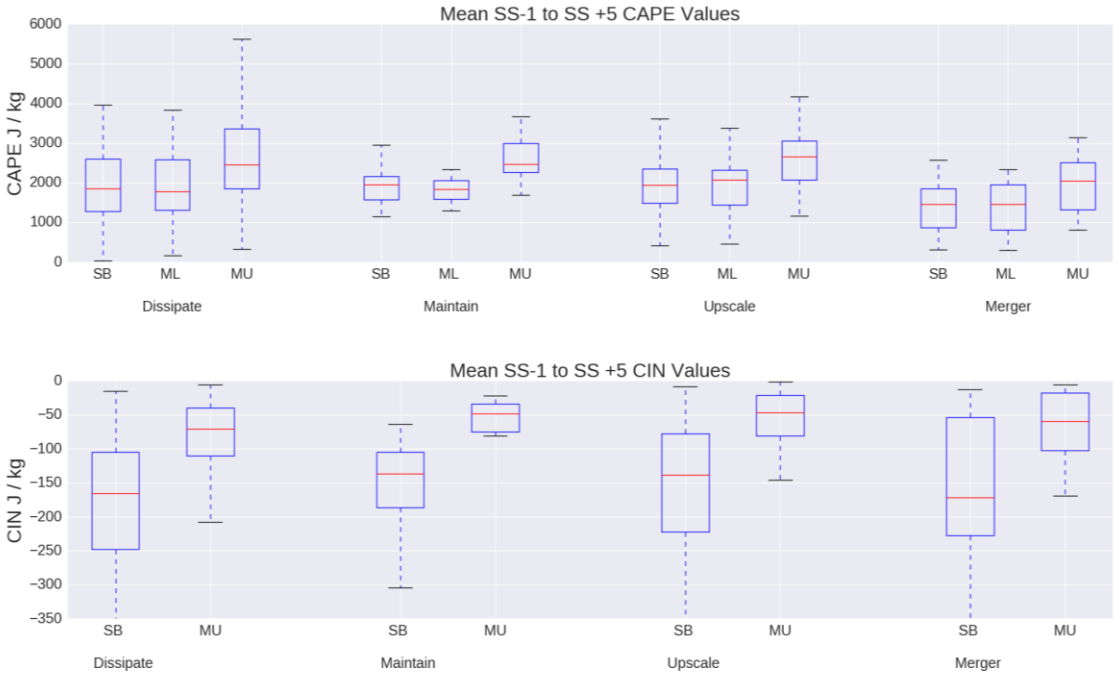

FIGURE 36: Cumulative SS -1 to SS +5 mean distributions for SB, ML, and MU CAPE (top panel) and SB and MU CIN (bottom panel) for each evolution type.

FIGURE 37: Mean change from SS -1 to SS +5 for SB, ML, and MU CAPE (top panel) and SB and MU CIN (bottom panel) for each evolution type.

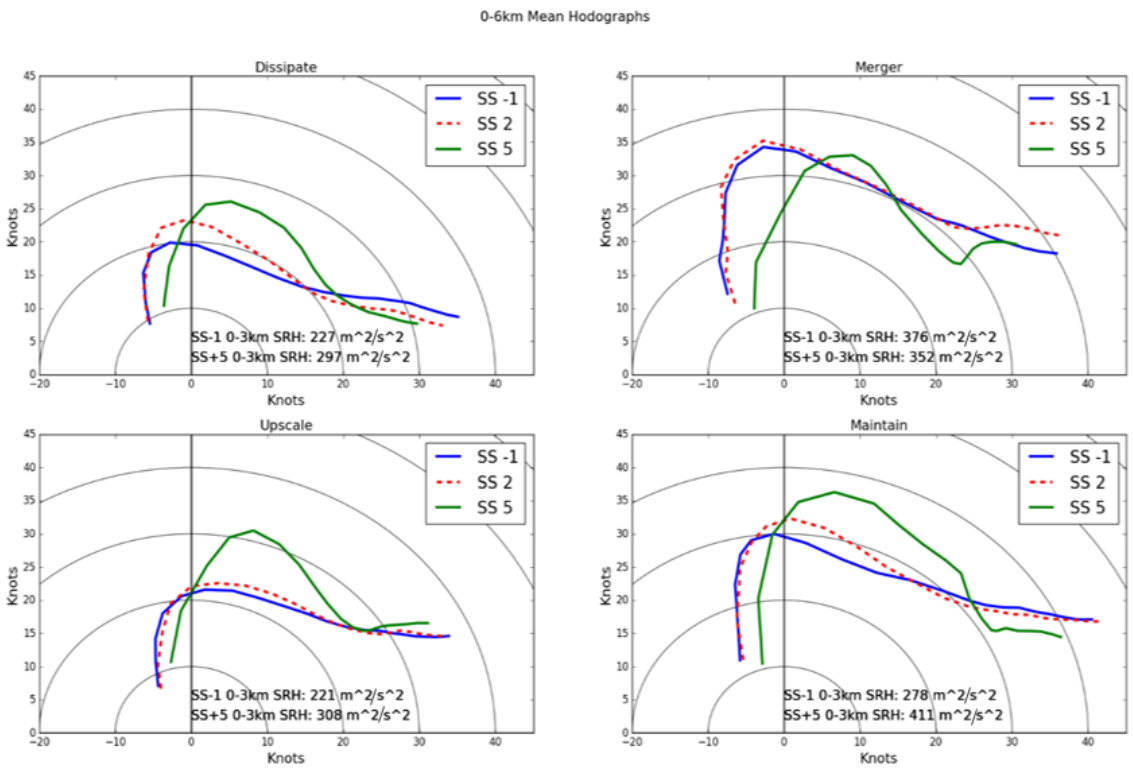

FIGURE 38: Composite 0-6 km hodographs for each evolution type at SS -1 (blue), SS +2 (red), and SS +5 (green)

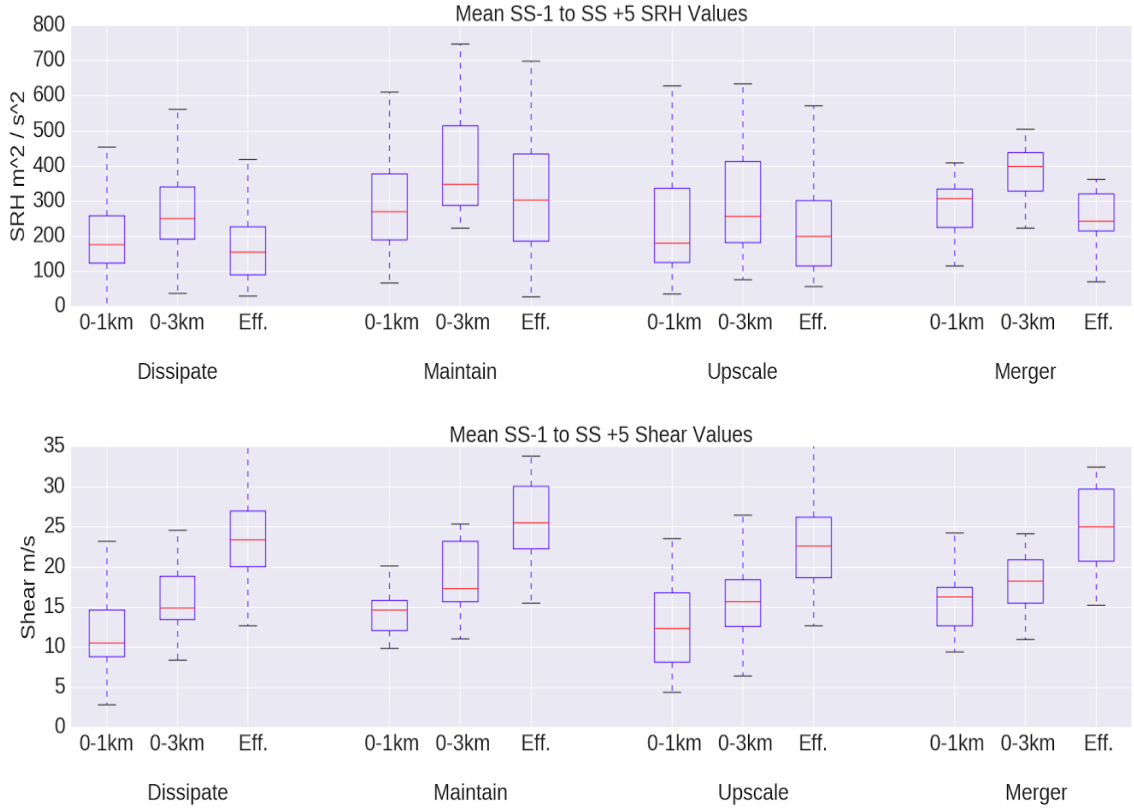

FIGURE 39: Cumulative SS -1 to SS +5 mean distributions for SRH (top panel) and 0-1 km, 0-3 km, and effective bulk layer shear (bottom panel) for each evolution type.

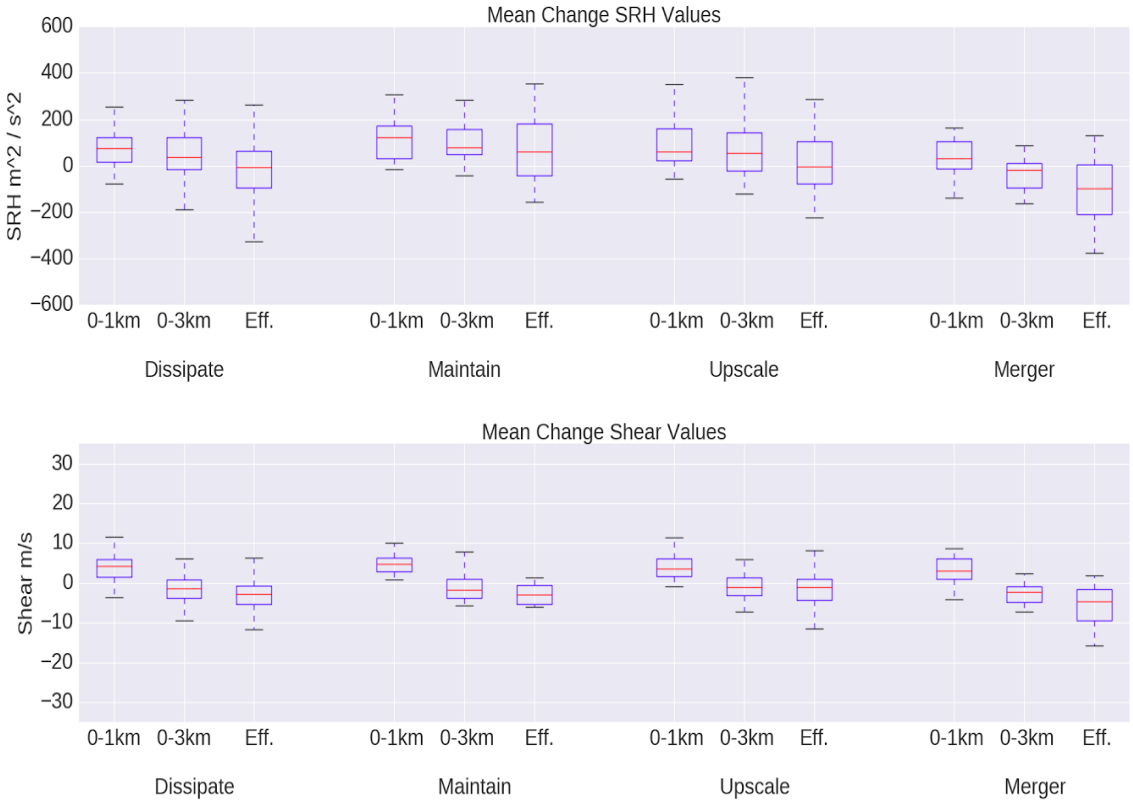

FIGURE 40: Mean change from SS -1 to SS +5 for SFC and MU CIN (top panel) and 0-1 km, 0-3 km, and effective layer shear (bottom panel) for each evolution type.

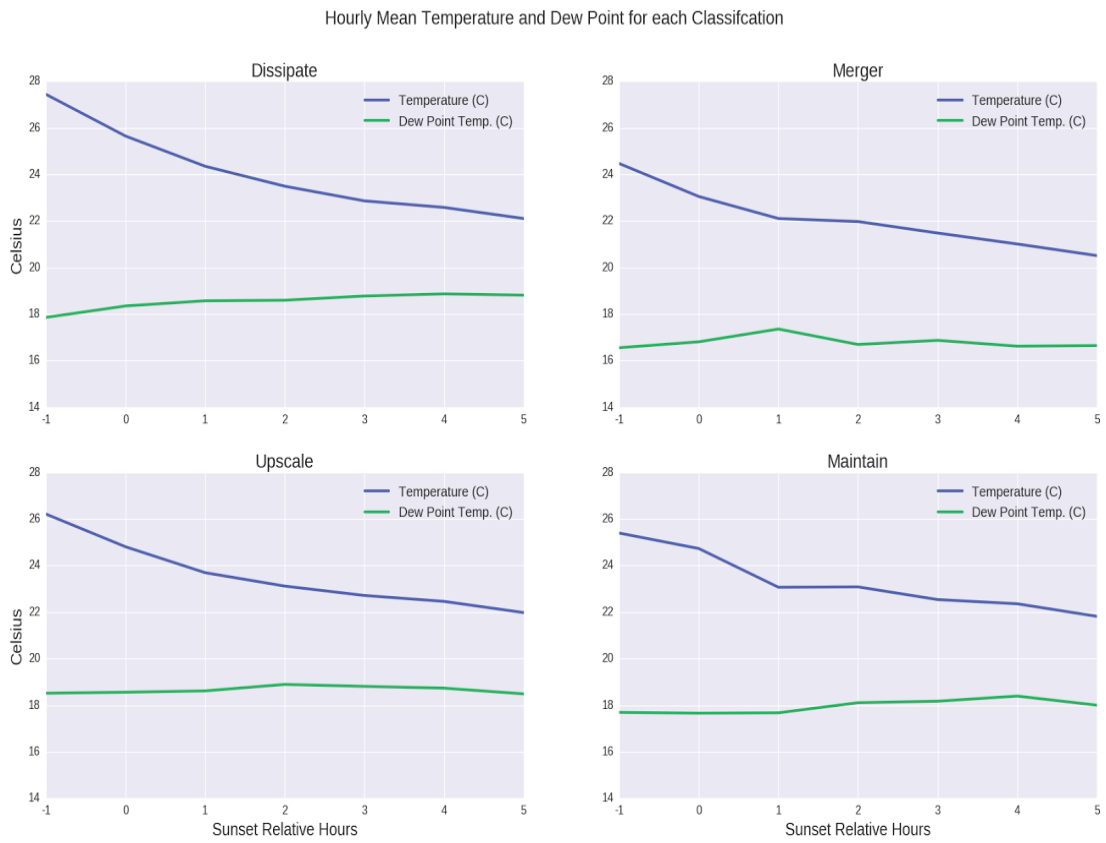

FIGURE 41: Time series from SS -1 to SS +5 of average surface temperature (blue) and dew point (green) for each classification.

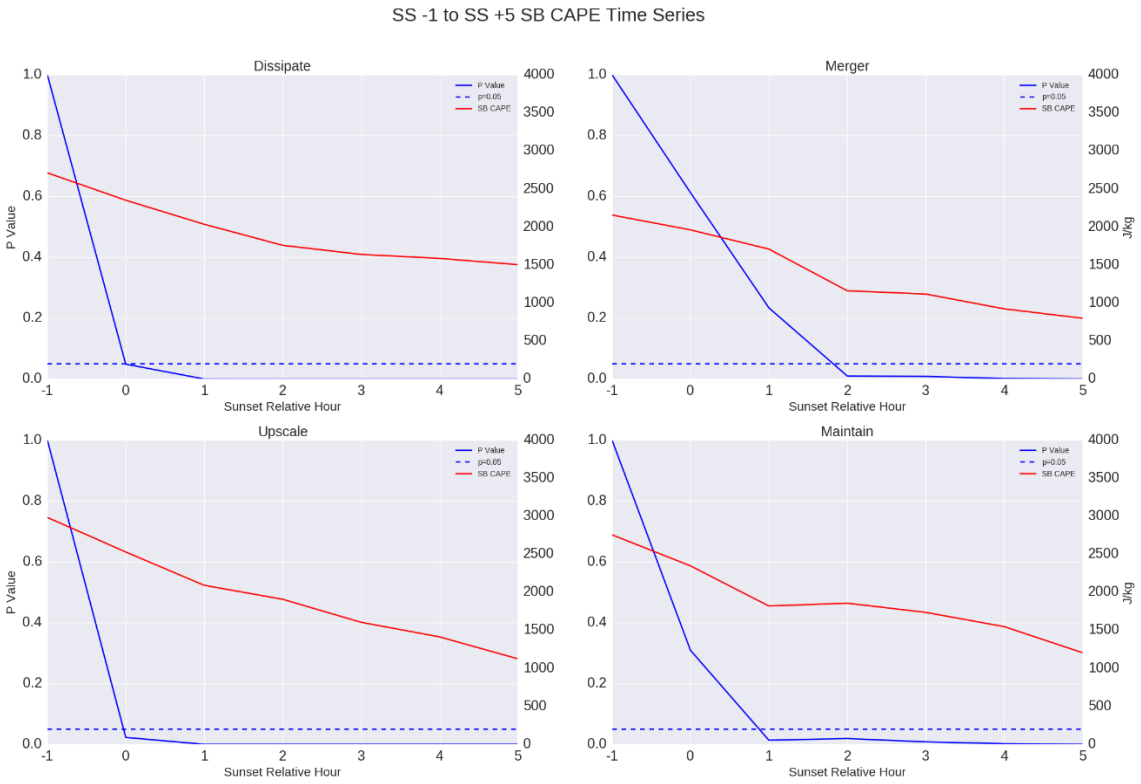

FIGURE 42: Time series of SB CAPE from SS -1 to SS +5 for each classification; dissipation (top left), merger (top right), upscale (bottom left), and maintained (bottom right). Average SB CAPE (red line), p value for the SS -1 hourly comparison (blue line) and the 0.05 significance level (dashed blue) are plotted.

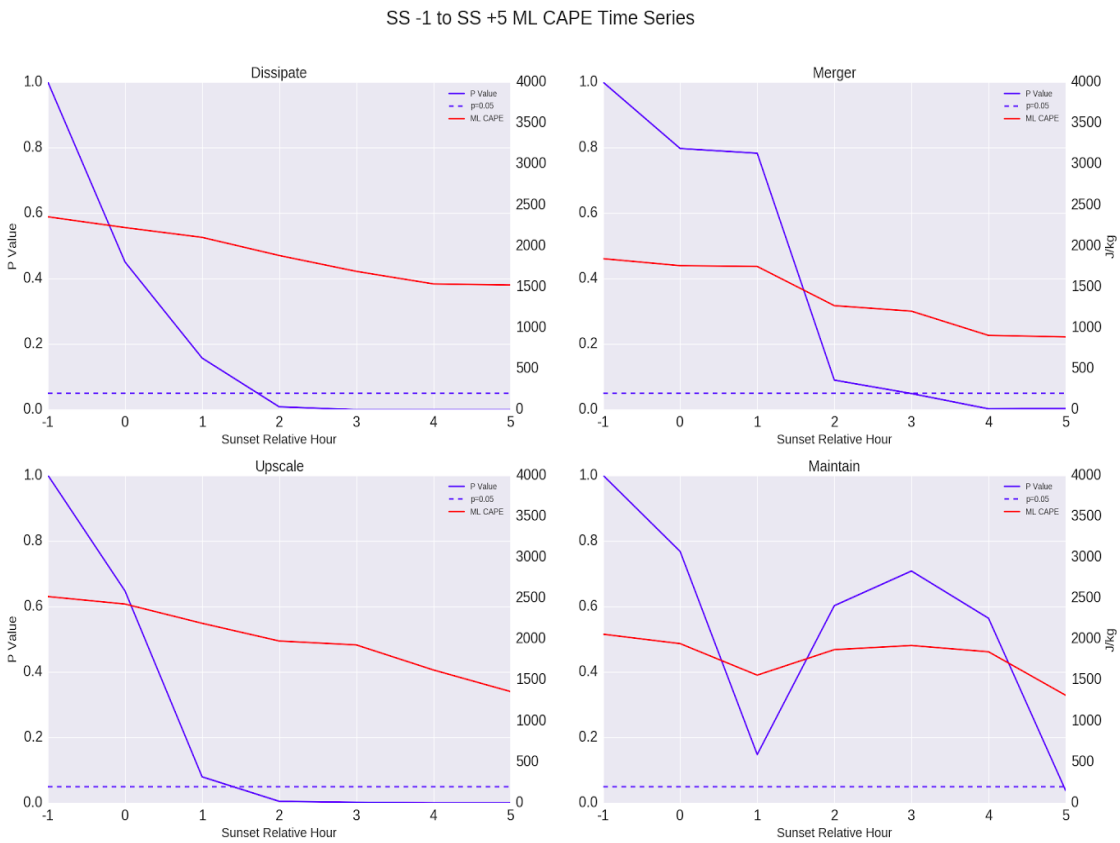

FIGURE **4**3: Same as Fig. 42, but with ML CAPE.

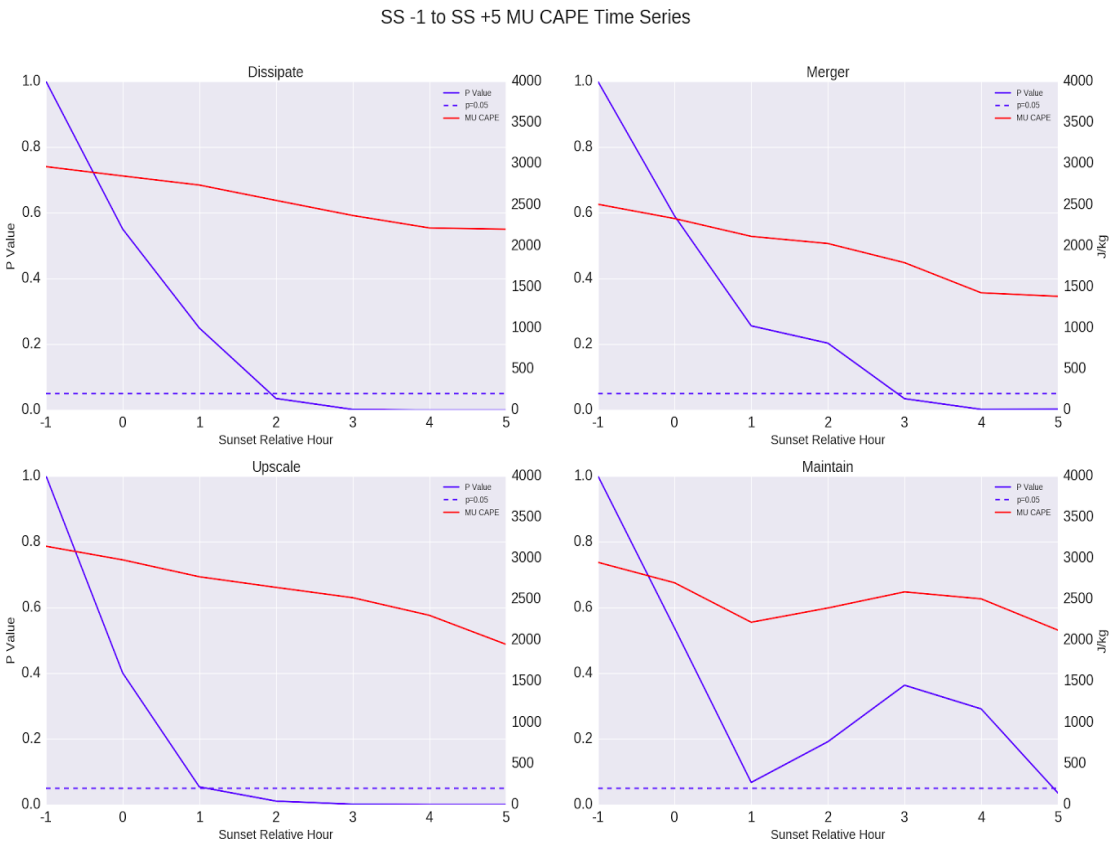

FIGURE 44: Same as Fig. 42, but with MU CAPE.

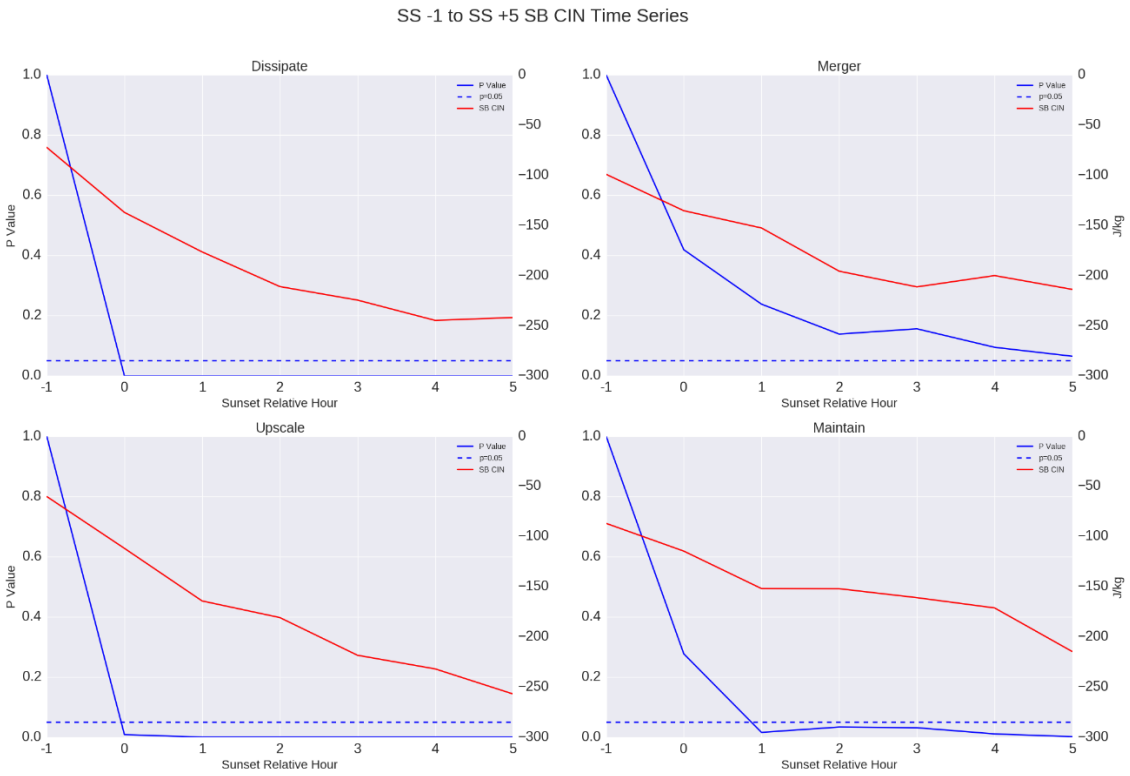

FIGURE 45: Same as Fig. 42, but with SB CIN.

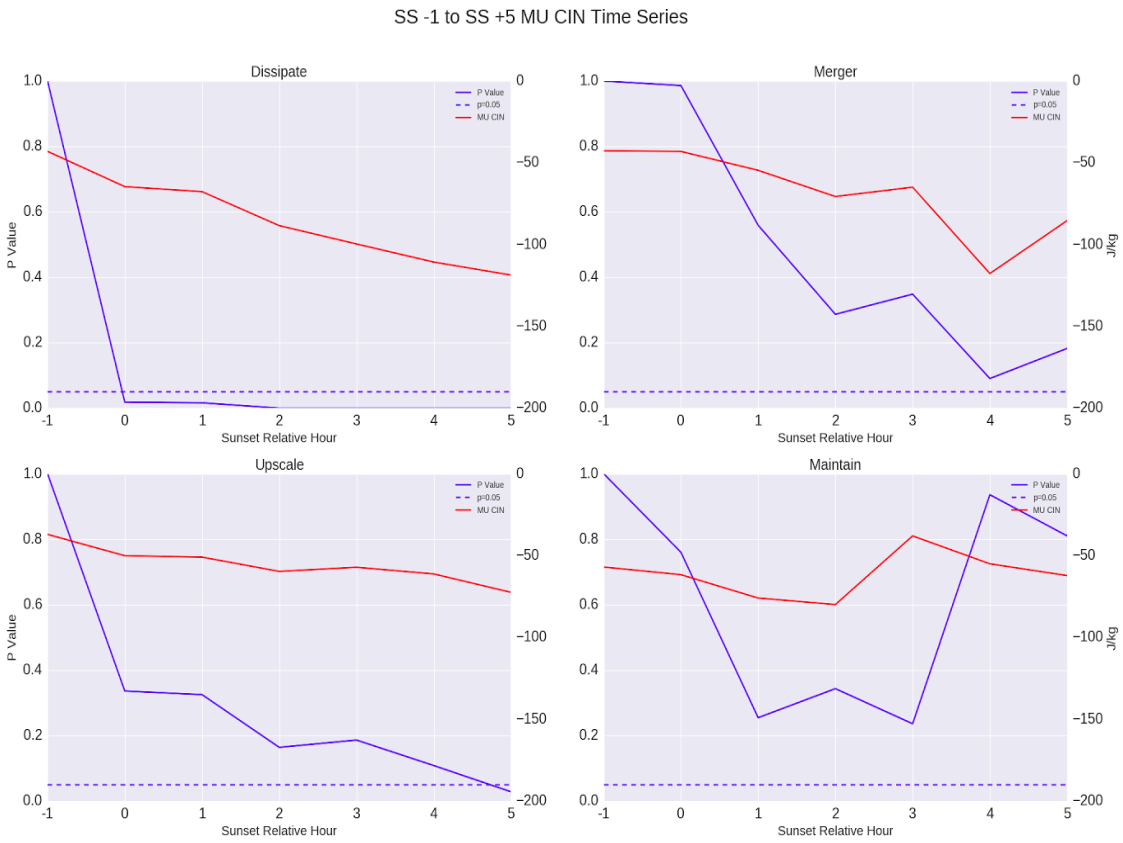

FIGURE 46: Same as Fig. 42, but with MU CIN.

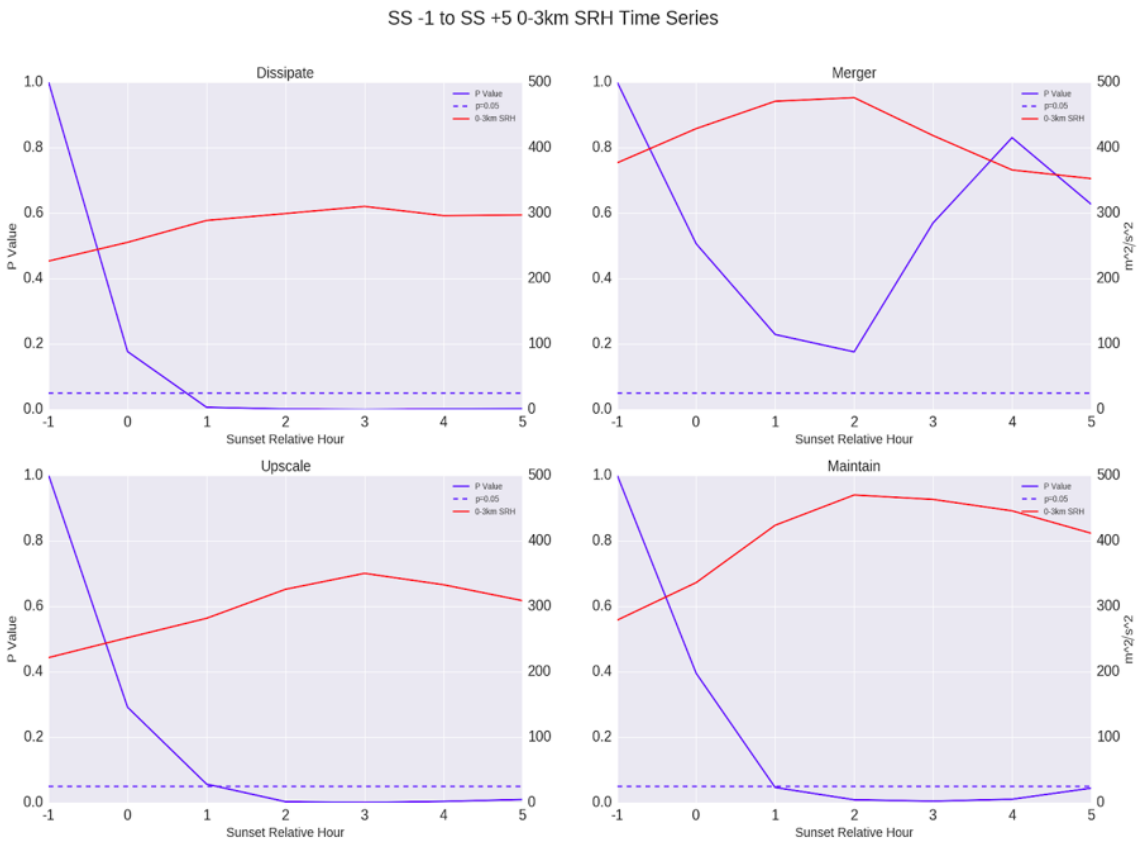

FIGURE 47: Same as Fig. 42, but with 0-3 km SRH.

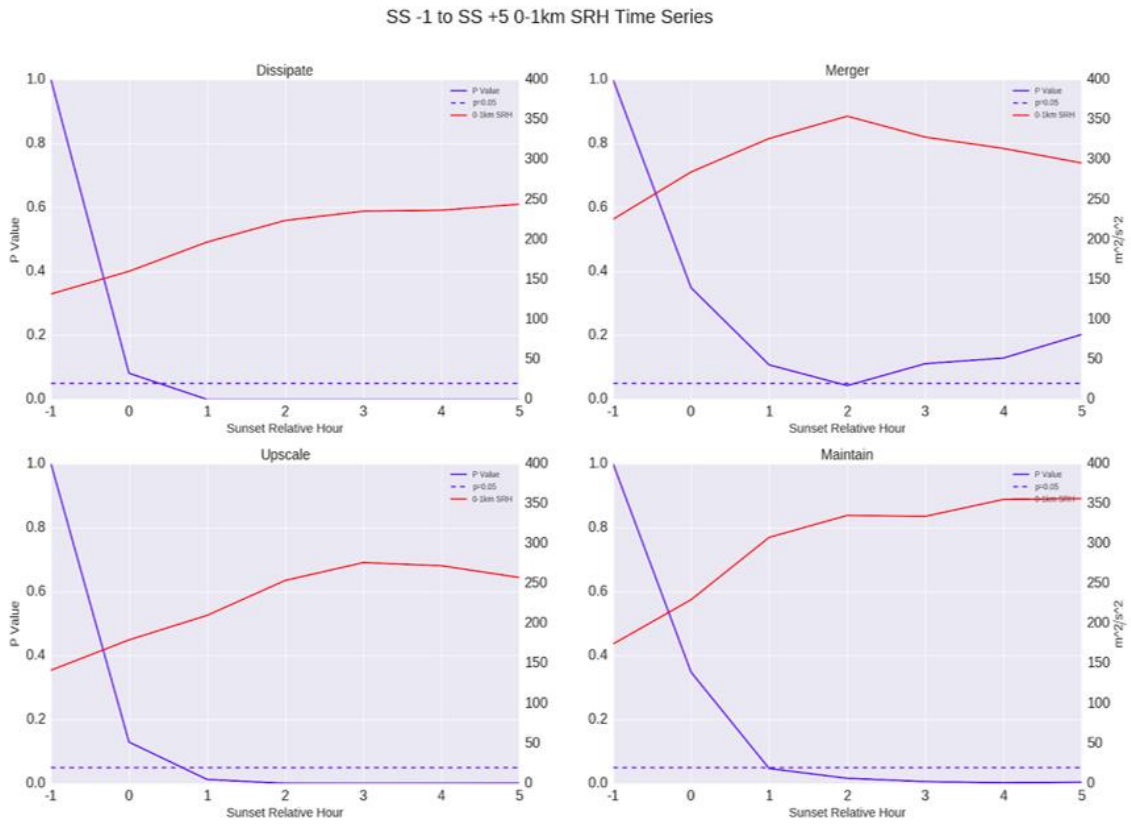

FIGURE 48: Same as Fig. 42, but with 0-1 km SRH.

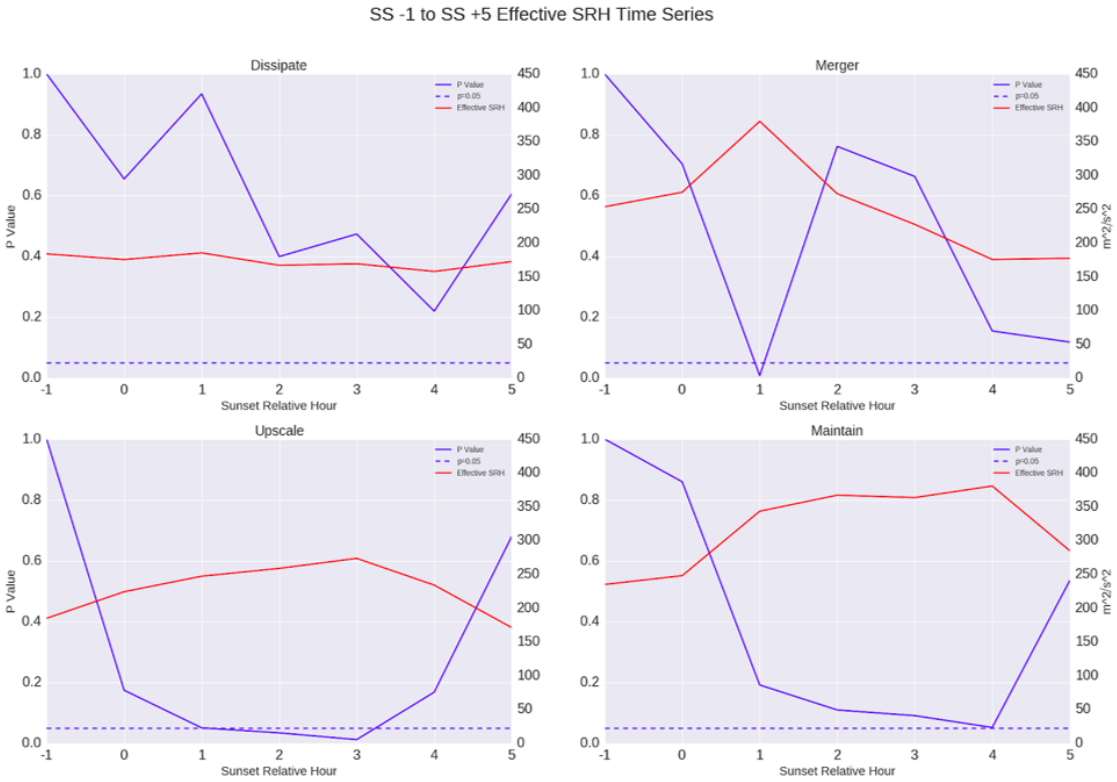

FIGURE 49: Same as Fig. 42, but with effective SRH.

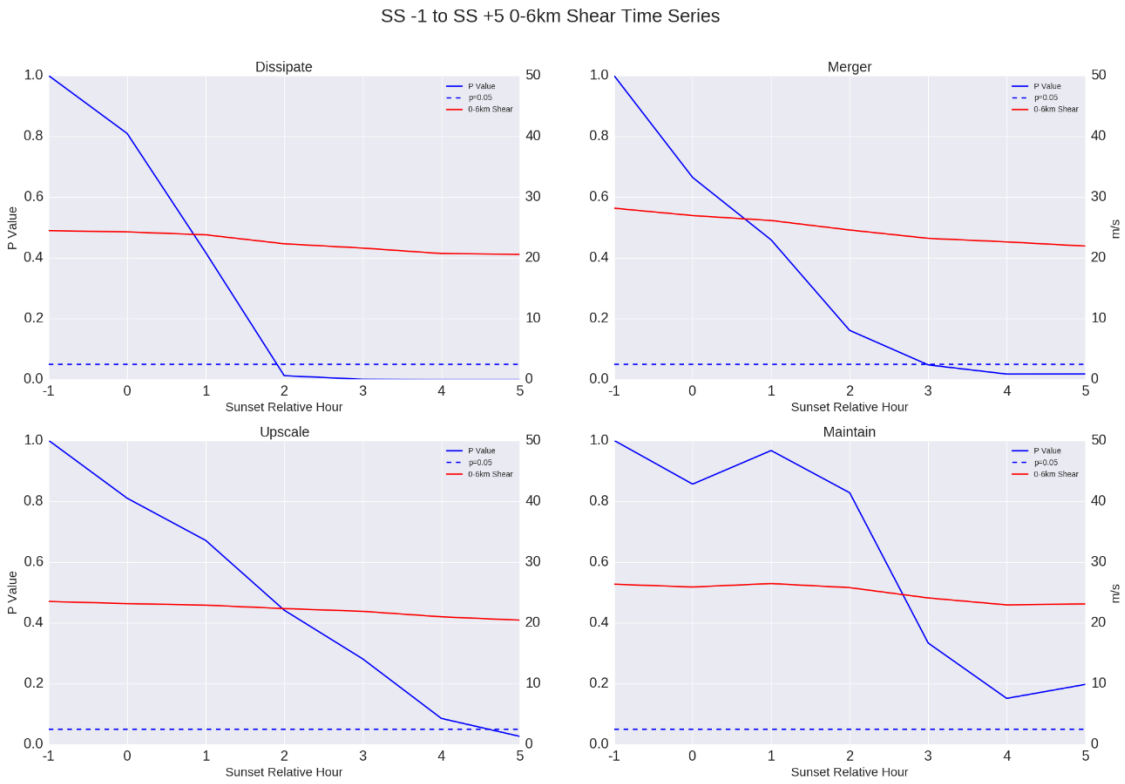

FIGURE 50: Same as Fig. 42, but with 0-6 km shear.

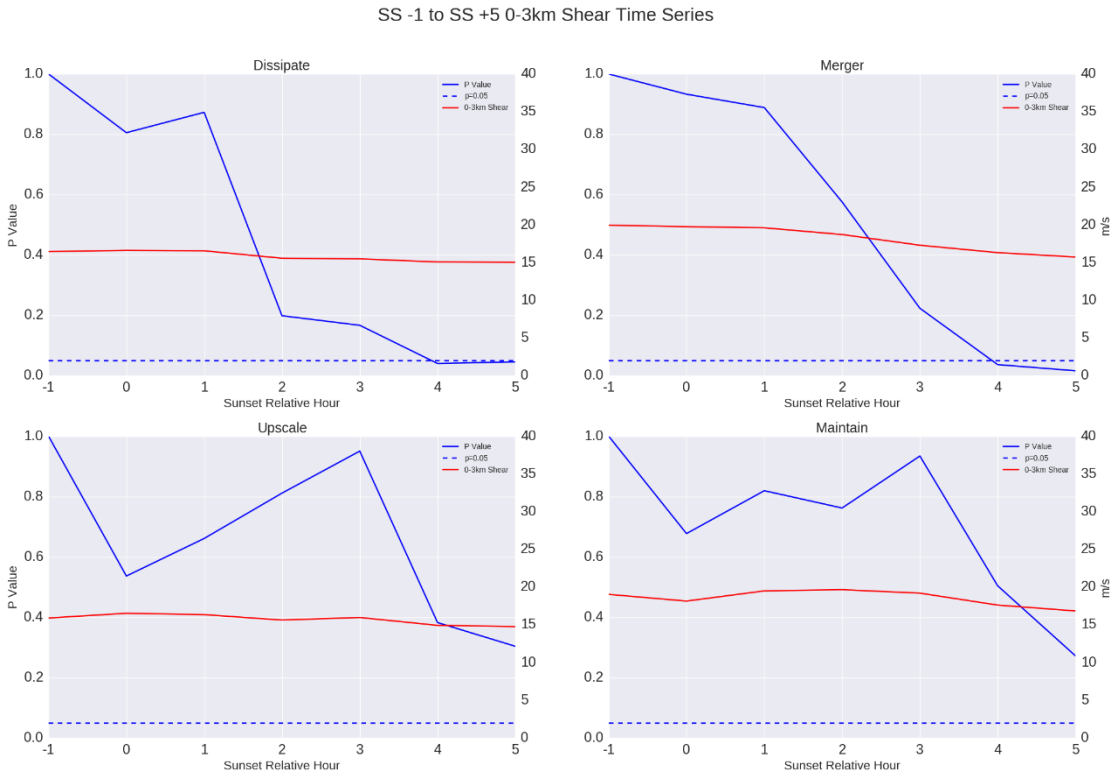

FIGURE 51: Same as Fig. 42, but with 0-3 km shear.

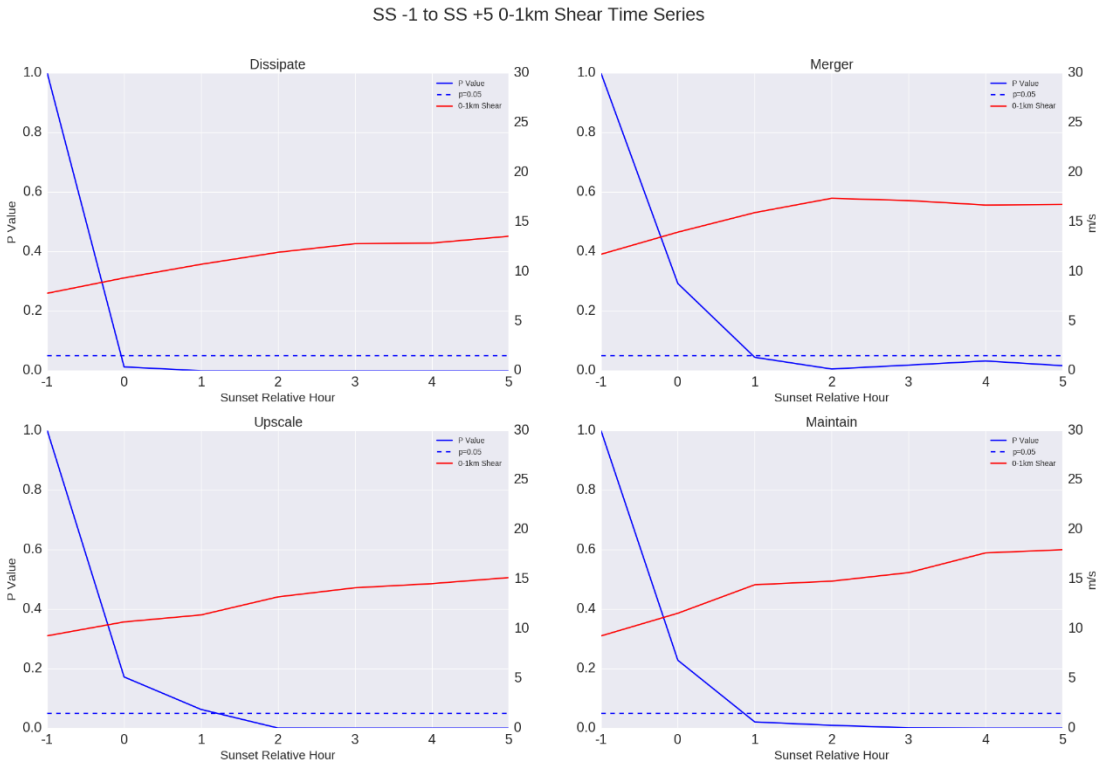

FIGURE 52: Same as Fig. 42, but with 0-1 km shear.

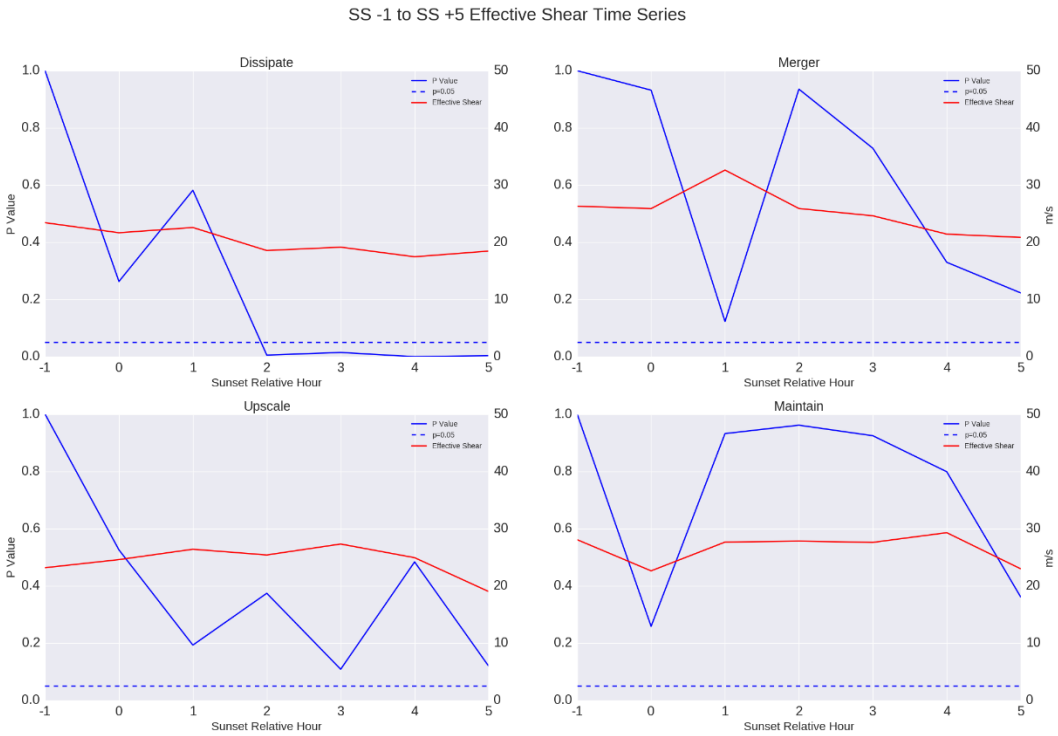

FIGURE 53: Same as Fig. 42, but with effective bulk shear.

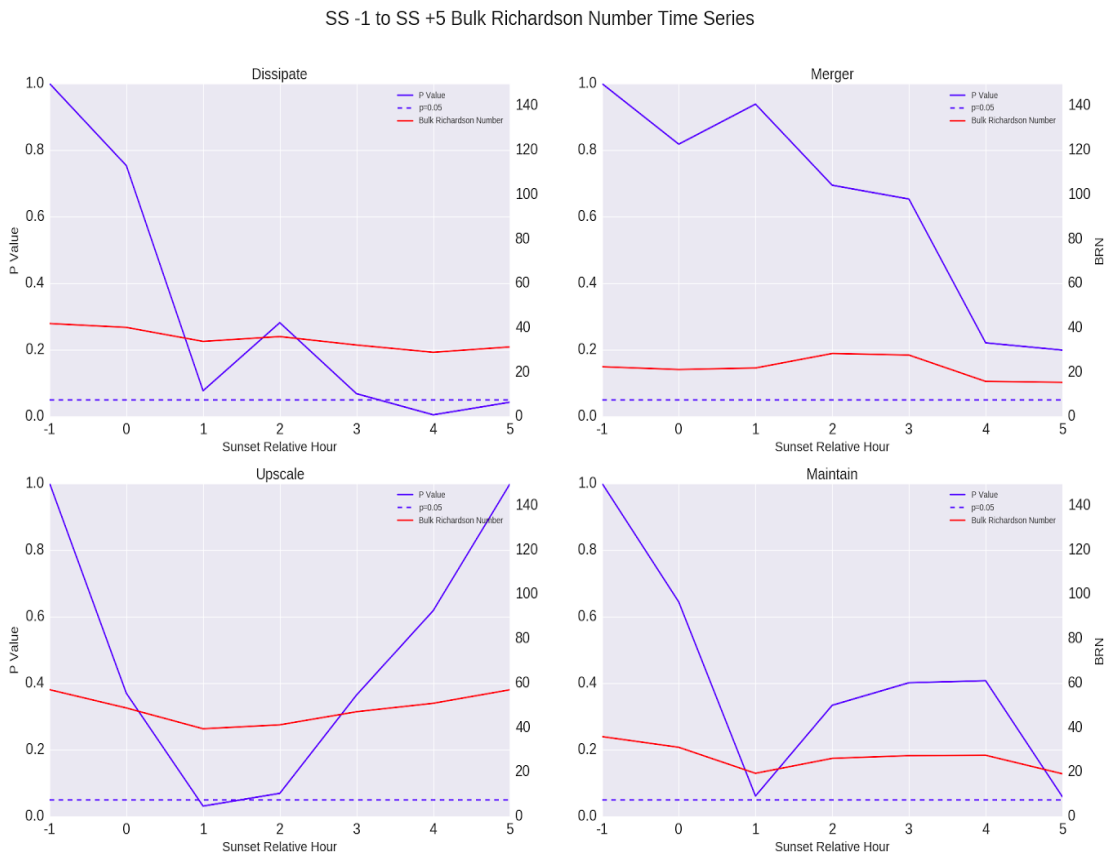

FIGURE 54: Same as Fig. 42, but with Bulk Richardson Number.

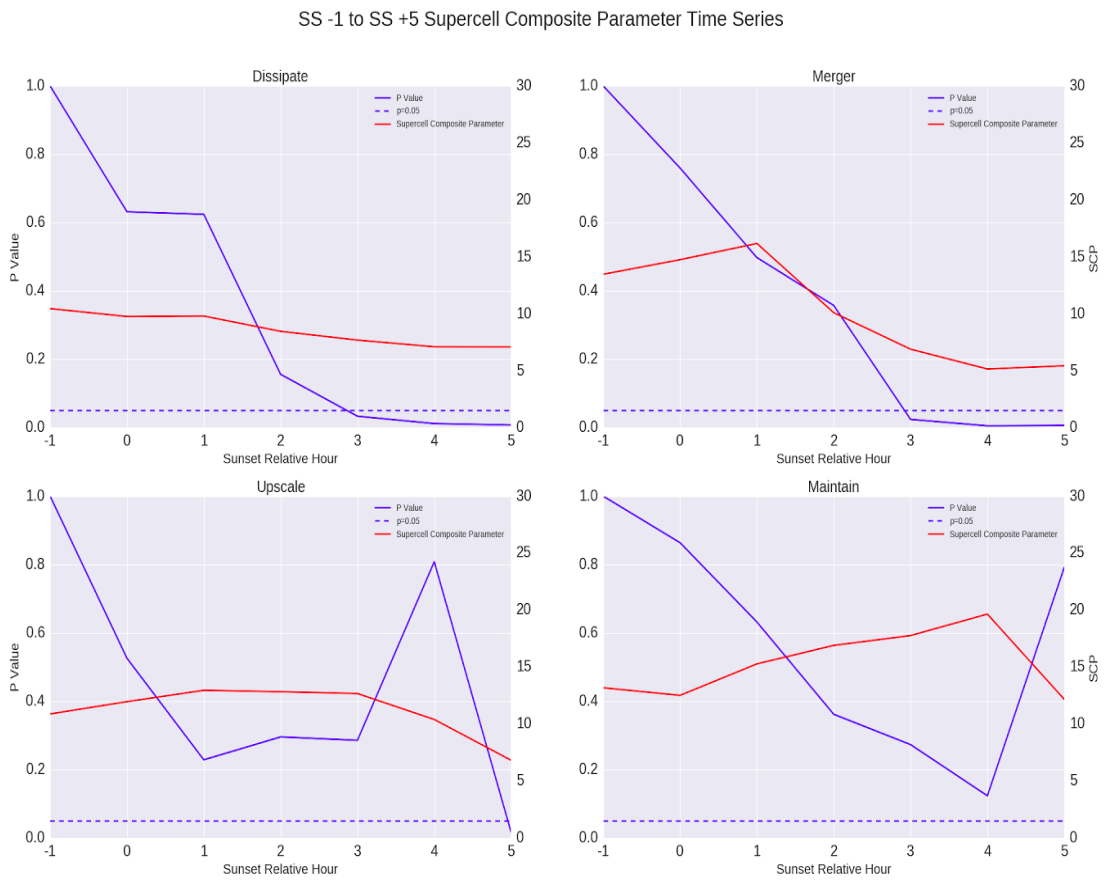

FIGURE 55: Same as Fig. 42, but with Supercell Composite Parameter.

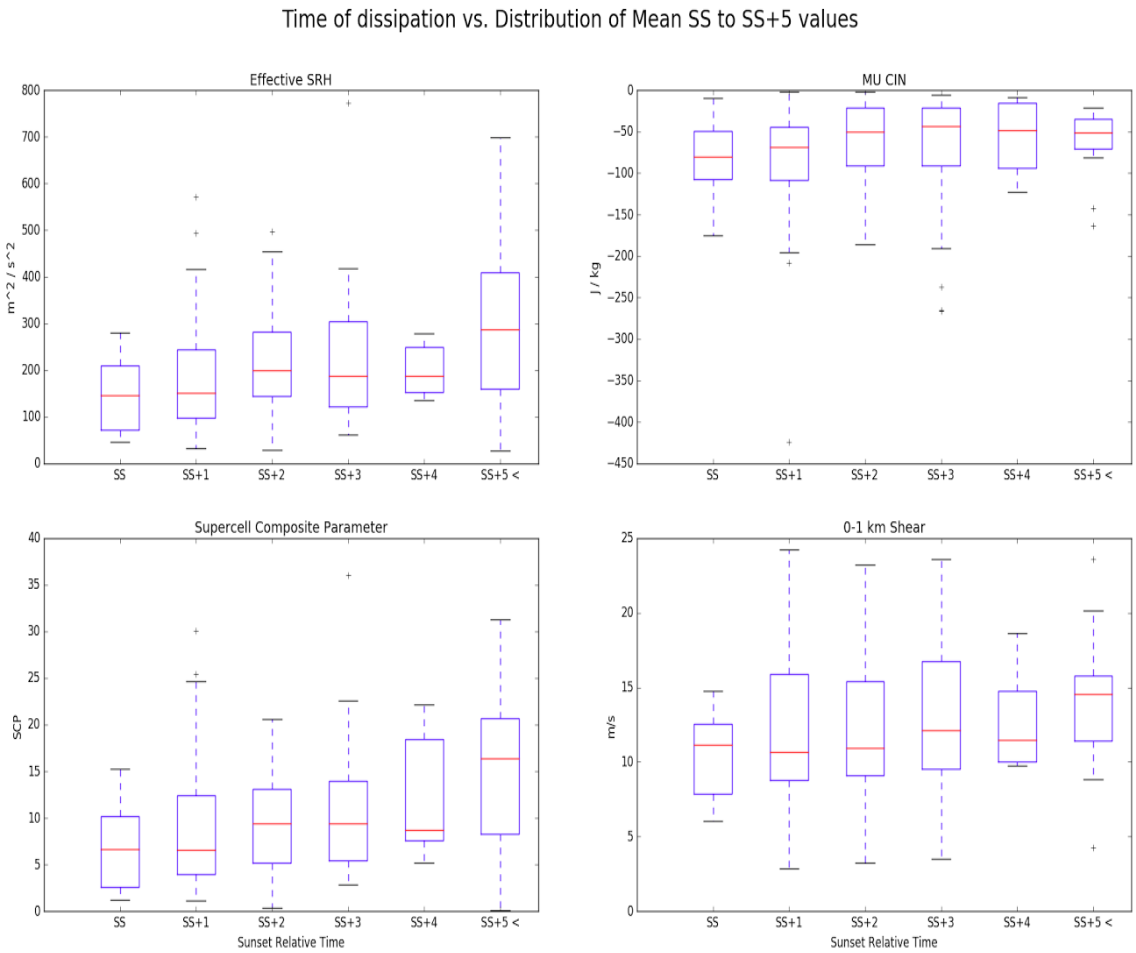

FIGURE 56: Bins based on time of evolution for all supercells. Values in the bins are the SS -1 to SS +5 cumulative mean for the given parameter.

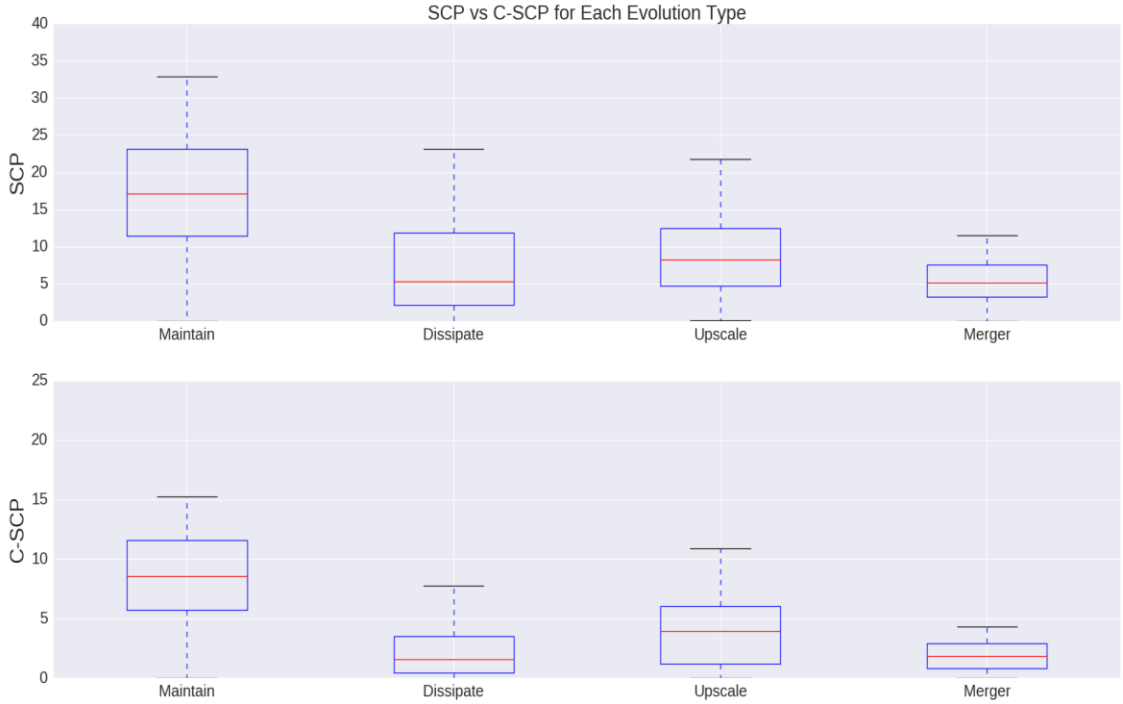

FIGURE 57: SS -1 to SS +5 mean distributions of SCP (top panel) and CIN SCP (bottom panel).

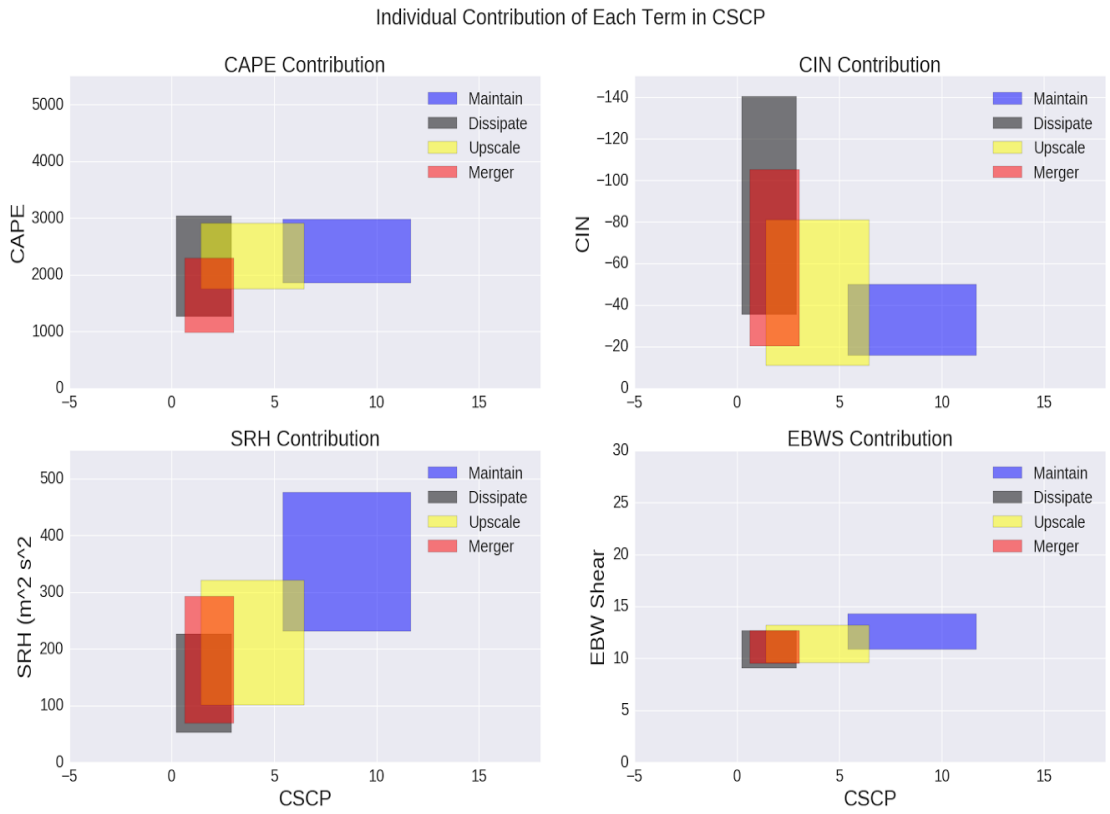

FIGURE 58: Individual contribution of each term in the CIN SCP equation; X axis is the SS -1 to SS +5 CSCP with the SS -1 to SS +5 mean of that particular term in the equation on the Y axis. The center of each box represents the SS-1 to SS+5 median value, while the horizontal and vertical extent of each box is plus or minus one median average deviation.

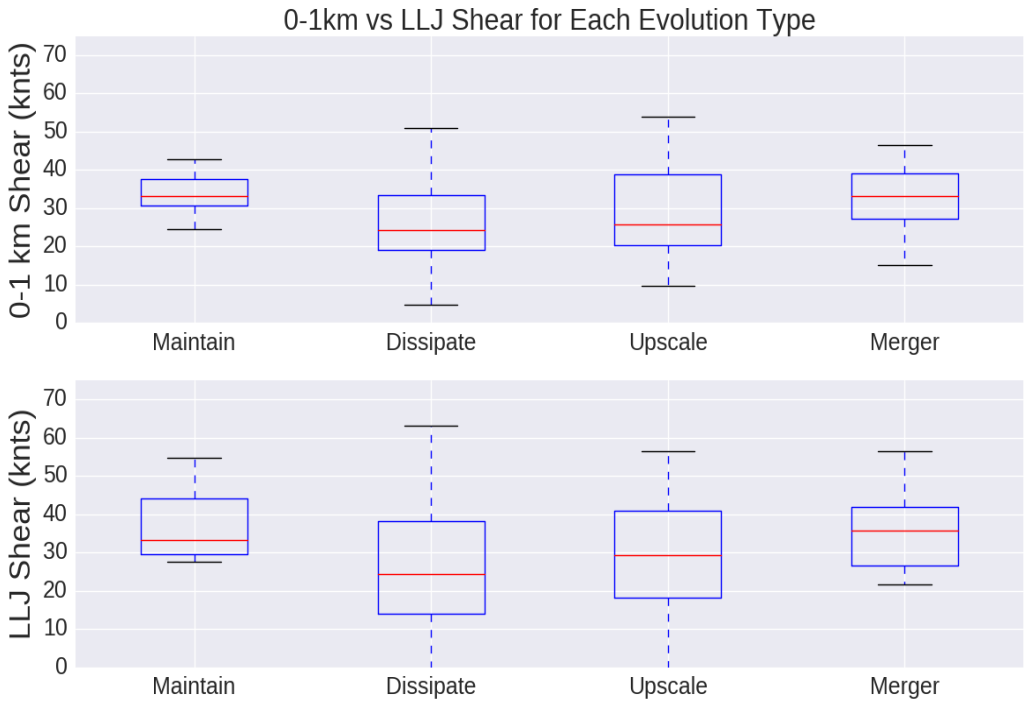

FIGURE 59: SS -1 to SS +5 mean distributions of 0-1 km shear (top panel) and Low Level Jet Shear (bottom shear)

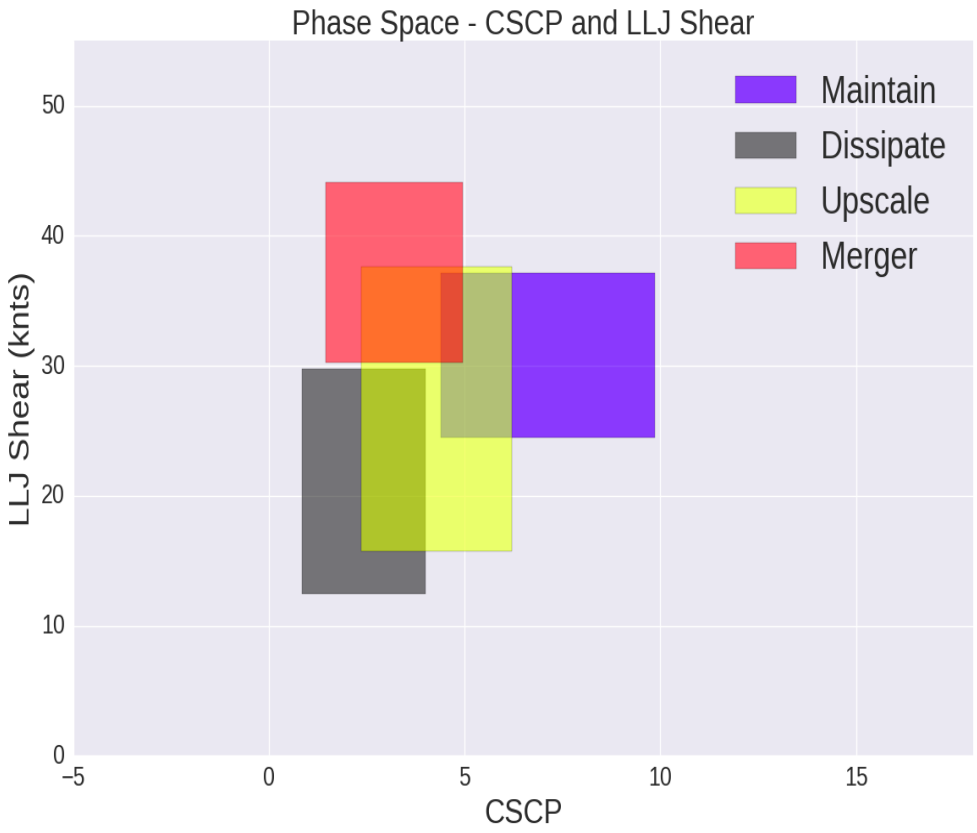

FIGURE 60: Phase space for each storm evolution classification; the center of each box represents the SS-1 to SS+5 median value, while the horizontal and vertical extent of each box is plus or minus one median average deviation. For example, dissipation events have a median of ~ 2.5 CSCP and ~22 knots of LLJ shear with a median average deviation of ~1.5 CSCP and ~ 10 knots of LLJ shear.

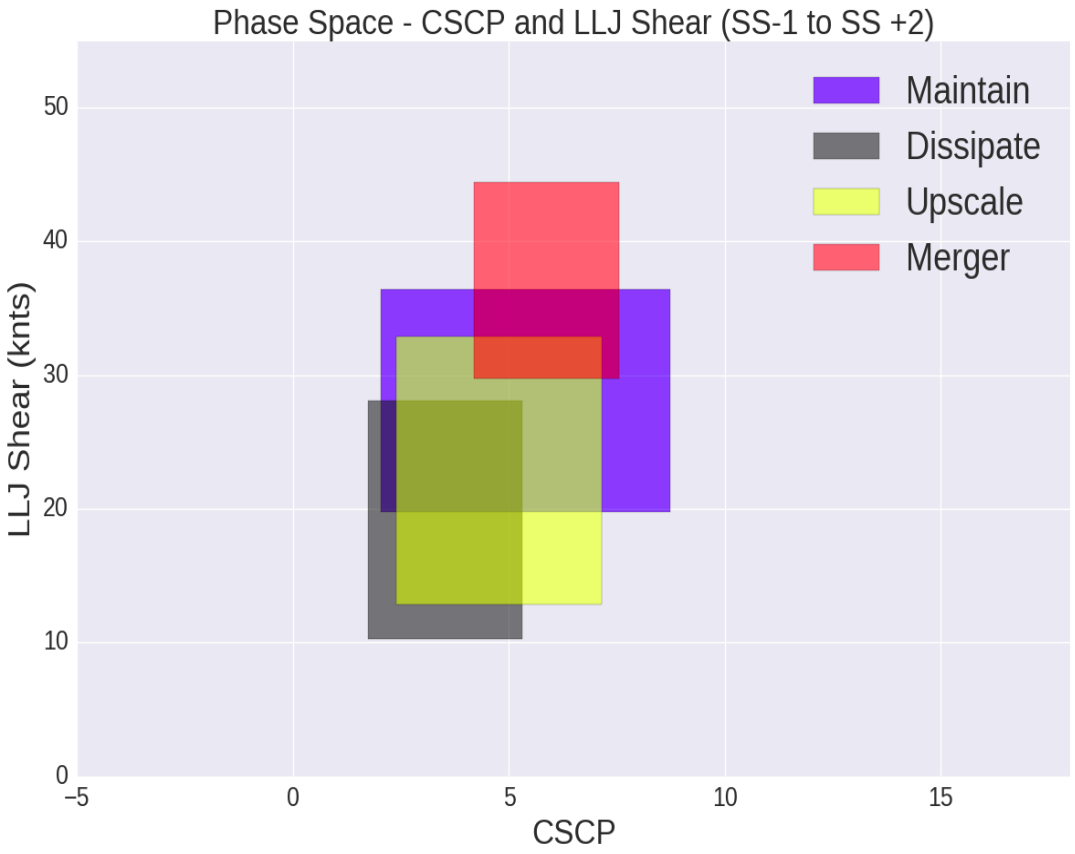

FIGURE 61: As in figure 48, but for median SS-1 to SS+2.

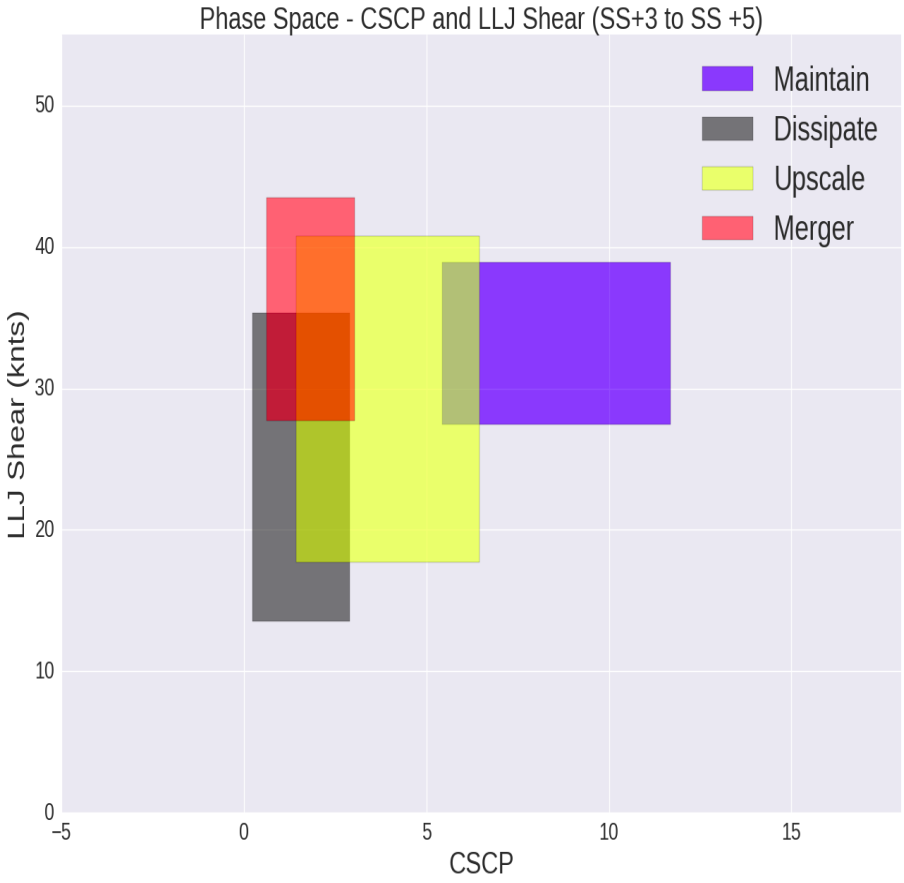

FIGURE 62: As in figure 48, but with median SS +3 to SS +5.

REFERENCES

2015: *NATIONAL PUBLIC WEATHER FORECAST PRODUCTS SPECIFICATION*. http://www.nws.noaa.gov/directives/sym/pd01005004curr.pdf (Accessed April 4, 2017).

Acevedo, O., and D. Fitzjarrald, 2001: The early evening surface-layer transition: Temporal and spatial variability. *Journal of the Atmospheric Sciences*, 58, 2650-2667, doi:10.1175/1520-0469(2001)058<2650:teeslt>2.0.co;2.

Ashley, W., A. Krmenec, and R. Schwantes, 2008: Vulnerability due to Nocturnal Tornadoes. *Weather and Forecasting*, 23, 795-807, doi:10.1175/2008waf2222132.1.

Benjamin, S. et al., 2016: A north American hourly assimilation and model forecast cycle: The rapid refresh. *Monthly Weather Review*, 144, 1669-1694, doi:10.1175/mwr-d-15-0242.1.

Benjamin, S., T. Smirnova, J. Brown, G. Grell, and R. Bleck, 2004: Mesoscale weather prediction with the RUC hybrid Isentropic–Terrain-Following coordinate model. *Monthly Weather Review*, 132, 473-494, doi:10.1175/1520-0493(2004)132<0473:mwpwtr>2.0.co;2.

Billings, J., and M. Parker, 2012: Evolution and maintenance of the 22–23 June 2003 nocturnal convection during BAMEX. *Weather and Forecasting*, 27, 279-300, doi:10.1175/waf-d-11-00056.1.

Blackadar, A., and K. Buajitti, 1957: Theoretical studies of diurnal wind-structure variations in the planetary boundary layer. *Quarterly Journal of the Royal Meteorological Society*, 83, 486-500, doi:10.1002/qj.49708335804.

Bluestein, H., 1999: *Tornado Alley: Monster Storms of the Great Plains*.

Bluestein, H., 1999: A history of severe-storm-intercept field programs. *Weather and Forecasting*, 14, 558-577, doi:10.1175/1520-0434(1999)014<0558:ahossi>2.0.co;2.

BONNER, W., 1968: CLIMATOLOGY OF THE LOW LEVEL JET. *Monthly Weather Review*, 96, 833-850, doi:10.1175/1520-0493(1968)096<0833:cotllj>2.0.co;2.

Bunkers, M., B. Klimowski, J. Grzywacz, L. Czepyha, J. Johnson, and M. Hjelmfelt, 2006: An observational examination of long-lived Supercells. Part II: Environmental conditions and forecasting. *Weather and Forecasting*, 21, 689-714, doi:10.1175/waf952.1.

Bunkers, M., M. Hjelmfelt, and P. Smith, 2006: An observational examination of long-lived Supercells. Part I: Characteristics, evolution, and demise. *Weather and Forecasting*, 21, 673-688, doi:10.1175/waf949.1.

Coffer, B., and M. Parker, 2015: Impacts of increasing low-level shear on Supercells during the early evening Transition*. *Monthly Weather Review*, 143, 1945-1969, doi:10.1175/mwr-d-14-00328.1.

Cohen, A., M. Coniglio, S. Cavallo, and H. Brooks, 2015: A review of planetary boundary layer Parameterization schemes and their sensitivity in Simulating southeastern U.S. Cold season severe weather environments. *Weather and Forecasting*, 30, 591-612, doi:10.1175/waf-d-14-00105.1.

Colman, B., 1990: Thunderstorms above Frontal Surfaces in Environments with Positive CAPE. Part 1: A Climatology. *Monthly Weather Review*, 118, 1103-1121.

Davenport, C., and M. Parker, 2015: Impact of environmental heterogeneity on the dynamics of a dissipating Supercell thunderstorm. *Monthly Weather Review*, 143, 4244-4277, doi:10.1175/mwr-d-15-0072.1.

Davenport, C., and M. Parker, 2015: Observations of the 9 June 2009 dissipating Supercell from VORTEX2. *Weather and Forecasting*, 30, 368-388, doi:10.1175/waf-d-14-00087.1.

Davies-Jones, R., 1984: Streamwise Vorticity: The origin of Updraft rotation in Supercell storms. *Journal of the Atmospheric Sciences*, 41, 2991-3006, doi:10.1175/1520-0469(1984)041<2991:svtoou>2.0.co;2.

French, A., and M. Parker, 2012: Observations of Mergers between Squall Lines and Isolated Supercell Thunderstorms. *Weather and Forecasting*, 27, 255-278, doi:10.1175/waf-d-11-00058.1.

Halbert, K., R. Thompson, P. Marsh, T. Supinie, W. Blumberg, and J. Hart, 2016: SHARPpy: An Open Source Sounding Analysis Toolkit for the Atmospheric Sciences. *Bull. Amer. Meteor. Soc.*,.

Helmus, J., and S. Collis, 2016: The Python ARM Radar Toolkit (Py-ART), a Library for Working with Weather Radar Data in the Python Programming Language. *Journal of Open Research Software*, 4, doi:10.5334/jors.119.

Horgan, K., S. Corfidi, J. Hales, D. Schultz, and R. Johns, 2007: A Five-Year Climatology of elevated severe Convective storms in the United States east of the Rocky Mountains. *Weather and Forecasting*, 22, 1031-1044, doi:10.1175/waf1032.1.

Janjić, Z., 1994: The step-mountain Eta coordinate model: Further developments of the convection, viscous Sublayer, and turbulence closure schemes. *Monthly Weather Review*, 122, 927-945, doi:10.1175/1520-0493(1994)122<0927:tsmecm>2.0.co;2.

Jones, T., K. McGrath, and J. Snow, 2004: Association between NSSL Mesocyclone detection algorithm-detected Vortices and tornadoes. *Weather and Forecasting*, 19, 872-890, doi:10.1175/1520-0434(2004)019<0872:abnmda>2.0.co;2.

Kerr, B., and G. Darkow, 1996: Storm-Relative Winds and Helicity in the Tornadic Thunderstorm Environment. *Weather and Forecasting*, 11, 489-505, doi:10.1175/1520-0434(1996)011<0489:srwahi>2.0.co;2.

Kis, A., and J. Straka, 2010: Nocturnal Tornado Climatology*. *Weather and Forecasting*, 25, 545-561, doi:10.1175/2009waf2222294.1.

Klemp, J., 1987: Dynamics of Tornadic thunderstorms. *Annual Review of Fluid Mechanics*, 19, 369-402, doi:10.1146/annurev.fluid.19.1.369.

Kumjian, M., J. Evans, and J. Guyer, 2006: The Relationship of the Great Plains Low Level Jet to Nocturnal MCS Development.

Lemon, L., and C. Doswell, 1979: Severe thunderstorm evolution and Mesocyclone structure as related to Tornadogenesis. *Monthly Weather Review*, 107, 1184-1197, doi:10.1175/1520-0493(1979)107<1184:steams>2.0.co;2.

Letkewicz, C., A. French, and M. Parker, 2013: Base-state substitution: An idealized modeling technique for Approximating environmental variability. *Monthly Weather Review*, 141, 3062-3086, doi:10.1175/mwr-d-12-00200.1.

Mead, C., and R. Thompson, 2011: Environmental Characteristics Associated with Nocturnal Significant Tornado Events in the Central and Southern Great Plains. *Electronic Journal of Severe Storms Meteorology*, 6, 1-35.

Nowotarski, C., P. Markowski, and Y. Richardson, 2011: The characteristics of numerically simulated Supercell storms situated over Statically stable boundary layers. *Monthly Weather Review*, 139, 3139-3162, doi:10.1175/mwr-d-10-05087.1.

Parker, M., 2008: Response of simulated squall lines to low-level cooling. *Journal of the Atmospheric Sciences*, 65, 1323-1341, doi:10.1175/2007jas2507.1.

Peters, J., and K. Eure, 2016: Factors that Influence Growth of Tornadic Supercells into MCSs after Sunset. *Severe Local Storms*, Pacific Grove, CA.

Rasmussen, E., and D. Blanchard, 1998: A Baseline Climatology of Sounding-Derived Supercell and Tornado Forecast Parameters. *Weather and Forecasting*, 13, 1148-1164, doi:10.1175/1520-0434(1998)013<1148:abcosd>2.0.co;2.

Markowski P., and Richardson, Y., 2010: *Mesoscale meteorology in Midlatitudes*. John Wiley & Sons, United States,.

Rotunno, R., and J. Klemp, 1985: On the rotation and propagation of simulated Supercell thunderstorms. *Journal of the Atmospheric Sciences*, 42, 271-292, doi:10.1175/1520-0469(1985)042<0271:otrapo>2.0.co;2.

Schultz, D., and S. Corfidi, 2008: Elevated convection and Castellanus: Ambiguities, significance, and questions. *Weather and Forecasting*, 23, 1280-1303, doi:10.1175/2008waf2222118.1.

Shapiro, A., E. Fedorovich, and S. Rahimi, 2016: A Unified Theory for the Great Plains Nocturnal Low-Level Jet. *Journal of the Atmospheric Sciences*, 73, 3037-3057, doi:10.1175/jas-d-15-0307.1.

Stensrud, D., J. Hwang, and M. Coniglio, 2010: Environmental factors in the upscale growth and longevity of MCSs derived from rapid update cycle analyses. *Monthly Weather Review*, 138, 3514-3539, doi:10.1175/2010mwr3233.1.

Stensrud, D., 2007: *Parameterization schemes: Keys to understanding numerical weather prediction models*. Cambridge University Press, Cambridge,.

Stull, R., 1988: *An introduction to boundary layer meteorology*. 1st ed. Kluwer Academic Publishers, Dordrecht,.

Stumpf, G., K. Thomas, M. Eilts, J. Johnson, P. Spencer, E. Mitchell, A. Witt, and D. Burgess, 1998: The national severe storms laboratory Mesocyclone detection algorithm for the WSR-88D*. *Weather and Forecasting*, 13, 304-326, doi:10.1175/1520-0434(1998)013<0304:tnsslm>2.0.co;2.

Mead C., and Thompson, R., 2011: Environmental characteristics associated with nocturnal significant-tornado events in the central and southern Great Plains. *Electronic J. Severe Storms Meteorology*, 6, 1-35.

Thompson, R., C. Mead, and R. Edwards, 2007: Effective storm-relative Helicity and bulk shear in Supercell thunderstorm environments. *Weather and Forecasting*, 22, 102-115, doi:10.1175/waf969.1.

Thompson, R., K. Elmore, J. Hart, R. Edwards, and P. Markowski, 2003: Close proximity soundings within Supercell environments obtained from the rapid update cycle. *Weather and Forecasting*, 18, 1243-1261, doi:10.1175/1520-0434(2003)018<1243:cpswse>2.0.co;2.

Thompson, R., R. Edwards, and C. Mead, 2004: An Update to the Supercell Composite and Significant Tornado Parameters. http://www.spc.noaa.gov/publications/thompson/stp_scp.pdf (Accessed April 6, 2017).

Thompson, W., and S. Burk, 1989: A vertically nested regional numerical weather prediction model with Second-Order closure physics. *Monthly Weather Review*, 117, 2305-2324, doi:10.1175/1520-0493(1989)117<2305:avnrnw>2.0.co;2.

Weisman, M., and H. Bluestein, 2000: The interaction of numerically simulated Supercells initiated along lines. *Monthly Weather Review*, 128, 3128-3149, doi:10.1175/1520-0493(2000)128<3128:tionss>2.0.co;2.

Weisman, M., and R. Rotunno, 2000: The Use of Vertical Wind Shear versus Helicity in Interpreting Supercell Dynamics. *Journal of the Atmospheric Sciences*, 57, 1452-1472, doi:10.1175/1520-0469(2000)057<1452:tuovws>2.0.co;2.

Weisman, M., J. Klemp, and R. Rotunno, 1988: A theory for strong, long-lived squall lines. *Journal of the Atmospheric Sciences*, 45, 463-485, doi:10.1175/1520-0469(1988)045<0463:atfsll>2.0.co;2.

Wurman, J., L. Wicker, D. Burgess, E. Rasmussen, P. Markowski, Y. Richardson, D. Dowell, and H. Bluestein, 2012: The Second verification of the origins of rotation in tornadoes experiment: VORTEX2. *Bulletin of the American Meteorological Society*, 93, 1147-1170, doi:10.1175/bams-d-11-00010.1.